Sastavljanje i dinamika antiparalelnih snopova mikrotubula u prometafazi mitoze

Matković, Jurica

Download date / Datum preuzimanja: **2024-07-17**

Repository / Repozitorij:

Repository of the Faculty of Science - University of Zagreb

UNIVERSITY OF ZAGREB

FACULTY OF SCIENCE

DEPARTMENT OF BIOLOGY

Jurica Matković

FORMATION AND DYNAMICS OF ANTIPARALLEL BUNDLES IN PROMETAPHASE OF MITOSIS

Graduation thesis

Zagreb, 2020.

Sveučilište u Zagrebu

Prirodoslovno-matematički fakultet

Biološki odsjek   Diplomski rad

Sastavljanje i dinamika antiparalelnih snopova mikrotubula u prometafazi mitoze

Jurica Matković

Rooseveltov trg 6, 10000 Zagreb, Hrvatska

Prilikom ulaska u mitozu, jezgrina ovojnica puca i formira se diobeno vreteno građeno od mikrotubula, motornih i nemotornih proteina. Pojedinačni mikrotubuli formiraju paralelne i antiparalelne snopove. Glavni marker antiparalelnih snopova je protein PRC1 (engl. *protein regulator of cytokinesis 1*). Prilikom mikroskopiranja primijećeno je da u stanicama u prometafazi PRC1 formira magličastu strukturu iz koje se u vremenu fokusiraju snopovi diobenog vretena. Inhibicijom kinaze aurora B ne dolazi do sastavljanja snopova sugerirajući da je lateralno vezanje kinetohora na mikrotubule vretena esencijalno za njihovo sastavljanje. Utišavanjem proteina Ndc80 dokazano je da prihvaćanje kinetohora na vrhove mikrotubula diobenog vretena ne utječe na sastavljanje antiparalelnih snopova. Također, uključenost proteina spindly u regulaciju broja antiparalelnih snopova dokazana je njegovim utišavanje, rezultirajući povećanjem broja snopova. Utišavanje proteina Haus6 rezultiralo je odsutnošću maglice proteina PRC1 u prometafazi. Protein Haus6, jedan od proteina augminskog kompleksa odgovornog za grananje mikrotubula, odgovoran je za nastanak maglice dokazujući time da je maglica razgranata mreža mikrotubula. Praćenje dinamike antiparalelnih snopova mikrotubula pokazalo je da novo formirani snopovi imaju isti obrazac kretanja u vremenu. Inhibicijom proteina Cenp-E i indukcijom mitoze s nerepliciranim genomom dokazano je da su sterička preklapanja krakova kromosoma koje se događaju kao posljedica njihove kongresije u metafaznu ravninu rezultat tog fenomena.

FORMATION AND DYNAMICS OF ANIPARALLEL BUNDLES IN PROMETPAHSE OF MITOSIS

Jurica Matković

Rooseveltov trg 6, 10000 Zagreb, Croatia

Cell division starts with nuclear envelope breakdown and the formation of mitotic spindle, composed of microtubules, motor and non-motor proteins. Microtubules form parallel and antiparallel bundles. Marker for antiparallel bundles is PRC1 protein (*protein regulator of cytokinesis 1*). During live cell imaging it is seen that in prometaphase PRC1 forms a mist from which bundles focus in time. Inhibition of aurora B kinase inhibited the formation of bundles suggesting that lateral attachment of kinetochores on microtubules is essential for their formation. By Ndc80 protein silencing it is shown that end-on attachment of kinetochores to microtubules does not affect antiparallel bundle formation. Moreover, role of spindly in the regulation of number of antiparallel bundles was shown by its silencing, resulting in their increase. Silencing of Haus6 protein resulted in no PRC1 mist formation in prometaphase. Protein Haus6 is one of the proteins of augmin complex responsible for branching of microtubules and is essential for mist formation proving that mist is a branched mesh of microtubules. Dynamics of antiparallel bundles showed that de novo formed bundles have the same pattern of movement in time. Cenp-E inhibition and induction of mitosis with un-replicated genomes showed that steric hindrance of chromosome arms during the chromosome congression is the main cause of bundle dynamics.

Table of Contents

1. INTRODUCTION

1.1 Mitosis

Of all the events that enable existence of life, perhaps the most critical is the ability of cells to accurately replicate and then faithfully segregate their chromosomes at each cell division. Every cell cycle culminates in mitosis. While the replication of chromosomes, which includes DNA replication and correct establishment of epigenetic chromatin marks, takes place in the interphase nucleus, segregation of duplicated chromosomes in daughter cells is the main function of complex and conserved microtubule-based structure, mitotic spindle. Mitotic spindle is formed after nuclear envelope breakdown (NEBD) in part of the cell cycle called mitosis. This segregation needs to be precise since the consequences of a single error are serious: aneuploid cells are either non-viable or, worse, they can become the first step on a road to cancerous transformation. The goal of mitosis is to ensure that daughter cells inherit identical genetic information transmitted in the form of duplicated chromosomes. Mitosis has been divided up into several stages for ease of description, but in reality it is a continuous process (**Figure 1**). The formation of mitotic spindle already starts in the first phase, prophase, when the interphase array of microtubule is replaced, as the duplicated centrosomes become more active in the microtubule nucleation. These microtubules are called asters, and as they grow, they push centrosomes on the opposite sides of the nucleus, which become poles of the mitotic spindle. The next phase, prometaphase, is marked by nuclear envelope breakdown. Microtubules assembled from the spindle pole growing in the direction of chromosomes are induced by nucleation factors recruited in the vicinity of chromosomes (O'Connell and Khodjakov, 2007). They are stabilized by lateral and end-on attachment of kinetochores, protein complexes that form on centromeres of chromosomes. Kinetochores are attachment points of chromosomes on the mitotic spindle. After attachment, chromosomes start their way to the middle of the spindle in the process known as congression. Prometaphase continues until all chromosomes are aligned in the metaphase plate, at which point cell enters a next stage, metaphase. The next stage, anaphase, is promoted by the activation of anaphase-promoting complex (APC) which promotes separation of sister chromatids by pulling forces of microtubules attached on kinetochores, known as anaphase A; and separation of spindle poles, anaphase B. Now that chromosomes have separated, the cell enters telophase. In this phase the nuclear envelope reforms, chromosomes decondense, spindle degrades and the cell is divided by a process known as cytokinesis. In the end of the

mitosis every daughter cell must receive one copy of the replicated chromosome (Lodish et al., 2008).
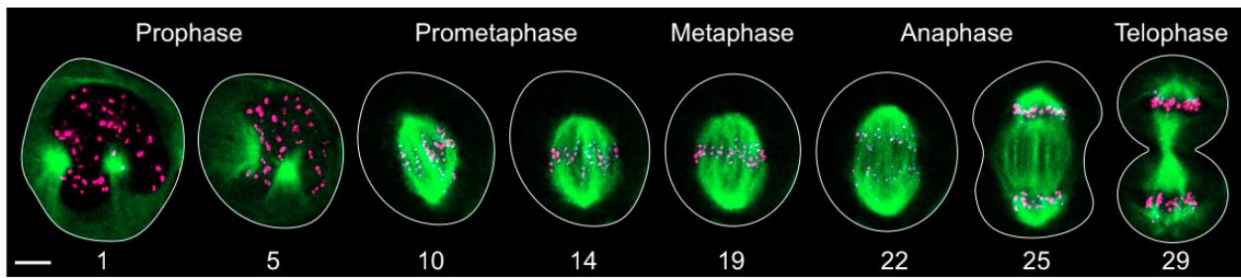
Figure 1. Mitosis in human U2OS cell line expressing CENP-A-GFP (pink) and mCherry-α-tubulin (green). Prophase is the first phase of mitosis in which spindle starts to form. Prometaphase starts with nuclear envelope breakdown and chromosome attachment to the microtubules. In metaphase all chromosomes are aligned at the metaphase plate, whereas in anaphase sister chromatids separate only to form two daughter cells in telophase, the last phase of mitosis. The white line marks the cell outline. Time is given in minutes; scale bare represents 5 μm (acquired from Tolić, 2017).

1.2 Classes of microtubules in the mitotic spindle

Chromosome movements during mitosis rely upon complex macromolecular machine known as the mitotic spindle. The spindle has three principal components: centrosomes, chromosomes and microtubules. It forms as chromosomes become connected to the two centrosomes or spindle poles by microtubule bundles that link each pole to a specialized macromolecular assembly on the chromosome body termed the kinetochore. Mitotic spindle is dynamic, self-assembling protein machine composed of more than a hundred different proteins. The main protein that constitutes microtubules, the main elements of the spindle, is tubulin. Purified soluble tubulin is a dimer consisting of two closely related subunits, α-tubulin and β-tubulin. They are conserved in all eukaryotes, with considerable expansion in the number of genes in multicellular organisms. All eukaryotes have genes coding for a third type of tubulin, γ-tubulin, which has a regulatory function. Tubulin polymerizes in microtubule filaments which consist of 13 laterally associated protofilaments forming a tubule whose external diameter is about 25 nm long, while diameter of inner hole is 15 nm long (**Figure 2**). Because protofilaments are composed of tubulin dimers, each protofilament has the α-subunit on the one side and β-subunit on the other side of the filament, so the protofilaments have an intrinsic polarity (Alberts et al., 2002). In a microtubule, all the

laterally associated protofilaments have the same polarity, so the microtubule also has an overall polarity. The plus (+) end of the microtubule favors polymerization and has β-subunits exposed, while minus (-) end favors depolymerization and has α-subunits exposed. Most microtubules in a cell consist of a simple tube, a singlet microtubule, built from 13 protofilaments (Saeidi et al., 2014). Microtubules nucleate from structures known as microtubule-organizing centers (MTOC) where minus end of the microtubule stays anchored in the MTOC, while plus end is growing from the MTOC towards the cell periphery. During mitosis, cell completely reorganizes its microtubule network to form a bipolar spindle, assembled from two MTOCs called spindle poles. Spindle poles are complex structures that have a dense matrix of γ-tubulin ring complex. Those are centers of the initial microtubule nucleation. Microtubules assemble by polymerization of αβ-tubulin dimer in a process that is catalyzed by the presence of microtubule associated factors (MAPs) (Lodish et al., 2008).
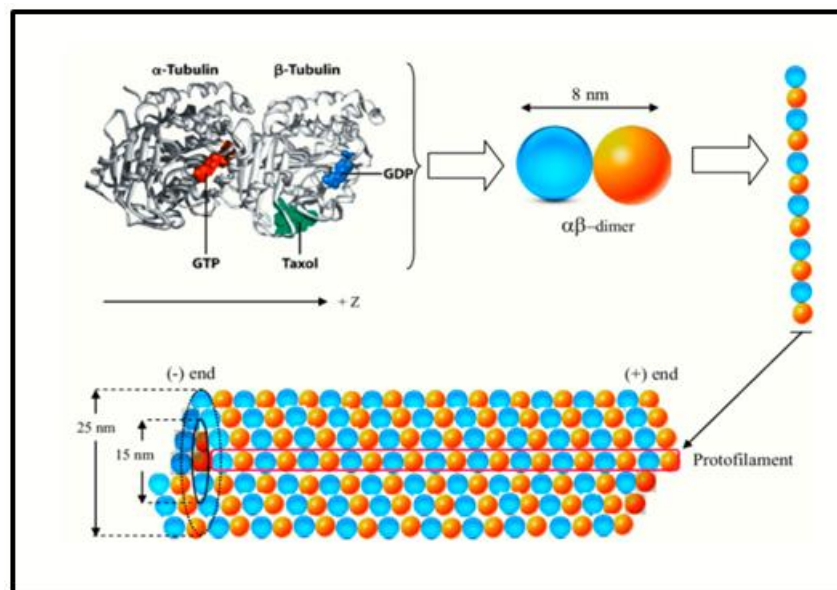
Figure 2. Schematic view of the αβ-tubulin dimer, which polymerizes end-to-end to form protofilaments. Protofilaments associate longitudinally to construct microtubules (MTs). The MT is a hollow cylindrical structure with a plus and a minus end, which typically has 13 parallel protofilaments. The length of αβ-tubulin dimer is 8 nm. The diameter of the inner hole of the microtubule is 15 nm, while the diameter of the whole cylinder is 25 nm (acquired from Saeidi et al., 2014)

The main characteristic of microtubules is that individual microtubules exhibit dynamic instability (Lodish et al., 2008). In essence, microtubule plus ends interconvert between polymerization and depolymerization states. Thus, at any given time an individual

microtubule grows or shrinks before it ultimately disassembles. Some microtubules grow in length, whereas others shorten very rapidly thus indicating two distinct populations of microtubules. Individual microtubules can grow and then suddenly undergo a catastrophe to a shrinking phase (**Figure 3**). Moreover, sometimes a depolymerizing microtubule end could go through a rescue and grow again (Lodish et al., 2008).

(A) assembly (elongation)

(B) disassembly (shrinkage)
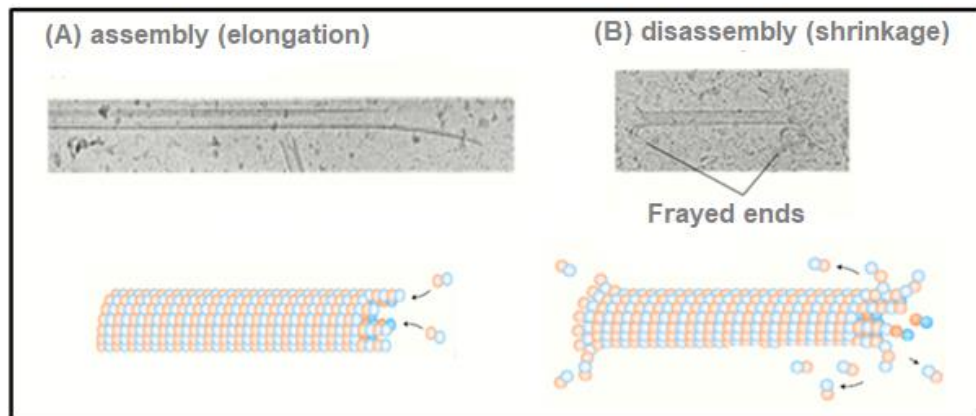
Frayed ends

Figure 3. **A.** Assembly of the microtubules by polymerization of αβ-dimer. **B.** Disassembly of the microtubule gives frayed ends on its end. Microtubules are captured in quickly frozen state in liquid ethane and examined with cryoelectron microscope (acquired and adapted from Lodish et al., 2008)

As microtubules grow from the spindle pole, more microtubules form lateral attachments facilitated by crosslinking proteins and motor proteins, forming bundles of microtubules (Bratman and Chang, 2008). Astral microtubules extend from the spindle pole to the cell cortex performing a critical role of orientating the spindle in the right axis for cell division (Nakayama et al., 2012). Parallel microtubules are connected by crosslinking proteins forming parallel bundles. Antiparallel microtubules that interdigitate from distinct poles are forming antiparallel bundles also with the help of some motor proteins and PRC1 (*protein regulator of cytokinesis 1*) cross linker protein. These two classes of bundles are forming a complex unit, composed of both antiparallel and parallel microtubules in a way that parallel bundles are connected to the kinetochore of chromosomes in metaphase and are called kinetochore fibers, whereas antiparallel bundles bridge two K-fibers from distinct poles forming bridging fiber (**Figure 4**) (Vukušić et al., 2017). The role of the bridge is balancing the forces between two K-fibers on kinetochores of chromosomes, and pole separation in anaphase B. All this structures start with their formation in the prometaphase in a way that is still unknown.
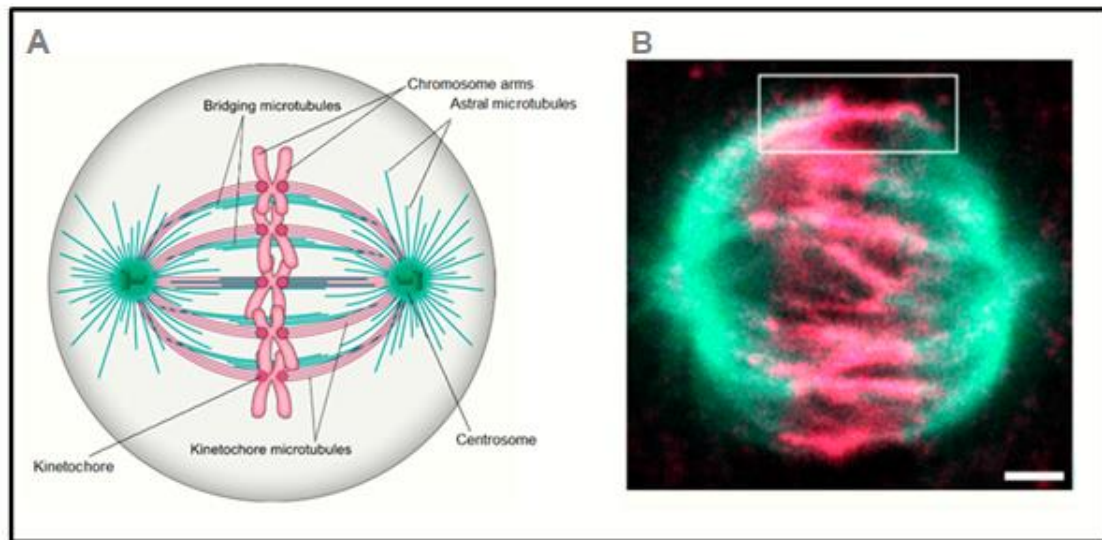
Figure 4. A. Schematic view of the mitotic spindle. Kinetochore microtubules are shown in purple. Other microtubules including bridging fibers are shown in green. Other components are designated on the scheme. **B.** Metaphase spindle in HeLa cells expressing tubulin-GFP (*green flourescent protein*) shown in green and endogenous PRC1 (immunostained), passive crosslinking protein that binds antiparallel microtubules representing bridge. Box region represents a complex unit of antiparalel and parralel microtubules. Scale bar is 5 µm (acquired and adapted from Polak et al., 2017).

1.3 Models of the spindle assembly

Several models have tried to explain spindle formation and chromosome segregation. First model that explained the spindle assembly was "search and capture" model (Mitchison and Kirchner, 1984). The core of this model is replicated centrosome. Each centrosome nucleates a radial array of highly dynamic astral microtubules. In this model, the plus ends of microtubules nucleated at centrosomes grow, shrink and regrow, randomly exploring the space. Contact with a kinetochore results in the capture of the chromosome and suppression of the microtubule dynamics. As a result, the kinetochore establishes a relatively stable connection to the pole. Over time, more and more microtubules become stabilized by repetitive capture so that the number of microtubules extending from centrosome to kinetochores increases, while the number of astral microtubules decreases proportionally, leading to the formation of a typical spindle-like structure (**Figure 5 A**). This model has some serious conceptual difficulties. Modern computational models predict that unbiased search and capture would require hours before each of the kinetochores on 46 chromosomes present in a typical human cell captures a single microtubule (Wollman et al., 2005). However,

mitosis takes less than 30 minutes in a diploid human cell (Magdison et al., 2011). Random probing of the cytoplasm for multiple small targets is likely to have a low probability of success and, therefore, is an inefficient mechanism. This implies that an additional mechanism facilitates spindle assembly by guiding microtubules growth towards the kinetochores and positioning chromosomes to the area with high density of microtubules.

The alternative model of the spindle assembly indicates that not centrosomes, but chromatin might drive the formation of the spindle. Ran-GTP is a protein from a large family of proteins called G proteins. They are included in signaling and transport in various processes in the cell. All G proteins have two conformations, of which one is active, ATP bound, and other is inactive, ADP bound. Ran promotes microtubule nucleation and stabilization and is present in a concentration gradient around mitotic chromosomes (**Figure 5 B**). The gradient is established throughout the activity of the chromosome associated guanine-nucleotide-exchange factor (GEF) RCC1 which promotes ADP for ATP exchange and shifts Ran from inactive to active state (Carazo-Salas et al., 1999). Ran has been proposed to effect the spindle formation through two mechanisms. First mechanism acts by creating a local concentration of microtubule stabilizing factors around the chromosomes to promote capture of astral microtubules. The second is direct nucleation of microtubules immediately adjacent to kinetochores after which microtubules assume proper orientation followed by the attachment of plus ends on the kinetochore. The classical search and capture mechanism and the chromosome mediated spindle assembly pathway appear to be interrelated (**Figure 5 C**). The chromosomes do not passively wait to be discovered by centrosomal microtubules. Instead, they actively form their own K-fibers by promoting local microtubule nucleation followed by capture at their kinetochores. K-microtubules emanating from kinetochores are captured by astral microtubules and are then transported poleward along the astral microtubules by dynein motors (O'Connell and Khodhakov, 2007). As such, centrosomes in animal cells serve as attraction points to which pre-assembled spindle components are transported and then integrated into a common spindle structure. Those are two different components that are probably included in the formation of K-fibers (Heald and Khodjakov, 2015).
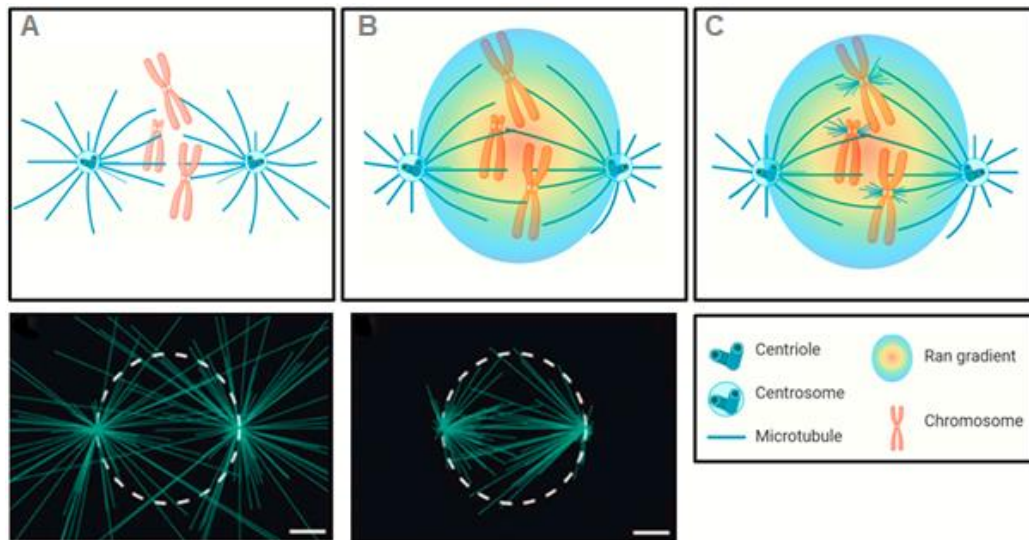
Figure 5. A. Schematic view of classical unbiased search and capture model shows capture of kinetochores by astral microtubules and their stabilization. **B.** Ran gradient biased model proposes growth of microtubules toward chromosomes due to accumulation of nucleating factors. **C.** Ran gradient biased model involving nucleation of microtubules on kinetochores. **D.** 2D projection of 3D simulation in the unbiased (left) and Ran gradient biased (B) model (acquired from Wollman et al., 2015).

Even more interesting phenomena observed during mitotic spindle formation, is the centrophilic behavior of the chromosomes. Shortly after the nuclear envelope breakdown, many chromosomes engage in lateral interactions with astral microtubules and move rapidly along them towards the pole, transported by dynein. As the spindle assembly proceeds, chromosomes continue to move towards the centrosomes, albeit more slowly, forming transient arrangement in a ring surrounding the central part of the spindle. There they reside until their sudden move back, congression, to the spindle equator.

Soon after the NEBD, kinetochores which are located in the inner parts of the nucleus are rapidly expelled from the central part of the spindle by spindle ejection force produced by plus end directed motor protein kinesin 10 (Kid) (Rieder and Salmon, 1994), while more peripheral kinetochores move inward. This rapid movement has as a consequence the formation of the ring configuration of chromosomes, with arms pointing outwards and the centromere inwards, towards the spindle axis so the chromosomes cover the spindle surface (Magdison et al., 2011). The space inside the ring is filled with microtubules forming prometaphase spindle. Most kinetochores reside at the boundary of the spindle interacting with microtubules in a lateral fashion (**Figure 6**). This model significantly differs from old search and capture model where kinetochores are captured by microtubules by only end on

attachment. In the next phase, congression, chromosomes move towards the spindle equator driven by plus end directed motor protein Cenp-E (Iemura and Tanaka, 2015).
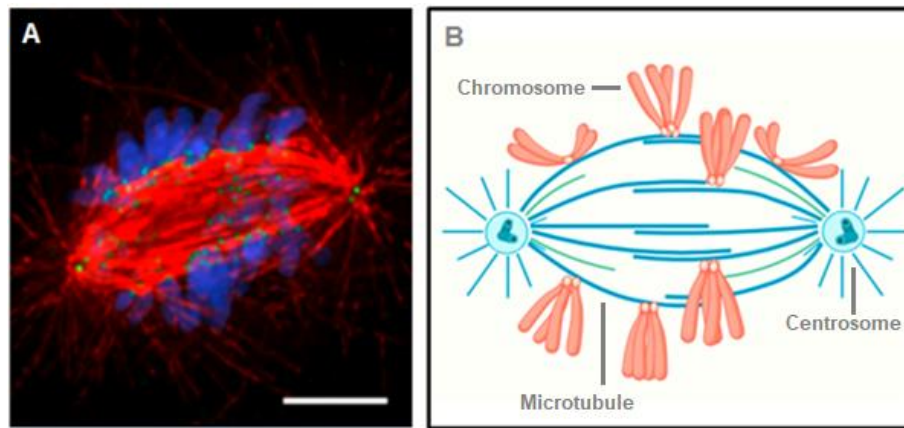
Figure 6. **A.** Immunofluorescence image of fixed RPE1 cell during mid prometaphase. Chromosomes are blue and microtubules are red. Kinetochores and centrosomes are green. Scale bar is 5 µm (acquired from Magidson et al., 2011). **B.** Schematic view of lateral attachments of kinetochores to the microtubules.

The initial translocation of chromosomes towards the spindle pole appears to be contra productive, given that it is in the opposite direction of the desired destination, metaphase plate. Yet this type of behavior is exhibited by many chromosomes during their initial attachment to the spindle, as well as during correction of chromosome attachment errors. As a result, centrosomes become positioned near spindle equator where kinetochores are exposed to the high density of microtubules that promotes formation of the stable amphitelic attachments. This ring provides means for a nonrandom distribution of chromosomes in daughter cells. That distribution of chromosomes is called toroidal and it facilitates the spindle assembly and the establishment of biorientation (Magidson et al., 2011). At the later stages of spindle formation, chromosomes move towards the central part of the spindle so that the toroidal distribution of kinetochores gradually converts into a typical metaphase plate with evenly spaced kinetochores. Therefore, lateral attachment is not just a transient, unstable initial attachment, but an important intermediate for developing bi-orientation.

1.4 Dual pathway of the spindle assembly

Every animal somatic cell spindle assembles by one of the two possible pathways: the classical prophase pathway and the prometaphase pathway. In the prophase pathway centrosomes migrate to the opposite sides of the nucleus ahead of the

nuclear envelope breakdown. When rupture of the nuclear membrane occurs, the bipolarity of the spindle is already set up with the chromosomes located in between the two poles (**Figure 7 A**). In the prometaphase pathway, centrosomes are both on the same side of the nucleus at NEBD and a spindle forms a monopolar structure that subsequently bipolarizes (**Figure 7 B**). Population of the prometaphase pathway cells contains cells with a broad range of intermediate stages of centrosome separation, including those that barely separated their centrosomes, to those which have well separated centrosomes, but still on the same side of the nucleus. These two pathways are not arbitrary points on a continuum of spindle assembly pathways, but are topologically and temporary distinct and genetically separable (Kaseda et al., 2012).

Because of the initial position of the spindle when NEBD occurs, in the prometaphase pathway, chromosomes quickly assemble around the nascent spindle, and cover its surface on the side facing the nucleus forming a special configuration called a prometaphase rosette. In contrast, when centrosomes reside at the opposite sides of nucleus at NEBD, as in the prophase pathway, chromosomes locating between the centrosomes directly move to the equator of the nascent spindle, while chromosomes outside of the spindle assemble to its surface, thus the typical prometaphase rosette is not formed in this instance. These two types of pathways are appearing at similar frequency (45.5% vs. 54.5%, respectively) in HeLa cells (Toso et al., 2009). Pathway of the spindle assembly directly depends on the time needed for separation of centrosomes. In the early prophase, plus end directed motor protein kinesin-5 (Eg5) is loaded on the centrosomes. Eg5 binds antiparallel microtubule bundles that are formed by crosslinking of astral microtubules from opposite spindle poles (**Figure 7 C**). It promotes sliding of antiparallel bundles walking towards the plus end of microtubules consequently separating the centrosomes (Leary et al., 2018). The distance between centrosomes at the time point immediately after NEBD shows no correlation with the onset of NEBD meaning that the mitotic clock controlling NEBD runs entirely independently of Eg5 driven centrosome separation. In other words, the timing of NEBD is uncoupled from the process of centrosome separation. The time interval between the start of Eg5 loading and NEBD is 9.2 ± 2.9 min in HeLa cells (Kaseda et al., 2012). This time frame represents the available interval for a cell to complete centrosome separation before NEBD which depends on the efficacy of Eg5 load. If it succeeds, the cell will form spindle by the prophase pathway. If it fails, spindle will form by the prometaphase pathway. Therefore prophase pathway cells have increased velocity of centrosome separation (Kaseda et al. 2012).
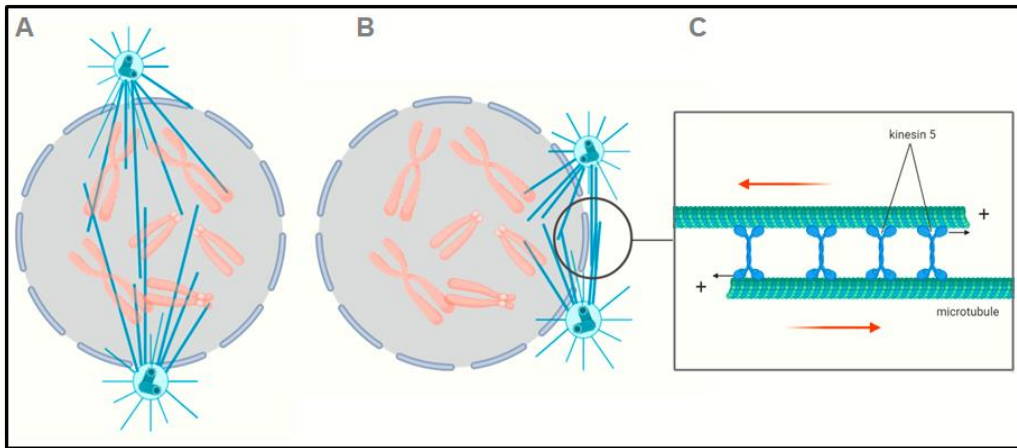
Figure 7. Schematic view of the two pathways of the spindle assembly. **A.** In the prophase pathway centrosomes migrate on the opposite sides of the nucleus before NEBD. **B.** In the prometaphase pathway centrosomes are on the same side of the nucleus at NEBD. **C.** Kinesin-5 drives pole separation due to antiparallel microtubule sliding.

Given that centrosome separation in the prophase is apparently dispensable, why do cells do it? One possibility is that the separation of centrosomes before NEBD makes the subsequent stages of mitosis faster. Other than that, prophase centrosome separation improves the overall fidelity of the chromosome segregation. Now the question is if the prophase pathway increases fidelity of mitosis, why half of the cells use the prometaphase pathway? The answer is simple. For 99 % of the cells to complete centrosome separation before NEBD would require 35 minutes. Clearly, improving the success for prophase centrosome separation is desirable, but to do so, cells would need to spend considerably more time waiting for prophase centrosome separation to complete. There is an evolutionary drive tending to minimize overall time spent in mitosis. So cells face a dilemma; they can either allow more time for the prophase centrosome separation, thereby reducing the mitotic error rate, or they can reduce the time spent in prophase centrosome separation, tolerate a slightly higher error rate, and complete mitosis faster. Cells solve this potential problem by requiring that prophase centrosome separation races against 9.2 minute countdown clock. By using this strategy, the cell population is split approximately 50:50 between the prophase and the prometaphase pathways and cells thereby achieve both a substantial overall improvement in the fidelity of chromosome segregation and an appreciable overall acceleration of mitosis. So the dual pathway is a biological strategy that improves both the speed and fidelity of mitosis, thereby reducing the risk of cancer and other genetic diseases (Kaseda et al., 2012).

1.5 Proteins involved in the prometaphase pathway of the spindle formation

Prometaphase spindle formation is driven by the interaction of kinetochores with microtubules that are growing from the spindle poles. As we have already addressed Eg5, plus directed motor protein from kinesin 5 family, responsible for pole separation before and after NEBD by antiparallel sliding of overlapping antiparallel microtubule bundles (Leary et al., 2018). For the faithful chromosome segregation in mitosis, kinetochores on all sister chromatid pairs have to establish bipolar attachment, or bi-orientation by attaching of sister kinetochores to microtubules emanating from the opposite spindle poles, and this is called end-on attachment (Toso et al., 2009). In contrast, kinetochores can also attach to the sides of microtubules, referred to as lateral attachment. They are efficiently captured by the lateral surface of the microtubules and transported towards the spindle. The majority of transient kinetochore components maximally localize to the kinetochores when the lateral attachments are formed, and such localization is mainly depended of aurora B kinase activity, including microtubule-interacting proteins (CLIP-170 and Cenp-E) as well as dynein related proteins (spindly, NDE1 and DIC), RZZ complex components (Zw10) responsible for dynein attachment to the kinetochores, and SAC components (BubR1) (Itoh et al., 2018). Two opposing motor proteins, minus end directed cytoplasmatic dynein and plus end directed Cenp-E motor from kinesin 7 family, are working at the interface between kinetochores and microtubules during lateral attachment. Kinetochore microtubule attachment is lost in the cells depleted of Hec1, Zw10 and Cenp-E in the early prometaphase, strongly suggesting that dynein and Cenp-E are involved in the lateral attachment itself, as well as in motility during lateral attachment (Itoh et al., 2018). The main functions of Cenp-E and dynein are temporary separated, making dynein more important immediately after NEBD in the formation of lateral attachments and positioning the chromosomes on the spindle on microtubules and driving chromosomes in the minus end direction to the poles, forming the prometaphase rosette (**Figure 8 A, B**). On the other hand, the main role of Cenp-E is driving congression of the chromosomes from poles to the methaphase plate where biorientation is established (Yu et al., 2019) (**Figure 8 C, D, E**). Their simultaneous existence on the spindle arises from the fact that dynein binds more effectively on tyrosinated microtubules which are commonly seen in unstable single microtubules, whereas Cenp-E works more efficiently on detyrosinated microtubules, which are enriched in stable, bundled microtubules that are formed later in the prometaphase. Such properties can explain the sequential chromosome motion along microtubule, first towards the spindle poles by dynein and then towards the spindle equator by Cenp-E.
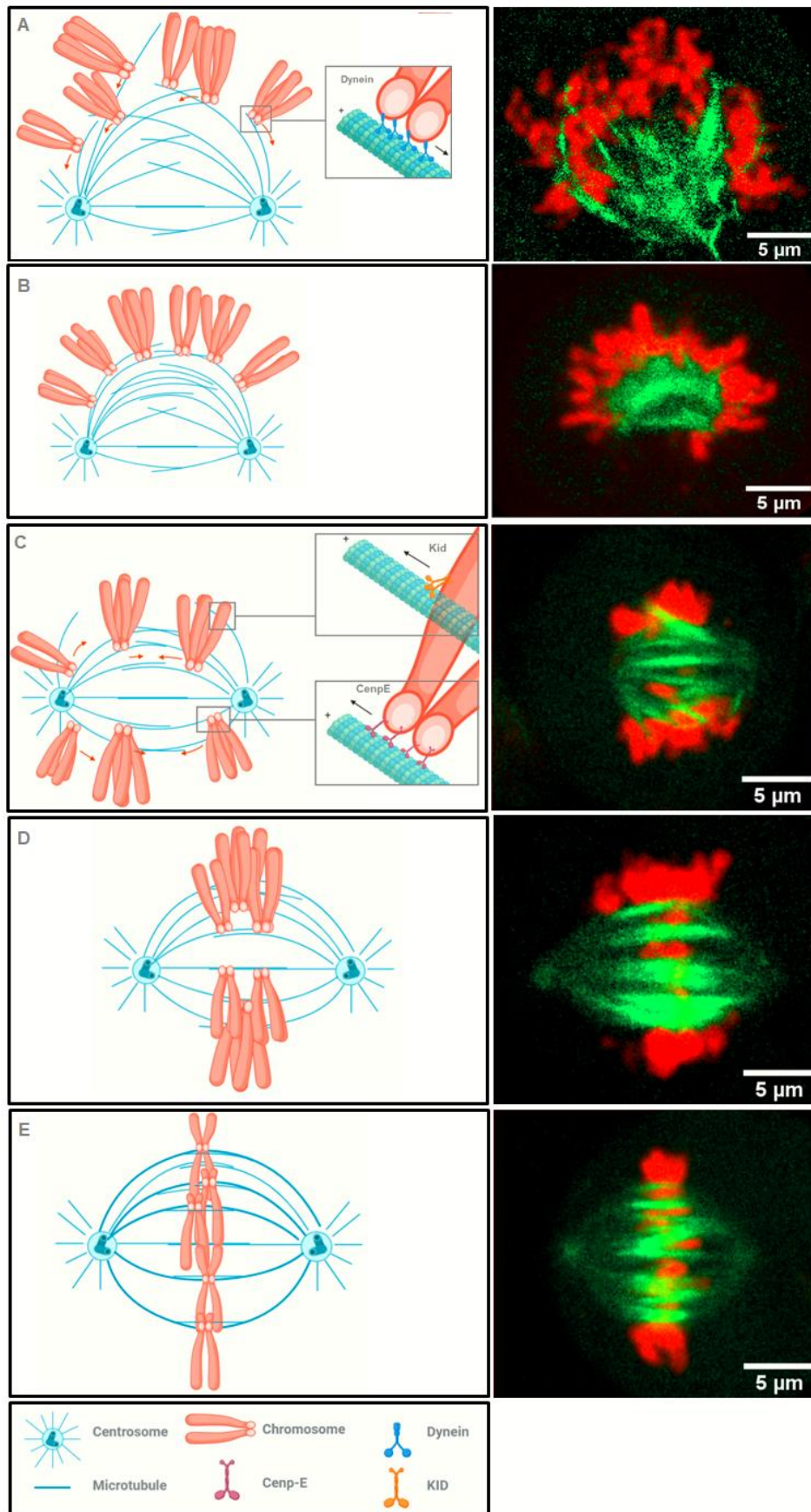
Figure 8. Kinetochore attachments to the microtubules and chromosome motion in the process of bi-orientation establishment through the prometaphase pathway. Schematic diagrams on the left are representations of live cell images shown on the right. **A.** Schematic

diagram shows the situation immediately after NEBD, showing growth of the microtubules towards the chromosomes, lateral attachment of chromosomes to the microtubules and poleward motion mediated by dynein motor protein. **B**. Typical prometaphase rosette configuration with chromosomes on the one side of the spindle. **C.** Congression of chromosomes driven by Cenp-E and KID motor. **D.** Before bi-orientation is established, laterally attached kinetochores align at the circumference of the spindle equator, referred to as the equatorial ring. **E.** Establishment of bi-orientation by conversion of lateral attachment to end-on attachment of kinetochores to the microtubules. Live cell images (right) represents HeLa PRC1 – GFP cell line in phases shown in schematic diagrams (left). PRC1 protein is colored green while chromosomes are colored red using SiR – DNA dye.

However, in the absence of dynein, CENP-E dependent kinetochore tethering to depolymerizing microtubule ends allows slow formation of the prometaphase rosette-like structures. Dynein also contributes to the efficient kinetochore accumulation on the spindle surface by counteracting the antipolar movement of chromosome arms called polar ejection force produced by another important player in the prometaphase spindle formation, chromokinesin Kid, motor protein from kinesin-10 family. In the early prometaphase, when there is no stable microtubules and microtubule bundles, chromosome congression is achieved by two mechanisms – by Kid which drives chromosome arms on microtubules towards their plus end, and through end-on attachment by establishing bi-orientation (Iemora and Tanaka, 2015). It was proposed that NuMa-dependent traction fiber based mechanism that pulls end on attached chromosomes to the spindle equator works in parallel with Kid mediated polar ejection force, but its contribution is minor (Haren et al., 2009). Contra intuitively, in the early prometaphase Cenp-E plays an inhibitory role in the chromosome congression. The reason for that is that Cenp-E cannot efficiently walk along unstable, less bundled microtubules in the absence of stabilized kinetochore fibers, rather it works as a microtubule tip-tracker on short or depolymerizing microtubules. So in the early prometaphase when the proportion of stabilized microtubules is small, Kid predominately drives chromosomes to the spindle equator while Cenp-E enables kinetochores to track spindle microtubules and suppresses chromosome congression by causing kinetochores to track short unstable microtubules and function like some kind of a break (**Figure 9 A**). In the late prometaphase, when the stabilized microtubules number is increased, Cenp-E shows high processivity and plays a predominant role in the congression of laterally attached chromosomes (**Figure 9 B**). The role of Kid may also be affected by the reduction of microtubules radiating outside the spindle in the late prometaphase. Aurora B kinase also plays a major function in the early prometaphase in

attaching the kinetochores on nascent spindle by regulating all the transient kinetochore components (Murata-Hori and Wang, 2002).
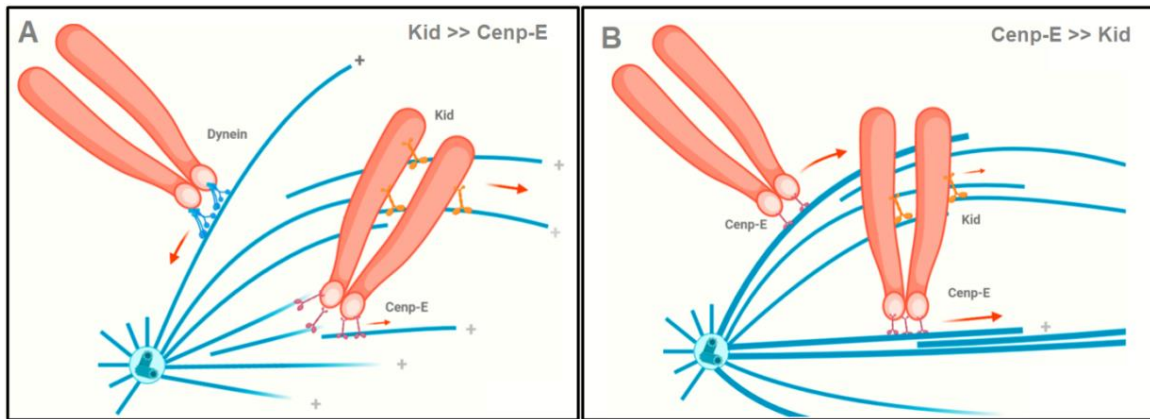
Figure 9. **A.** In the early prometaphase Kid predominantly drives laterally attached chromosomes towards the spindle equator, whereas Cenp-E suppresses chromosome congression by causing kinetochores to track short unstable microtubules while at the same time dynein drives kinetochores to the pole. **B.** Later in the prometaphase when stabile microtubules are abundant, they serve as tracks for Cenp-E, which is now predominant motor protein that drives congression.

1.6 Prometaphase rosette can be divided in few chronologically addressed configurations

The process of chromosome alignment is categorized into five distinct phases: NEBD, prometaphase rosette, congression, equatorial ring and biorientation. The equatorial ring was defined previously as the chromosome ring formed at the spindle equator in which chromosomes are laterally attached to microtubules (**Figure 8 D**). The phase between the prometaphase rosette and the equatorial ring is categorized as the congression phase in which chromosomes move along the spindle surface towards the spindle equator (**Figure 8 C**). When lateral attachment in the equatorial ring is converted to end-on attachment, during which bi-orientation is established, the chromosome ring is transformed into the metaphase plate, filling the space inside the ring with chromosomes (**Figure 8 E**) (Itoh et al., 2018).

1.7 Significance of the prometaphase rosette configuration

The prometaphase rosette is observed in nearly half of the mitotic events in HeLa cells. At first it was only seen in cells cultured on plates, on which cells are flattened. Flatness could potentially be causing chromosome scattering outside the spindle (Lanchester et al., 2013). However, prometaphase rosettes are also seen in the subcutaneous tumors derived from HeLa cells transplanted into SCID (severe combined immunodeficiency) mice. More importantly, they are confirmed in the tissue samples of human gastric cancer cells (Itoh et al., 2018). There are few theories why formation of lateral attachments and prometaphase rosette can be evolutionary important mechanism for the spindle assembly. When spindle poles are close to each other, a single kinetochore can be captured by microtubules from both spindle poles, leading to the formation of merotelic attachments and increased rates of chromosome missegregation (Silkworth et al., 2012). In this respect, it would be advantageous to form lateral rather that end-on attachments, to avoid merotelic attachments in the prometaphase rosette when spindle poles are at the one side of a chromosome mass. In contrast to the mechanism for end-on attachment that is essential, defects in lateral attachment are likely to be tolerable, but still affect fidelity of chromosome segregation, which makes it more observable in living cells, especially cancer cells.

1.8 Microtubule bundle formation

The variety of microtubule structures made by different cell types require a diverse group of proteins to assemble, stabilize and dynamically control these microtubules arrays. It is now clear that different cytoskeletal architectures arise from the interplay between motor proteins which can crosslink and move microtubules relative to one another, and non-motor microtubule associated proteins (MAPs), which can crosslink microtubules to stabilize the specific orientations of microtubules. MAPs include both motor and non-motor proteins. Several we have already addressed. Non-motor MAPs that crosslink microtubules (NuMa, NuSAP, Mia1p and PRC1) are known to play important roles in dividing and non-dividing cells, arranging microtubules in antiparallel or parallel bundles. The polarity of microtubules within a bundle is crucial to the action of motor proteins (Eg5, Dynein, Kif10, kinesin-4) that slide filaments past each other and drive the movement of chromosomes (Walczak and Shaw, 2010). Parallel bundles are formed by the microtubules emanating from the same spindle pole, while antiparallel bundles are formed by microtubules emanating from the opposite spindle poles. Parallel bundles are mainly in form of kinetochore fibers (K-fiber) connected to the

kinetochore. Non-kinetochore microtubules can be found as single microtubules, in the parallel bundles or in the antiparallel bundles. When divided with respect to their location, non-kinetochore microtubules include those that grow from the spindle pole towards the cell cortex, known as astral microtubules, those that grow toward the spindle equator and have free ends, which are often called polar, and those that form antiparallel bundles in the central part of the spindle, known as inter-polar or overlap microtubules forming interpolar bundles (Bratman and Chang, 2008). The process of the formation of microtubule bundles in human cells is not well understood. Presumably, interpolar bundles form during early mitosis through interaction of microtubules growing from the opposite spindle pole. Those overlaps are important for structural integrity of the spindle during its formation in the prometaphase as in dynamics of chromosome segregation in anaphase (Vukušić, Buđa and Tolić, 2019). Major class of proteins which crosslink microtubules into microtubule arrays is the PRC1 family, stressing their role in the organization of central spindle during cytokinesis. PRC1 protein bounds preferentially to the microtubules that overlap in antiparallel regions (**Figure 10 A**). PRC1 is not a molecular motor, but instead works in concern with motor proteins to organize arrays of microtubules. Thus, PRC1 can be used to visualize the overlap zones of interpolar microtubules through the spindle (Subramanian et al., 2010). PRC1 has three prominent domains: the N-terminal domain, which contains the major site for binding to the microtubules; the central domain; and the intrinsically disordered C-terminal domain with a large number of positively charged residues, which is a common feature of the regions that interact with microtubules (**Figure 10 A**). By binding on the crosslinked microtubules, PRC1 molecules take on more structured configuration than those bound to the single microtubules (Subramanian et al., 2010). This suggests that crosslinking itself converts PRC1 from a flexible molecule to a rigid one, which may enhance PRC1 crosslinking activity. PRC1 interacts with one αβ-tubulin heterodimer and extends as a single rod shape almost perpendicular to the microtubule lattice. PRC1 directly interacts with Kif4 kinesin motor protein whose motility plays an active role in bundle architecture controlling the length of the antiparallel bundles (**Figure 10 C**) (Bieling et al., 2010). Another important protein that interacts with PRC1 is kinesin-5. As we already addressed, kinesin-5 proteins are responsible for establishing bipolarity of spindles during the early stages of mitosis by actively sliding apart microtubules of opposite polarity and for progression of anaphase B (Leary et al., 2018). PRC1 does not significantly resist microtubule sliding by kinesin 5, indicating that moderate binding affinities and diffusive microtubule interactions of PRC1 can permit microtubule movement while maintaining the attachment (**Figure 10 B**). However, new results suggest that PRC1 ensembles act like a mechanical dashpot, producing a significant resistance against

the fast motions, but minimal resistance against the slow motions, allowing for the integration of diverse motor activities into a single mechanical outcome (Gaska et al., 2019).
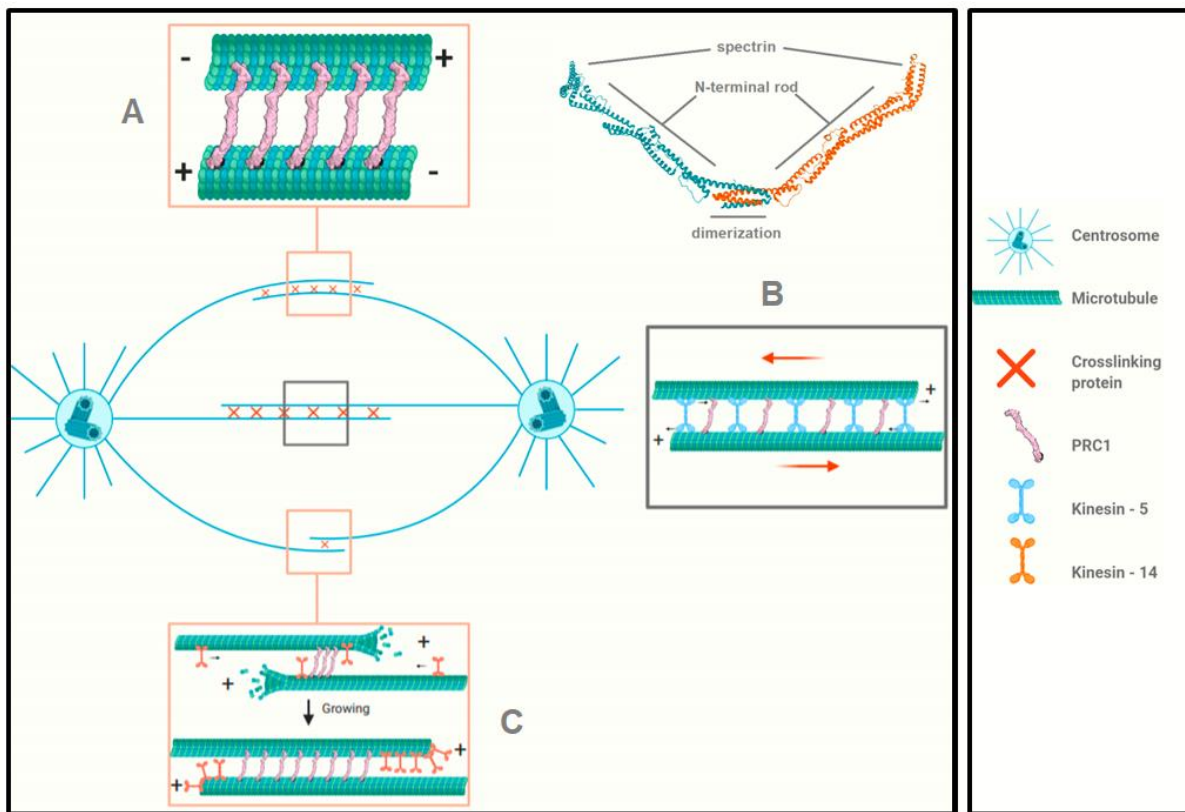
Figure 10. A. Protein regulator of cytokinesis 1 crosslinks microtubules that interact in an antiparallel fashion (left). PRC1 is composed of 3 domains; spectrin domain for binding the microtubules, N-terminal rod domain and dimerization domain (right) which forms a homodimer. **B.** When kinesin 5 is added to the crosslinked microtubules, PRC1 maintains the crosslinks despite the sliding action. **C.** The interaction of kinesin 4 with PRC1 increases the dwell time of kinesin 4 on microtubules, which in turn limits the length of the overlap region by blocking microtubule growth at the plus ends.

On the other hand, formation of K-fibers, parallel bundles connected to the kinetochores, requires another set of proteins. The number of microtubules in a kinetochore fiber increases as mitosis progresses and the fiber matures. In HeLa cells, a metaphase kinetochore fiber consists of on average 17 microtubules. A mature K-fiber consists of about 20 parallel microtubules (McEwen et al., 1997). This thick fiber is formed most likely by stepwise addition of new microtubules to the immature fiber. One candidate for its formation is kinesin-14 which is recruited on the plus end of microtubules and guides its growth along another microtubule (Molodtsov et al., 2016). The microtubules in a kinetochore fiber are linked by clatrin in a complex with transforming acidic coiled-coil protein 3 (TACC3), and hepatic tumor overexpressed gene (ch-TOG) (Royle et al., 2005). The exact mechanism of K-

fiber formation is yet unknown, but there are a few theories. One mechanism includes old search and capture model with some modifications. Kinetochore microtubules from the spindle pole do not grow straight-forward, rather they rotate about pivot at the spindle pole body (Kalinina et al., 2013). This angular motion may be important because this motion helps the microtubules as they search for the targets such as kinetochores, cortical anchors, or other microtubules exploring the space performing rotational diffusion and ultimately approaching one another which in turns allows crosslinking proteins to connect microtubules in the stable bundles (Pavin and Tolić, 2014, Prelogović et al., 2019). Also, microtubules can be formed at the locations other than the spindle pole – growing nucleated from the preexisting microtubules by augmin complex. The last, simplest mechanism is growing along preexisting microtubule, guided growth (Simunić and Tolić, 2016). Microtubule is nucleated either in the pole or in the preexisting microtubule by augmin complex (**Figure 11**).

1.9 Complex interactions between the antiparallel and parallel microtubules.

Today we know that antiparallel interpolar bundles and parallel kinetochore bundles are functionally and physically connected, and are in close contact in various types of cells in the metaphase spindle. The minus ends of interpolar microtubules are not clustered in poles like K-microtubules, but they are found in the bundles of kinetochore microtubules. It is known that discrete bundles of PRC1 labeled antiparallel microtubules connect a pair of kinetochore fibers bound to the sister kinetochores interacting through parallel overlaps in the region close to the spindle poles (Kajtez et al., 2016). However, the nature of this interaction is unknown. This interpolar bundle looks like a bridge between sister kinetochore fibers, hence it is called bridging fiber. Bridging fiber is strongly linked to the kinetochore fibers. They form a single mechanical unit, whose role is to balance the tension between sister kinetochores and compression at the spindle pole. The bridging fiber consists of 10-15 microtubules arranged in an antiparallel manner, based on observation that they bind PRC1. The number of PRC1 decorated bundles per spindle roughly matches the number of kinetochore pairs, indicating nearly 1:1 relationship between interpolar bundles and chromosomes (Polak et al., 2017). The existence of that bridge and their links is important in force balance in the spindle and chromosome movement because the forces generated by non-kinetochore microtubules, in particular by interpolar bundles, are transmitted to the kinetochore fibers and hence to the kinetochores through these connections (Tolić, 2017).

1.10 The origin and assembly of parallel and antiparallel bundles into a mechanical unit

The assembly of the microtubule bundles and mechanisms under their physical coupling are still unknown. There are few scenarios that are still just speculations. Which assembled first, bridge fiber or kinetochore fiber, and how they assemble in one mechanical unit? In support to the bridge first scenario is that most kinetochores at the prometaphase make lateral attachments in the prometaphase rosette which was mentioned earlier (Itoh et al., 2018). Then they congress into the metaphase plate on the interpolar bundles, which are stabilized by bound PRC1 and tyrosinated, without stabile bi-orientation and end-on attachment. In the bridge first scenario, the kinetochore only has one K-fiber and it is not bi-oriented, while the second K-fiber is assembled when kinetochore reaches the equator (**Figure 11**). In support to the K-fiber first scenario, it has been shown that chromosomes near the equatorial plate can be bi-oriented without Cenp-E activity but that happens rarely (McEwen et al., 2001). Also, chromosomes on the one spindle pole would have very small probability to be connected on the opposite spindle pole by k-microtubule (Wollman et al., 2005). An interesting hypothesis is that interpolar bundle that the chromosome uses for congression can interact with the K-fiber and create a bridging fiber. Also, bridging bundles can serve as tracks that guide nucleating kinetochores microtubules as they grow (Putkey et al., 2002). Then, the K fiber can mature by those three mechanisms that we already addressed, by growth from the pole, or nucleation from the existing microtubule by augmin complex, or by pivoting microtubule crosslinking. Another possibility is that kinetochore microtubules nucleate from the kinetochore itself. The kinetochore captures short microtubules that are nucleated within the vicinity of chromosome by Ran gradient (Maiato et al., 2004). Once captured, the plus end of the microtubule polymerizes at the kinetochore, where the minus end pushes towards the pole and is integrated into the spindle pole by dynein motor (O'Connell and Khodjakov, 2007). Once the first kinetochore microtubules have been stabilized at the kinetochore, subsequent ones could also be recruited from the microtubules that nucleate from the augmin complexes that are positioned on the preexisting microtubules. Sometimes, microtubule bundles already present in the cell cytoplasm can be transported with their minus end to the centrosome by dynein or HSET motor and help the spindle assembly, which is often seen in acentrosomal spindles, but can contribute to the assembly of centrosomal spindles, as well (Mahoney et al., 2006). Also, regardless of the nucleation mechanism that is used, the bridging fiber can be nucleated away from the K-fiber, or even well before or later, as a part of the interpolar antiparallel bundles. Then, it could be attached by crosslinking proteins on the K-fiber after

they are already fully formed, forming a unique mechanical module observed in the metaphase spindle (Simunić and Tolić, 2018).
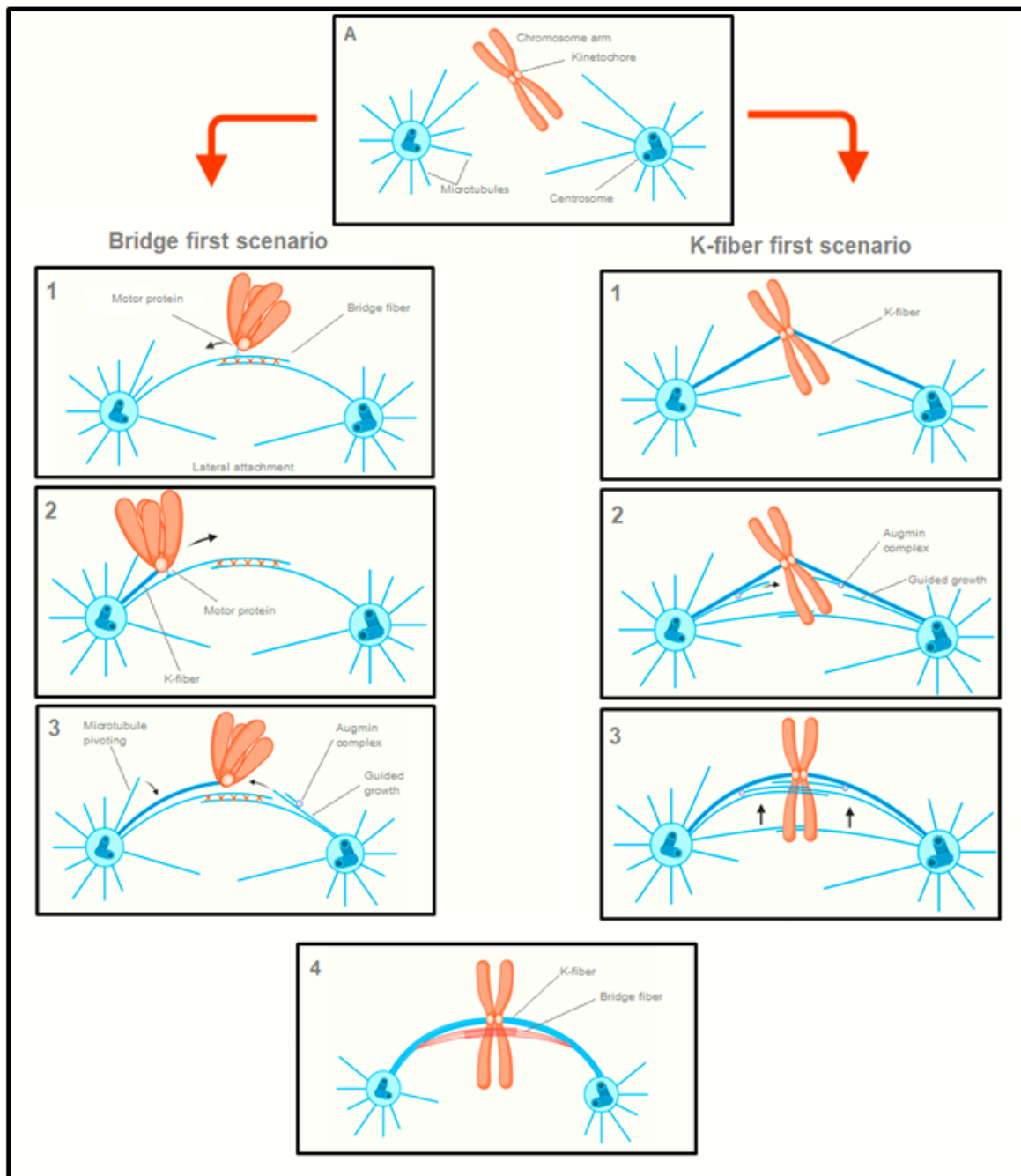
Figure 11. Two theoretical scenarios of the bundle formation. In the bridge first scenario antiparallel overlaps form first and are used as rails for poleward movement of chromosomes in the early prometaphase (1) and chromosome congression (2) later. First kinetochore fiber forms when chromosome approaches the spindle pole (3). Second K-fiber catches chromosome when it comes to the metaphase plate (4). In K-fiber first scenario chromosome is first captured by K-fibers (1) and then overlaps form (2). There are few mechanisms of the overlap formation; crosslinking from the opposite poles, association with k-fiber or nucleation from existing k-fiber by the augmin complex and crosslinking by the augmin complex (3).

2. REASERCH AIM

The goal of this research is to reveal the mechanisms underlying antiparallel bundle formation and formation of the whole spindle. I started with the fact that number of overlapping microtubules in cell is proportional to the number of kinetochores (Polak et al., 2017). I decided to use HeLa cell line stably expressing PRC1 protein labeled with GFP, marker of antiparallel microtubule bundles as the main experimental system for antiparallel bundle formation investigation. The question was whether the spindle starts to form with a fixed number of bundles or the number of bundles increases in time. Also the aim of this study is to determine mechanisms underlying the antiparallel bundle formation. Three possible models of the formation are proposed; formation of one big bundle or mass of microtubules that splits into several bundles (**Figure 12 A**), spontaneous formation of the microtubule bundles by crosslinking in random places in the spindle (**Figure 12 B**), or formation from the mesh of microtubules that subsequently form bundles (**Figure 12 C**). Also, I was interested in finding out which proteins are involved in their formation. To answer those questions, live cell imaging and immunostaining techniques in combination with silencing of candidate proteins and their inhibition using specific inhibitors was used.
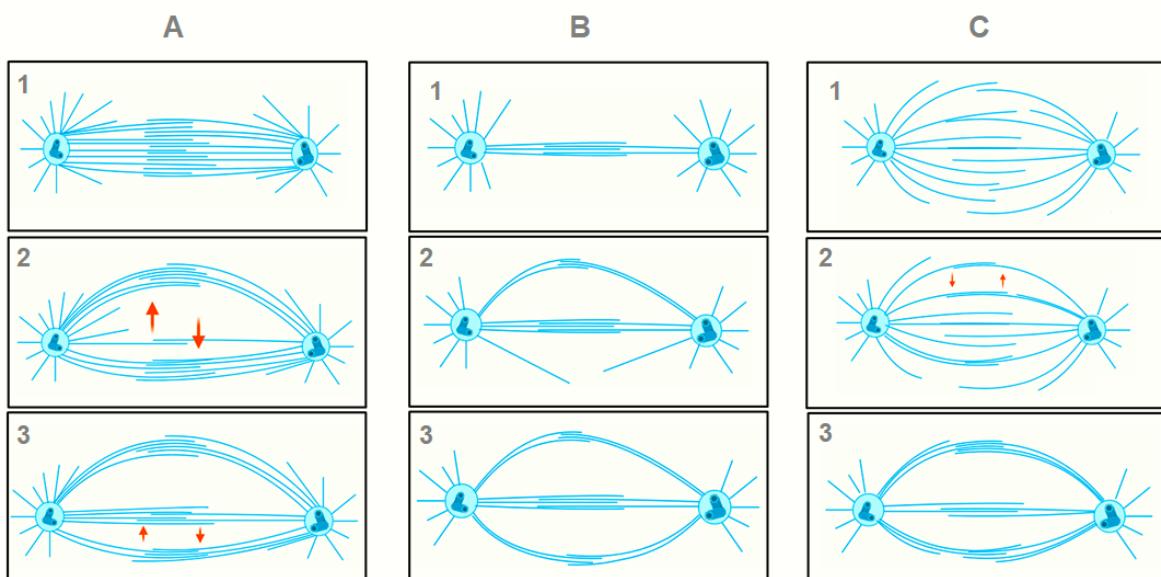
Figure 12. Models for the antiparallel bundle formation mechanism. **A.** One or a few large bundles split in smaller bundles. **B.** Bundle formation is localized in defined places during the spindle formation. **C.** Formation of the bundles from a large mesh of disorganized microtubules by fusion of microtubules.

3. METHODS

3.1 Cell lines

In all experiments human tumor and non-tumor cell lines were used. HeLa-Kyoto BAC lines stably expressing PRC1-GFP are courtesy of Ina Poser and Tony Hyman (Max Planck Institute of Molecular Cell Biology and Genetics, Dresden, Germany). Non-tumor immortalized retinal pigment epithelium 1 (RPE1) cells expressing CENP-A-GFP and Centrin1-GFP and human bone Osteosarcoma epithelial cells (U2OS) stably expressing tubulin-RFP and CenpA-GFP were also used in this experiments.

Cells were grown in Dulbecco's modified Eagle's medium (DMEM) (Lonza, Basel, Switzerland) supplemented with 10% fetal bovine serum (FBS; Life Technologies, Carlsbad, CA, USA), penicillin, streptomycin, and geneticin (Santa Cruz Biotechnology Inc., Dallas, TX, USA). The cells were kept at 37 °C and 5% CO_2 in a humidified incubator (Galaxy 170S CO_2, Eppendorf, Hamburg, Germany).

When cells reached 90% confluence, DMEM medium was removed from the flask and the cells were washed with 5 mL of 1% PBS (phosphate-buffered saline), and 1 mL of 1% Trypsin/EDTA (Biochrom AG, Berlin, Germany) was added to the cells. After 5 min incubation at 37°C and 5% CO_2 in a humidified incubator, trypsin was blocked by adding 2 mL of DMEM medium. Cells were seeded and cultured 1 day prior to microscopy in 2 ml DMEM medium with same supplements (as above) at 37 °C and 5% CO2 on 35 mm glass coverslip uncoated dishes with 0.17mm (#1.5 coverglass) glass thickness (MatTek Corporation, Ashland, MA, USA)

3.2 Confocal microscopy

Cells were imaged using Bruker Opterra Multipoint Scanning Confocal Microscope (Bruker Nano Surfaces, Middleton, WI, USA). The system was mounted on a Nikon Ti-E inverted microscope equipped with a Nikon CFI Plan Apo VC 100x/1.4 numerical aperture oil objective (Nikon, Tokyo, Japan). The system was controlled with the Prairie View Imaging Software (Bruker). During imaging, cells were maintained at 37°C in Okolab Cage Incubator (Okolab, Pozzuoli, NA, Italy). For optimal resolution and signal to noise ratio, 22 nm slit was used. For excitation of GFP 488 nm diode laser line was used, while for mCherry

fluorescence a 561 nm diode laser line were used. The excitation light was separated from the emitted fluorescence by using Opterra Dichroic and Barrier Filter Set 405/488/561/640. Images were captured with an Evolve 512 Delta EMCCD Camera (Photometrics, Tucson, AZ, USA) using 150-200 ms exposure times.

Imaging protocols:

For studies of increasing number of bundles Z-stacks were acquired compromising 41 focal planes with 0.5 µm spacing to cover the whole spindle. The horizontal prometaphase spindles of HeLa PRC1-GFP with added SiR-DNA dye and RPE1 CENP-A, Centrin1-mCherry with added SiR-tubulin dye were filmed every 10 and 5 minutes, respectively. Prometaphase cells were recognized by non-congressed chromosomes and relatively small spindle size. Zero time was set as the first time metaphase plate was seen.

For filming the dynamics of the spindle formation only vertically oriented spindles of HeLa PRC1-GFP cells with added SiR-DNA dye were selected and fastest acquisition mode was used. Imaging sequence was next: first the 41 plane Z-stack with 0.5 µm spacing was acquired to cover the whole spindle using both 488 nm and 633 nm excitation light. Then the T-series of images was required using only 488 nm excitation light. Every repetition recorded 9 middle frames of the vertical spindle, forming a stack of 9 slices separated by 0.5µm. Time between repetitions was 2.7 seconds. After T-series, the second Z-stack was acquired, again using both excitation lasers. Total time lapse of the movie was 4 minutes and 30 seconds. That time was estimated to be the longest time the cell can endure without photo-damage and bleaching. The cells filmed that way successfully formed metaphase plate and some of them entered anaphase.

To gain an insight into the behavior of chromosomes during this time frame, some cells were filmed with both 488 nm and 633 nm excitation light during T-series in the same way as described above.

Other experiments are imaged on Andor Dragonfly multi-point confocal microscope (Andor, Oxford instruments, UK) for high-speed and high-sensitivity imaging. The system was mounted on Nikon Ti2 inverted microscope (single deck) equipped with CFI P-Apo 60x Lambda / NA 1.40/ WD 0.13 mm – oil (MRD01605) objective (Nikon, Tokyo, Japan). Following emission filters were used: 521/38, 594/43, 620/60 and 478/37. Images were captured with 1x Andor iXon EMCCD camera (Andor, Oxford instruments, UK) using 100 ms exposure time. No binning was performed. The xy-pixel size in the image was 100 nm.

The system was controlled with the Imaris Imaging Software (Imaris, Oxford instruments, UK).

Imaging protocols:

To explore the mechanism of the antiparallel bundle formation in HeLa PRC1-GFP cell lines similar protocol as above was designed. Only cells with vertically oriented spindles were imaged following the next imaging sequence: first the 41 plane Z-stack was acquired to cover the whole spindle using both 478 nm and 620 nm excitation light. Then the T-series of images was required using only 478 nm excitation light. Every repetition recorded 9 middle frames of the vertical spindle, forming a stack of 9 slices separated 0.5 µm. Time between repetitions was 5.4 seconds. After T-series, the second Z-stack was acquired, again using both excitation lasers. Total time lapse movie was 8 minutes and 35 seconds long.

The same protocol was used for experiments with the wild type cells, cells in which a specific protein was silenced using siRNA interference (Haus6 protein, see below in siRNA silencing), and cells with chronic inhibition of certain proteins with specific inhibitors (chronic Aurora B and Cenp-E inhibition, see bellow in drug treatments).

For other experiments and treatments (metaphase spindles of Haus6 siRNA, Ndc80 siRNA, Spindly siRNA, GSK and Barasertib treated cells and cells with induced mitosis with un-replicated genomes, see below in drug treatments and siRNA silencing) only Z-stack images were acquired compromising of 41 planes separated by 0.5 µm to cover the whole spindle. HeLa PRC1 cells were imaged using 478 nm and 620 nm excitation light to visualize GFP labeled PRC1 and chromosomes, respectively. RPE1 CenpA-GFP, Centrin-GFP cells were imaged using 478 nm and 620 nm excitation light to visualize GFP labeled Cenp-A and Centrin and tubulin stained with SiR-Tubulin dye, respectively. U2OS cells were filmed using 478 nm, 620 nm and 521 nm excitation light to visualize GFP labeled Cenp-A, SiR-DNA labeled chromosomes and RFP labeled tubulin protein, respectively.

Due to a specific phenotype, spindle formation in Haus6 siRNA treated HeLa PRC-GFP and RPE1 CenpA-GFP, Centrin-GFP cells were filmed using different customized protocol. HeLa PRC1- GFP cells were filmed using T-series protocol. Only GFP channel (478 nm excitation) light was acquired. Number of repetitions was 100. Every repetition recorded 15 middle frames of the cell forming stack of 15 slices separated by 1 µm. Time between repetitions was 10 seconds. The same protocol was used for RPE1 CenpA-GFP, Centrin1-GFP cell with some adaptations: both 478 nm channel and 620 nm channels were used. Here the number of

repetitions was 50 and time between repetitions was 20 seconds. For both experiments total time lapse was 16.6 minutes long.

3.3 Visualization dyes

To visualize chromosomes and determine the phase of the prometaphase, in experiments with live cell imaging, rhodamine SiR-DNA (Spirochrome AG, Stein am Rhein, Switzerland) was added to the dish containing the cells. The amount of 0.1 µL of SiR-DNA per 1 mL of medium was added in the dish with HeLa PRC1-GFP and U2OS tubulin-RFP, Cenp-A-GFP cells 15 minutes before imaging for chromosome visualization. For visualization of tubulin in RPE1 Cenp-A-GFP, Centrin-GFP, the amount 0.1 µL of SiR – Tubulin dye (Spirochrome AG, Stein am Rhein, Switzerland) per 1 µL od DMEM was added in a cell dish 8 hours before imaging.

3.4 Drug treatments

The stock solution of S-trytil-L-cysteine (STLC), Barasertib (AZD1152) and GSK-923295 inhibitors were prepared in dimethyl sulfoxide (DMSO) to a final concentration of 1 mM. All drugs and solvents were obtained from Sigma-Aldrich. The working solution was prepared in DMEM at appropriate concentration. At the time of treatment, the working solution was added to cells at 1:1 volume (volume of drug solution: volume of cell medium) ratio to obtain a final concentration.

If a specific inhibitor was added just before imaging started (when a target cell was already found under the microscope), I called that acute inhibition of the target protein. If the inhibitor was added at least 30 minutes before the imaging started, I called that chronic inhibition. For acute inhibition "one dish, one experiment" approach was used.

STLC was used in the final concentration of 20 µM for Eg5 inhibition in the cells with vertically oriented prometaphase spindle (Wu et al., 2018). STLC was added acutely, just after the cell of interest was found. For acute inhibition of Eg5, STCL working solution was added in the cell culture dish immediately after one Z-stack was acquired. Then T-series were acquired (described above in imaging protocols) after which last Z-stack was acquired.

Cenp-E protein was inhibited by GSK inhibitor acutely in order to determine its effect on the bundle dynamics in vertically positioned prometaphase spindles. and chronically 2 hours before imaging for size parameters analysis of horizontally positioned metaphase spindles. Both HeLa PRC1-GFP and RPE1 CenpA-GFP, Centrin1-GFP cell lines were treated. Final concentration of GSK inhibitor was 200 nM for live cell imaging. Appearance of un-congressed chromosomes in the neighborhood of the imaged spindle confirmed the effect of GSK inhibitor (Bennett et al., 2015).

Aurora B kinase was inhibited using Barasertib (AZD1152) acutely and chronically in order to determine its effect on the bundle formation on vertically positioned prometaphase spindles and chronically 2 hours before imaging on horizontally positioned metaphase spindles. Final concentration for Barasertib inhibitor was 300 nM for live cell imaging. Only HeLa PRC1-GFP cell lines were treated (Helfrich et al., 2016).

For mock-treated experiments, cells were treated with the same concentration of DMSO that was used for preparation of the inhibitors.

3.5 siRNA silencing

Haus6 siRNA (L-018372-01-0005, Dharmacon, Lafayette, CO, SAD), CDCC9 siRNA (Spindly siRNA), Ndc80 siRNA and control siRNA *Non-Targeting Pool* (D-001910-10-05, Dharmacon, Lafayette, CO, SAD) were prepared according to the manufacturer's instructions. Lyophilized siRNA (n = 10.0 nm) was dissolved in 100 µL of 1 x siRNA Buffer (prepared by dilution of 5 x siRNA Buffer, (B-002000-UB-100, Dharmacon) in RNAase free water, (B-003000-WB-100, Dharmacon). Final concentration of stock solution was 100 µM stored at 20°C. After 24 hours stock solution was ready for transfection by Lipofectamine RNAiMAX Reagent Protocol 2013. Two solutions were prepared for every sample. First solution was prepared by adding 9 µL of lipofectamine Lipofectamine RNAiMAX Reagent in 150 µL Opti-MeM Medium. Second solution was prepared by adding 1 µL siRNA (c = 100 µM) in 150 µM Opti-Mem Medium. These two solutions were mixed and incubated at 37°C, 5 min. Then 360 µL of this solution was added in a dish with previously plated cells in 740 µL DMEM medium. Cells were incubated at 37°C and 5% CO_2 for 4 hours. The medium with lipofectamine was washed and replaced with 1 mL of DMEM. Cells were again incubated at 37°C and 5% CO_2. Cells transfected with Ndc80, Spindly and Haus6 siRNA were imaged 24, 48 and 72 hours after transfection, respectively. HeLa PRC1-GFP cells were transfected with

all three siRNA, while RPE1 CenpA-GFP, Centrin-GFP cells were transfected with Haus6 and Ndc80 siRNA. To check whether siRNA silencing of Spindly, Ndc80, and Haus6 protein was successful, immunocytochemistry staining to those proteins was performed. However, for Ndc80 silencing, full dish of cells locked in equatorial ring configuration was appropriate conformation that Ndc80 is silenced indeed (McCleland et al., 2003).

3.6 Immunocytochemistry

To determine the efficiency of siRNA silencing of Haus6, Ndc80 and Spindly protein, immunocytochemical staining is performed. Immunocytochemistry staining enables visualization of protein of interest in fixated cells. Efficiency of siRNA silencing was performed on HeLa PRC1-GFP cell line. The cells were fixed 72 hours after transfection with Haus6 siRNA, 42 hours after transfection with Spindly siRNA and 24 hours after transfection with Ndc80 siRNA. The same procedure was implemented on the cells treated with control siRNA. The medium was removed from the dish and 1 ml of 4% formaldehyde (Biognost, Zagreb, Croatia) was added. Cells were incubated in 4 % formaldehyde for 5 minutes on a shaker. Then the cells were washed 2 times for 5 minutes with 1 ml of PBS. After that cells were incubated in 1 mL of 0.5% Triton X-100 for 15 minutes in the purpose of membrane permeabilization. Again, cells were washed 2 times for 5 minutes in 1 ml PBS. To avoid nonspecific binding of antibody cells were incubated in 1 ml of 3% BSA-PBS (blocking buffer prepared by dissolving of 3g of pure BSA (bovine serum albumin) in 100 ml PBS) for 1 hour. After incubation, primary antibody was added to the cells and incubated overnight at 4 °C. Primary antibody was prepared according to manufacturer instructions (Table 1.)

Protein of interest	Antibody		Manufacturer	Dilution in PBS
Haus6	Primary	Rabbit ab-150806	Abcam, Cambridge, UK	1 : 250
	Secondary	Alexa Fluor 594-conjugated donkey anti-rabbit antibody	Abcam, Cambridge, UK	1 : 500
Ndc80 (Hec1)	Primary	Mouse ab-3613	Abcam, Cambridge, UK	1 : 500
	Secondary	Alexa Fluor 594-conjugated donkey anti-mouse antibody	Abcam, Cambridge, UK	1 : 1000
Spindly	Primary	Rabbit A301-354A	BETHYL Laboratories, Inc.	1 : 500

Secondary	Alexa Fluor 594-conjugated donkey anti-rabbit antibod	Abcam, Cambridge, UK	1 : 500

After the incubation with the primary antibody, cells were washed in PBS, 2 times for 5 minutes. Secondary antibody was prepared according to manufacturer instructions (Table 1). Secondary antibody was added to the cells and incubated for 1 hour on a shaker at room temperature. After incubation, cells were washed 2 times for 5 minutes with 3% BSA-PBS. Then DAPI (1µg/ml) was added to the cells and incubated for 15 minutes. After incubation cells were washed 2 times for 5 minutes in PBS. Cells are stored in PBS on +4 till the next day. During all incubations, samples were placed on the shaker. Cells were imaged using 405, 478 and 594 nm excitation light on Dragonfly confocal microscope.

3.7 Inducing mitosis with un-replicated genomes (MUG)

MUG is induced by incubation of cells in hydroxyurea and caffeine (Brinkey et al., 1988). Hydroxyurea and caffeine were a gift from the organic chemistry laboratory (Institute Ruđer Bošković, Zagreb). The amount of 0.0470 g caffetine and 0.0273 g of hydroxyurea was weighed on analytical balance. The stock solutions of hydroxyurea and caffeine were prepared by dissolution of 0.047 g of caffeine and 0.0 273 g of hydroxyurea in 1936 µL and 1775 µl of water to acquire the stock solutions of concentration of 175 mM and 200 mM, respectively. The stock solution was diluted in DMEM medium to the final concentration of 2mM for hydroxyurea and 5mM for caffeine. The amount of $1x10^5$ cells were seeded and cultured in 2 ml DMEM medium at 37 °C and 5% CO2 on 35 mm glass coverslip uncoated dishes with 0.17mm (#1.5 coverglass) glass thickness (MatTek Corporation, Ashland, MA, USA). Cells were counted using the Improved Neubauer chamber (BRAND GMBH + CO KG, Wertheim, Germany). The cells were incubated for 12 hours at 37 °C and 5% CO2. After 12 hours medium was replaced with 2 mL DMEM containing 2mM hydroxyurea and incubated for 20 hours at 37C and 5% CO2. After 20 hours medium was again replaced with medium containing 2mM hydroxyurea and 5mM caffeine and the cells were again incubated at 37C and 5% CO2. The cells were imaged 18 hours later. MUG was induced on HeLa PRC1-GFP and U2OS tubulin-RFP and CenpA-GFP.

3.8 Image analysis

Microscopy images were analyzed in Fiji Software and Imaris Viewing Software.

3.9 Transformation of horizontal spindle images to vertical orientation.

To count the number of bundles, horizontally imaged spindles were transformed in vertical orientation. Then vertical spindle cross section appears as dots (**Figure 13**). This was done using the code written in R programming language in R Studio (R Core Team., 2016). Before the transformation, the Z-stack of the spindle in a single channel was rotated in Fiji so that the spindle major axis was approximately parallel to the x-axis. The program is written so that after the transformation of image from horizontal to vertical, orientation of the coordinate system corresponds to rotation of the image without mirroring. The aberrations caused by refractive index mismatch between immersion oil and aqueous sample are taken into account in program by multiplying Z-step size by a correction factor of 0.81 to obtain the correct Z-distance. This factor is calculated as a ratio of the cell diameter in y and z direction, assuming that a mitotic cell is spherical.
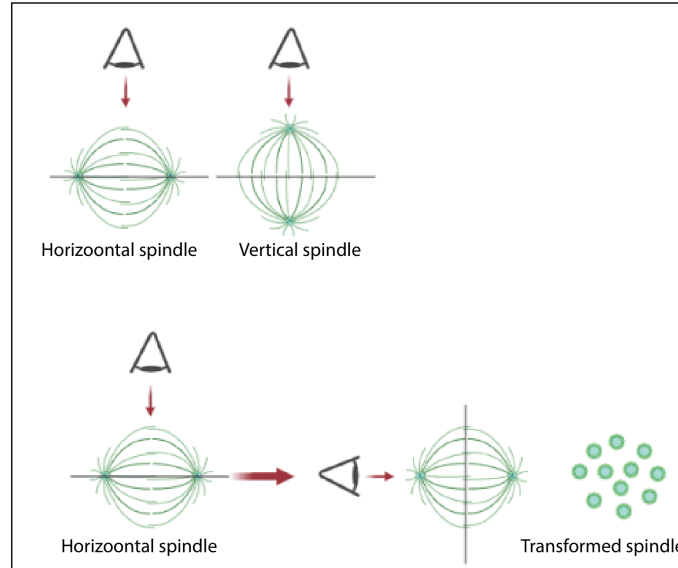

Figure 13. Schematic view of the spindle orientation. Upper images shows two possible orientation of the mitotic spindle; horizontal (left) and vertical spindle (right). Bottom image shows the transformation of horizontal spindle in vertical using R software. Transformed image shows cross section of spindle.

Bundles were counted on the sum intensity images of 5 central planes of the transformed vertical spindle. The number of bundles is determined by counting the bright spots using Multi point tool in ImageJ program (**Figure 14 B**). Bright spots are taken to represent microtubule bundles. Big spots were counted as one whole bundle. Zero time point was set as the first image of methaphase spindle.

3.10   Intensity measurements

Intensities were measured on the cells imaged vertically and horizontally. In time lapse movies of vertical cells imaged for bundle formation, intensities were measured using Fiji software to determine the changes in intensities in time in one central plane of the cross section of the vertical spindle. The square of the defined size was used to frame the region of the spindle and the intensity of the frame was measured in every frame out of 100 in time series (time between every frame is 5.4 s) (**Figure 14 D**). The average and maximum intensity was measured. Correction for bleaching and background subtraction was performed by subtracting the mean intensity of cytoplasm from mean and maximum intensity of the spindle territory (Bancaud et al., 2010). It is assumed that the drop of intensity in the cytoplasm is due to bleaching only (**Figure 14 C**).

Mean intensity of the spindle cross section = Mean intensity of the square which frames territory of the spindle cross section – Mean intensity of the cytoplasm

Maximum intensity of the spindle cross section = Maximum intensity of the square which frames territory of the spindle cross section – mean intensity of the cytoplasm

Normalization of the intensity change was performed dividing the mean/maximum intensity of the spindle with the mean/maximum intensity of the spindle in first frame of T series.

$$Normalized\ mean\ intensity = \frac{mean\ intensity\ of\ the\ spindle\ cross\ section}{mean\ intensity\ of\ the\ spindle\ cross\ section\ in\ the\ first\ time\ frame}$$

$$Normalized\ maximum\ intensity = \frac{maximum\ intensity\ of\ the\ spindle\ cross\ section}{maximum\ intensity\ of\ the\ spindle\ cross\ section\ in\ the\ first\ time\ frame}$$

Intensity profile of the bundle was measured using Line tool in Fiji in every 10th frame (**Figure 14 E**). 3D illustrations of the individual bundle formation and whole spindle formation were made using 3D Surface plot in Fiji in selected frames.

Measuring intensities of individual bundle in formation was measured in one middle slice in all time frames of vertically oriented spindle. The position of the individual bundle formation was framed in square of defined area that was determined as area that can frame fully formed

bundle in last time frame. Analogously, drop of intensity in the vicinity of the bundle was measured in the same way using the square of the same size as for the neighbor bundle (**Figure 14 F**).

When calculating the change in the intensity of the whole spindle, mean intensity and maximum intensity were determined using the sum of all Z slices of Z stack that was imaged before and after the T series was taken (described in confocal microscopy: imaging protocols). Only the region of the spindle was outlined using Polygon Selection tool in Fiji (**Figure 14 G**). Mean and maximum intensity were measured. Bleaching was corrected by subtracting mean intensity of the cytoplasm as described above.
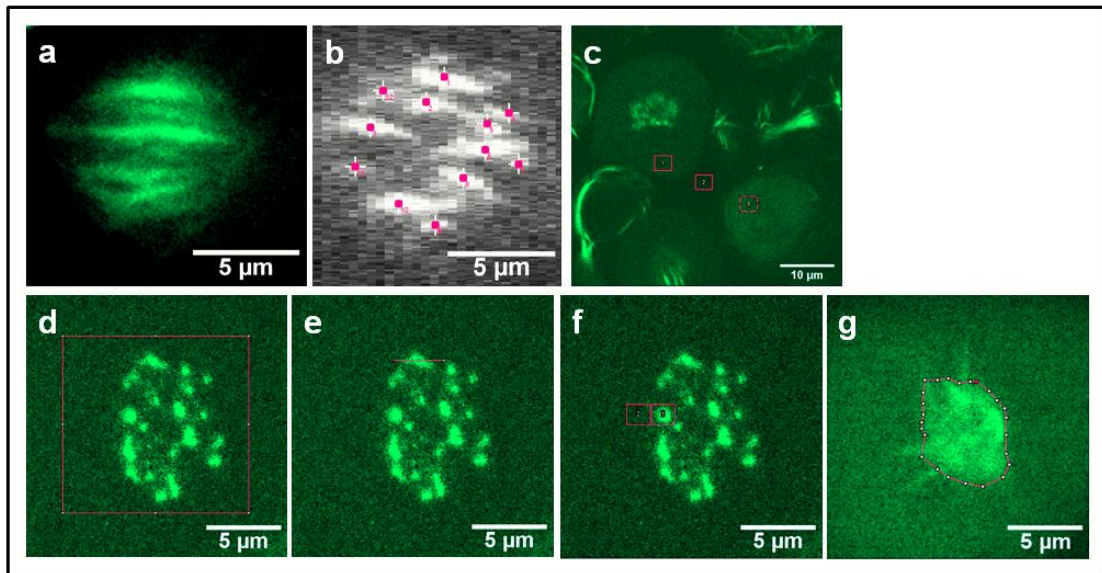
Figure 14. Illustrations of the measurements using Fiji tools. **A.** Sum of intensities of 41 plane Z stack. **B.** Image of the transformed spindle shows the cross section. Bundle cross section is seen as white dots. Bundles are counted using Multi point tool in Fiji software. **C.** Intensity measurements of the cytoplasm background using Rectangle tool in Fiji. **D.** Intensity measurement of the spindle cross section territory in the middle plane. **E.** Intensity line profile measurement of one bundle in the spindle cross section. **F.** Measuring of the mean intensity of the bundle and local cytoplasm using Rectangle tool in Fiji software. **G.** Measuring the whole spindle intensity on the sum of the intensity of 41 plane Z stack using Free hand selection tool.

3.11   Segmentation and quantification of the prometaphase spindle

Segmentation was performed using Squash (Rizk et al., 2014). Squash uses a segmentation method that directly connects the image-segmentation task with biological reality through a prior knowledge about imaged object, the image formation process and the noise present in the image. This allows the same method to be applied to a wide spectrum of images by adjusting the prior knowledge (changing parameter values). In addition, the segmentation method used here provides theoretical performance and robustness guarantee, and is independent of the manual initialization and directly corrects for microscope blur and detector noise, yielding optimally de-convolved segmentations. This last feature is achieved by accounting for the microscope spread function (PSF), improving the capacity to segment objects with sizes close to the resolution limit. The algorithm makes no assumptions about the expected shape of the segmented objects, hence minimally biasing the results. The segmentation algorithm is implemented in a user-friendly multithreaded software plugin for free open-source bio-image processing frameworks ImageJ and Fiji, as a part of the MosaicSuite. The idea was that during the formation of the bundles, discrete objects and spots are formed that can be detected and measured by this segmentation plugin. The procedure starts with the object detection and separation, followed by an estimation of the local background and object intensities and computation of the optimal segmentation (**Figure 15**). Background subtraction is performed first. Background variations are nonspecific signals and are corrected using rolling-ball algorithm. This algorithm computes intensity histograms in a window moving across the image. The edge length of the window is set by the user. This segmentation method corrects for microscope blur and detector noise, yielding optimally de-convolved segmentation. This feature is achieved by accounting for the microscopes point spread function (PSF), improving the capacity to segment objects with sizes close to the resolution limit. Here the theoretical PSF for the correction for diffraction blur was used. The theoretical PSF model was used by specifying the imaging conditions parameters in the "Segmentation parameters" options "Estimate PSF from objective properties sub window". The software provides models for confocal microscopy. Our values were standard deviation in xy (in pixels) 0.79 and standard deviation in z was also in pixels 0.79. In each window, the most frequently occurring intensity value is taken at the local background estimate. This is based on the assumption that the objects of interest are smaller than the window size and covers less than a half of the total window area. In main graphical user interface squash window we set the parameter for Background subtraction options entering the window edge lengths in units of 14 pixels. This length should be large enough so that the square with that

edge length cannot fit inside the objects to be detected, but smaller that the length scale of background variations.
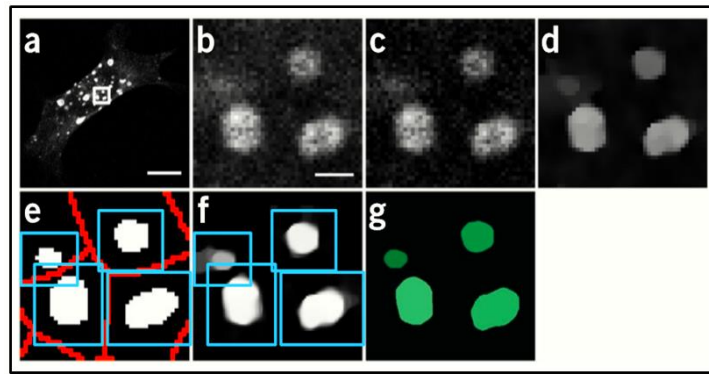

Figure 15. Work flow of the Squash protocol illustrated on an endosome segmentation. **A.** Original image of a Cherry-RAB5–transfected HEK293 cell; scale bar: 10 µm. **B.** Close-up of the region highlighted by the white square in a; scale bar: 1 µm. **C.** The same close-up after the background subtraction. **D.** Object model image found by Squash. Intuitively, this is a de-noised and de-convolved version of c taking into account the microscopes PSF. **E.** Objects (white) obtained by thresholding image d. The image is decomposed into regions (blue boxes), and objects are separated by red lines. **F.** Refined sub-pixel object model images obtained by applying the Squash segmentation method inside each region with individual estimates for the local object and background intensities. **G.** Final segmentation with the estimated object intensities displayed in shades of green (acquired from Rizk et al., 2014).

Object detection was performed over the entire image. This stage is not the final segmentation, but only serves to find regions in the image that contain objects of interest. This was set by varying regularization parameter and threshold. The higher value of the regularization parameter of 0.1 (typical values are between 0.05 and 0.25) was used to avoid the segmenting noise-induced small intensity peaks. Thresholding of the initial detection reveals the initial objects. All objects with peak intensities lower than this threshold are discarded, and the others are retained. This parameter allows the user to control sensitivity of the analysis. Connected regions were identified as individual objects. Then the threshold for the minimum object intensity to be considered was set. Intensity values were normalized between 0 for the smallest value occurring in the image and 1 for the largest value. Low values were used for increased sensitivity and high values to force object separation. The parameter of 0.001 (smallest value) was used (**Figure 16**).
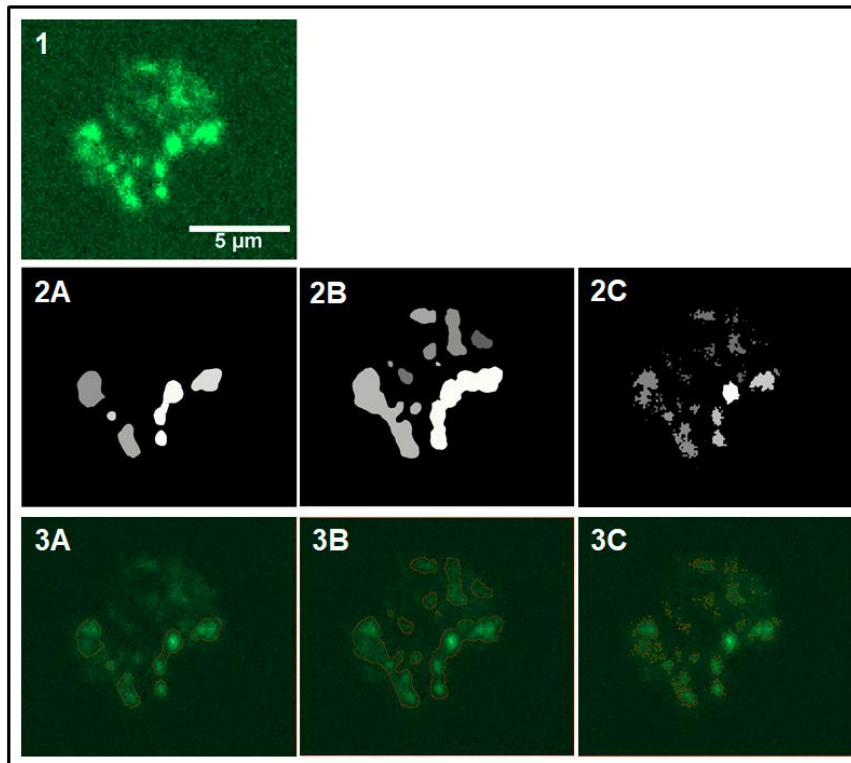
Figure 16. Illustration of how the parameters affect segmentation results by using prometaphase spindle cross section. Green spots represent cross sections of the antiparallel bundles. **1.** Cross section of the prometaphase spindle. Row **2** and **3** represent Object intensity output and Object outlines output, respectively. **A** Segmentation with the minimum intensity threshold set to 0.001 and the regularization weight set to 0.2. **B** Segmentation with the same minimum intensity threshold (0.001) and with the regularization parameter set to 0.002. **C** Segmentation with the minimum intensity threshold increased to 0.1 and regularization 0.002.

The sub-pixel segmentation to compute segmentations with sub-pixel resolution was selected. The resolution of the segmentation is increased by an oversampling factor of 8 for 2D images. Local intensity estimation parameter was set to automatic. The poisson model, recommended for confocal microscopes, was set. (**Figure 17**).
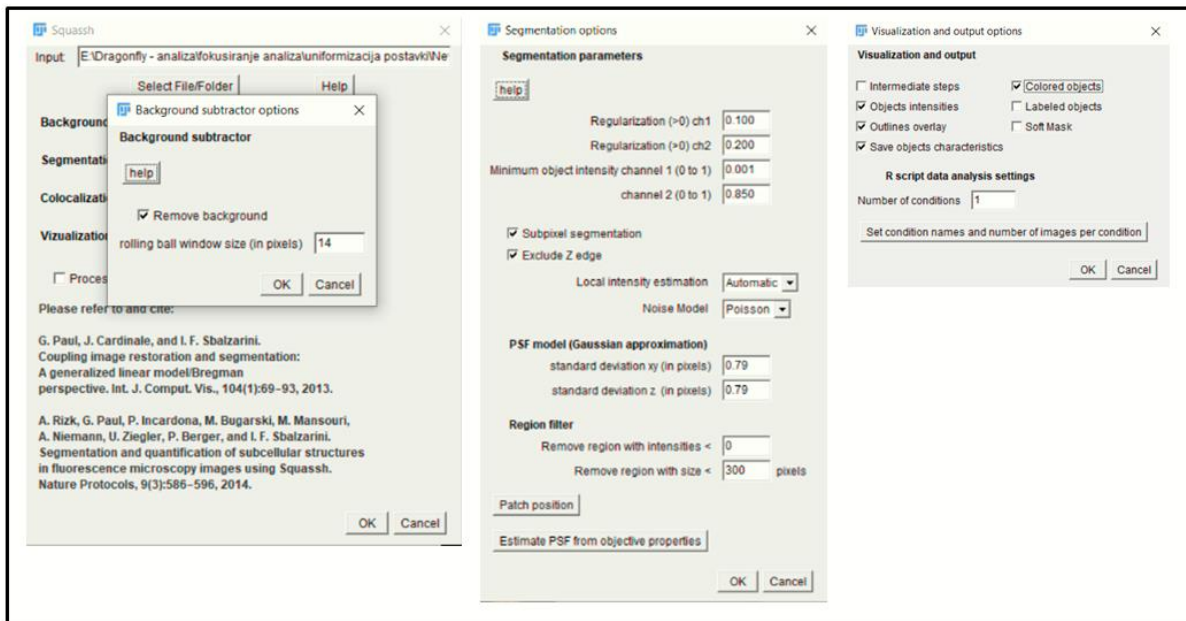
Figure 17. Parameters set for segmentation analysis.

Next visualization options were selected: Colored objects, Object intensities and Object outlines. With colored objects visualization, every object is visualized in a different, random color. Object intensities display objects in their estimated fluorescence intensities. Object outlines show an overlay of the original image with the segmented outlines in red. "Save object and image characteristics" was also selected. Output files are saved in the folder containing tiff image for analysis. The file "Image data" contains the mean object features from the each image. It stores the number of objects found in the image, the mean object size in terms of area, the mean object surface (perimeter for 2D images), the mean length of the objects (the maximum extension in the most extended direction, and the main fluorescence intensity in the objects). In files "ObjectsData" are individual, per-object features. Each object is indexed by its segmentation label, and the sizes and intensities of all the objects.

3.12   Measuring the spindle parameters

Spindle length and width were measured on the horizontal metaphase cells using line tool in Fiji. Spindle length in the prometaphase vertical cells was measured by multiplying the number of slices in Z stack in which spindle part was seen with the distance between two Z planes.

3.13   Low Light Tracking Tool (LLTT)

This software is a tool for the tracking of the low-light sub-resolution objects in the fluorescent microscopy. It can be applied in other fields, as well. Bundles were tracked in time using Low Light Tracking Tool (LLTT), an ImageJ plugin (Krull et al., 2014). Dots of tracking tools were placed randomly on the area of high intensity. Every dot tracked the signal to the last frame. The output of Y kymograph was showing the dynamics of the bundles in Y axis.

3.14   Manual tracking tool

The 2D trajectories of the bundles and their coordinates were tracked using Manual tracking tool to represent bundle trajectories. The movement of all the bundles was corrected to the central bundle/bundles as a reference bundle present in all filmed cells, using Manual drift correction plugin in Fiji. Those bundles are first formed and were not bearing chromosomes.

Morphological analysis of the cells were done using Imaris 3D viewer. Length of the spindle was measured on the vertically oriented spindle Z stacks. The spacing between slices was 0.5 µm. The length was measured by multiplying the number of slices in which the spindle was present with the spacing of 0.5 µm.

3.15   Statistical analysis.

Graphs were generated in the BioVinci software. Fiji was used to scale images and adjust brightness and contrast. Figures were assembled in Biorender and Ilustrator. Data are given as mean ± s.e.m., unless otherwise stated. Significance of the data was estimated by Student's t-test (two-tailed and two-sample unequal-variance). The value of $p < 0.05$ was considered statistically significant. Values of all the significant differences are given with degree of significance indicated (*$0.01 < p < 0.05$, **$0.001 < p < 0.01$, ***$p < 0.001$). The number of analyzed cells and microtubule bundles are given in the respective figure panel.

4. RESULTS

4.1 Number of bundles

HeLa PRC1-GFP cells with horizontal prometaphase spindles were selected. Z stack of 41 planes was acquired every 10 minutes of the same cell starting from the early prometaphase. After rotating cells using R-code, it was seen that the number of antiparallel bundles increased in time. Number of PRC1 labeled bundles increased from 13 ± 0.657 in prometaphase to 25 ± 0.841 (n = 15) (**Figure 18 A, C**). Same experiment was performed with RPE1 CenpA-GFP, Centrin1-GFP cells, with exception that cells were imaged every 5 minutes. Here, bundles were labeled with tubulin binding dye, SiR-Tubulin and they represent general bundles in the cell (antiparallel and parallel bundles). Number of bundles in RPE1 cells also increased in time, starting from 12 ± 1.235 in the early prometaphase to 26 ± 2.048 (n = 16) in metaphase (**Figure 18 B, C**).
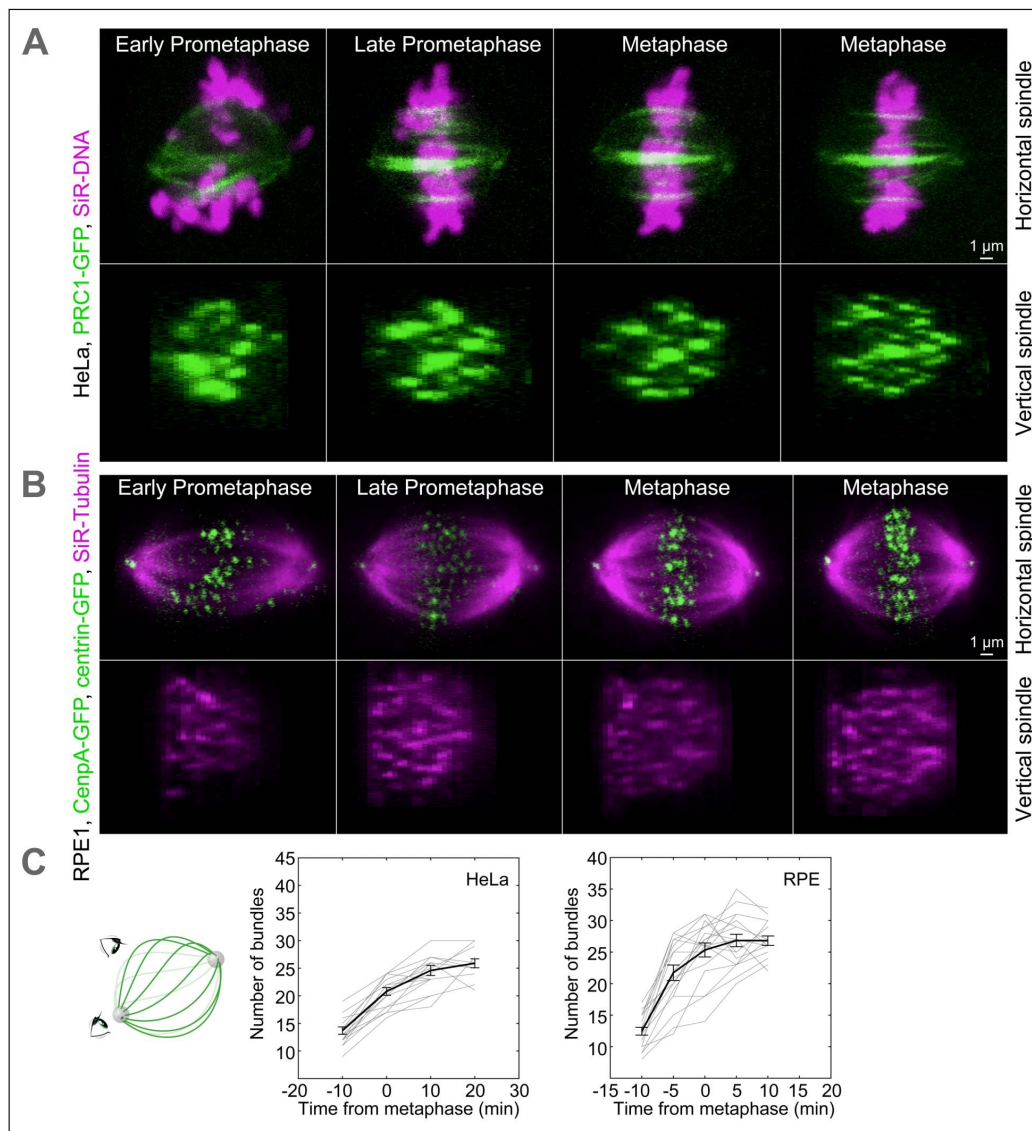
Figure 18. A. HeLa PRC1-GFP cells with added SiR-DNA dye (pink). First row are horizontal cells in the early prometaphase, late prometaphase and methaphase acquired in intervals of 10 minutes. Second row shows cross section (middle plane) of the corresponding spindle in the first row generated using the R software. Only PRC1-GFP channel was transformed. **B.** RPE1 cells with labeled kinetochore protein Cenp-A and Centrin1 labeled with GFP (green). Microtubules are labeled with SiR-Tubulin dye (pink). First row represents horizontal cells and second row corresponding cross sections. Only SiR-Tubulin channel was transformed. **C.** Schematic representation of horizontal and vertical view of the spindle (left). Plots on the right represent the number of bundles as a function of time for HeLa and RPE1 cells (from left to right). In both cell lines, number of bundles increases in time.

4.2 Antiparallel bundle formation

All the experiments in this section were performed on HeLa PRC1 – GFP cell line. To determine the mechanism of antiparallel bundle formation, the search for rare cells with vertically oriented prometaphase spindle began. From now "antiparallel bundles" will be called only "bundles" by default. Vertically oriented prometaphase spindle was recognized in PRC1-GFP channel as a relatively small circle of higher intensity in the cell with a few dots which correspond to the cross sections of early formed antiparallel bundles (**Figure 19 A**). The territory of the spindle cross section was recognized by amorphous stain of GFP labeled PRC1 protein that was higher in intensity compared with the rest of the cell cytoplasm. I called this structure a prometaphase mist. It was noticed that in all cells chromosomes were surrounding the mist and were positioned on the surface of the spindle cross section which is in agreement with previous studies. Interestingly, the circle of chromosomes was not closed around the prometaphase mist. Chromosomes are located predominately on the one side of the prometaphase spindle which matches to the rossete configuration. That suggests that searching for vertical spindles selected only cells with prometaphase pathway of mitosis that begins with the rossete configuration. For further description of parameters of the spindle, region of the spindle cross section free of chromosomes was annotated as "top" and side opposite to it, "bottom" of the cross section (**Figure 19 B**). In the top region of the spindle cross section free of chromosomes, one or two fully formed bundles were present in all cells, while rest of the spindle territory was forming a mist. A spindle cross section is referred as "spindle territory" for ease of description.
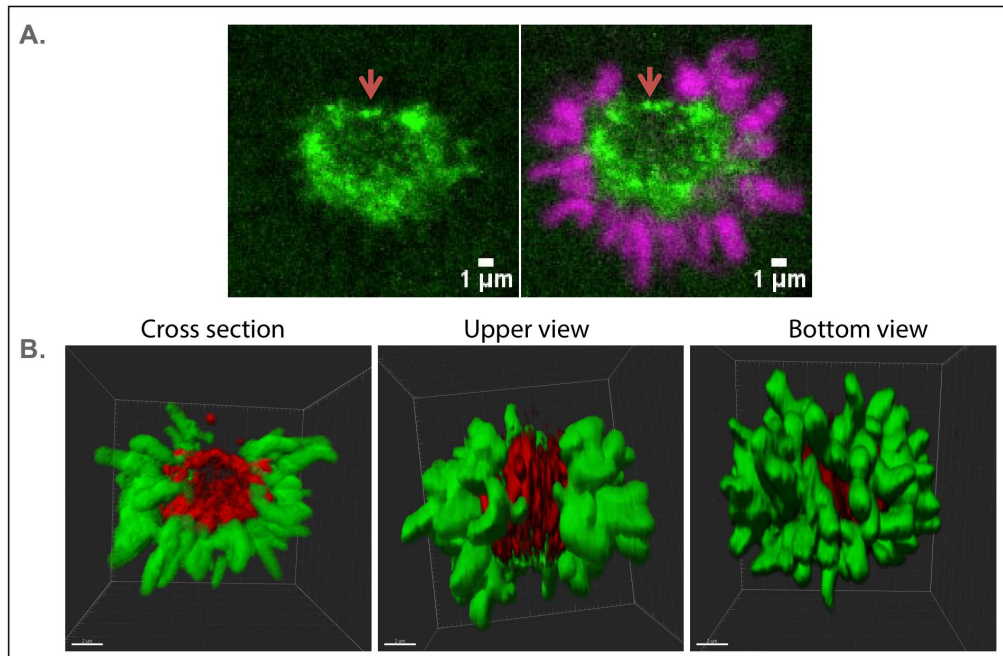
Figure 19. A. Cross section of vertically oriented early prometaphase spindle in HeLa PRC1-GFP cell line. Only GFP channel (left) shows PRC1 protein that aggregates in one region called prometaphase mist. Chromosomes (right, pink) are positioned on the surface of the prometaphase spindle mist and they form a circle around the cross section of the spindle. The circle is not closed, therefore making a region of the spindle free of chromosomes. Red arrows show fully formed 2 bundles on the top of the spindle cross section. **B.** 3D view of vertically positioned prometaphase spindle made in Imaris 3D viewer shows the cross section (left), the upper surface (middle) and the bottom surface (right) of the spindle. Microtubules are colored red and chromosomes green.

Imaging live prometaphase vertical spindle in time according to the imaging protocol showed appearance of bright dots of PRC1-GFP protein in time. These dots represent bundle cross sections indicating that antiparallel bundles form in time. Those dots gradually form in the territory of the prometaphase mist of PRC1-GFP protein. Except for the formation of bundles, rearrangements of chromosomes were also observed. They changed the position from the bottom and side spindle surface before imaging to fill the entire area of spindle cross section forming methaphase plate at the end of T series (**Figure 20**).
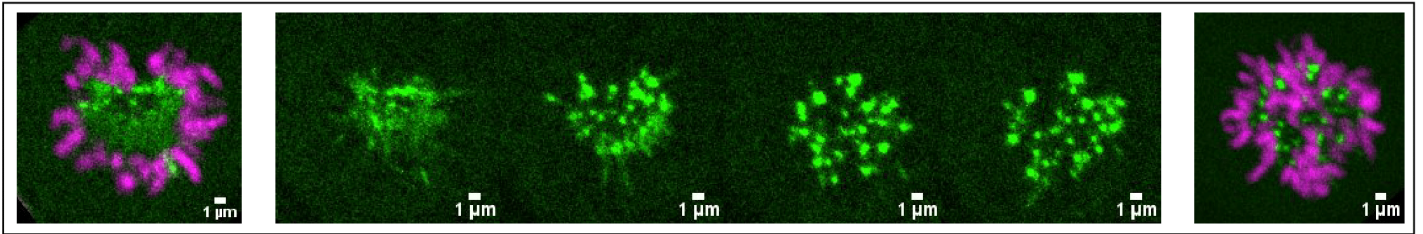
Figure 20. Time lapse of vertically oriented spindle formation in HeLa PRC1-GFP cell line with DNA labeled using SiR-DNA dye (pink). Time interval between two frames was 5.4 seconds. Time lapse shows concentration of PRC1 protein in discrete spots that represents cross sections of antiparallel bundles.

To analyze and quantify the process of antiparallel bundle formation, the segmentation analysis is performed using Squash plugin in Fiji software. As time passes, few large patches of PRC1 in the first frame fragment in a larger number of smaller segments (**Figure 21 A, B**). The numbers of surfaces, called segments, increases significantly in time from 5.300 ± 0.760 (n=10) in the first frame to 17.000 ± 1.461 (n=6) in the last frame (p = 4.197×10^{-8}) (**Figure 21 B, C**). The mean size (mean surface) of the objects and the mean perimeter per frame decrease; from 460.089 ± 151.375 pixels (n=10) to 51.943 ± 12.056 pixels (p = 0.214×10^{-2} n=6) and from 144.477 ± 32.787 pixels (n=10) to 38.35578 ± 2.043 pixels (p = 0.269×10^{-2} n=6), respectively (**Figure 21 B, D, E**).

Figure 21. A. Time lapse of the prometaphase vertical spindle formation in HeLa PRC1-GFP cell line. **B.** Outlines of the mist segments after squash segmentation analysis colored white. Color brightness is proportional to the signal intensity (gray represents smaller signal intensity and bright white represents higher intensity). **D.** Number of segments increases in time. **E.** Mean size of the objects per frame decreases in time. **F.** Mean perimeter of the objects per frame also decreases in time. In plots C, D and E pi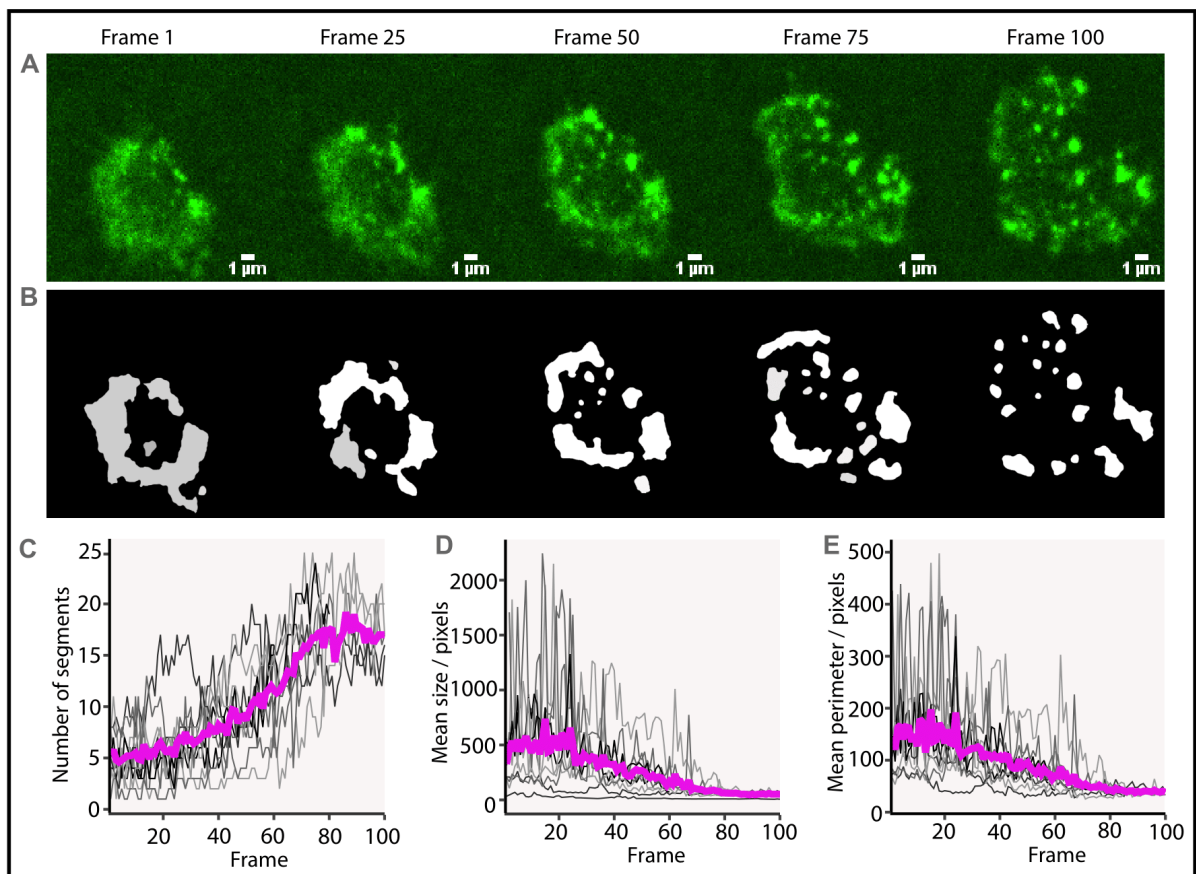nk line represents the mean and gray lines correspond to the particular cells. Time interval between two frames was 5.4 seconds.

Next, the size distribution of individual segment in time showed that in all 10 cells, objects of maximum size show abrupt decrease in size as the time passes (**Figure 22 A**). Maximum sized segments in the last five frames make up 28.764 ± 5.669 % of the size of the maximum sized segments in the first five frames (n = 10), while segments of the smallest size in the last five frames make up 75.454 ± 11.192 % of the size of smallest segments in the first five frames. That is means that larger segments fragment 3.477 times while the smallest segments fragment only 1.325 times (n = 19) (**Figure 22 A**). In addition to the large segments, small segments are also present in the first frames and their number is increasing in every next frame due to segmentation of larger segments. If we take into account only the largest segments in every frame, drop of the size would have reverse sigmoid like curve. The presence of small segments in the first frames suggests existence of small local regions of higher intensity that is recognized by the software. Those segments have not permanent location and size and they are probably artifacts of the software or dynamic unstable patches of higher intensity signal that are recognized.

In contrast, mean intensity of every frame showed an increasing trend. The histogram of mean intensity of the frame is skewed right, meaning that mean intensity of the segments in every next time frame grows (**Figure 22 B**). Mean frame intensity grows 2.059 ± 0.159 times in relation to the first frame. Sum of the intensity of all segments per frame shows steeper intensity growth than mean intensity growth (**Figure 22 C**), reflecting increasing number of segments and an increase in their intensity. The sum of the mean frame intensity grows 7.355 ± 0.964 times in relation to the first frame (n = 10). In summary, these results suggest that number of segments grows and that mean intensity of segment grows, while the size of the segment and perimeter drop in value.
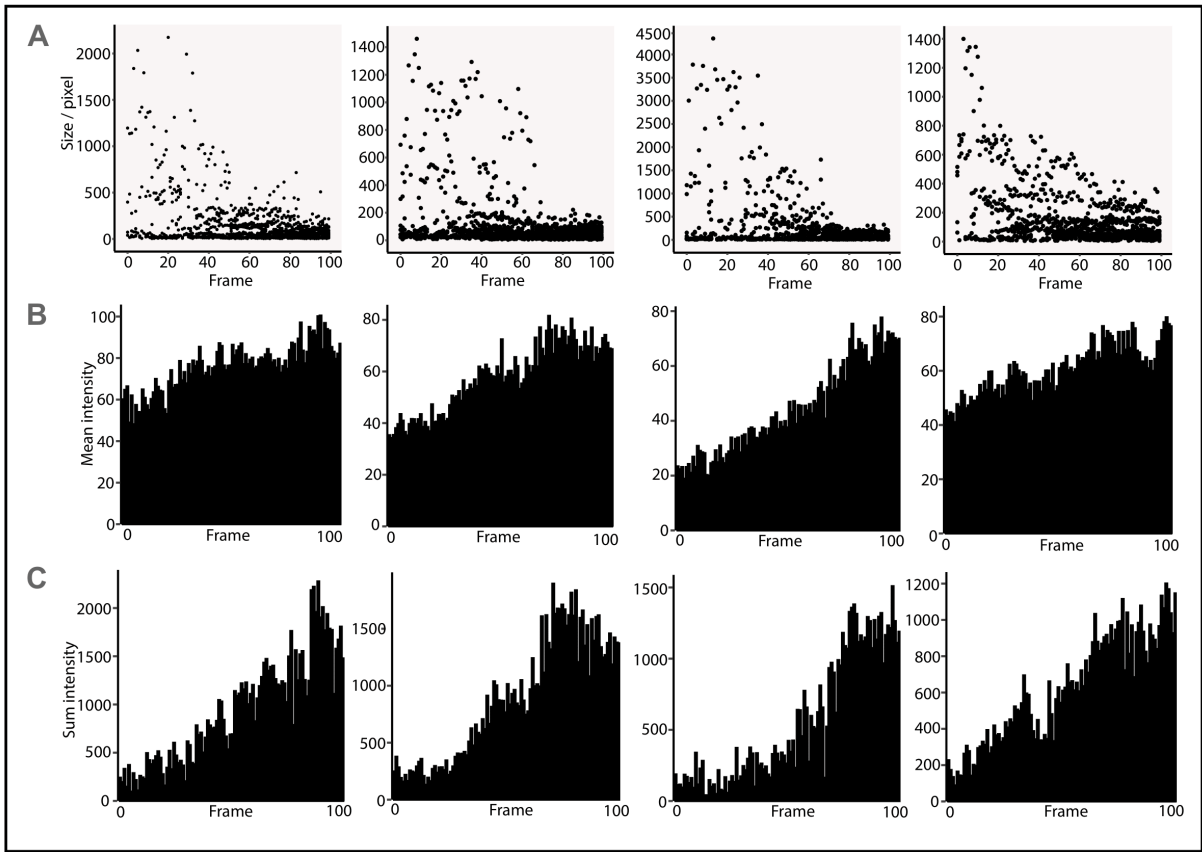
Figure 22. A. The size distribution of segments in time. Size of segments drops in time. **B.** Mean segment frame intensity increases in time. **C.** Sum of object intensity increases in time. For every parameter, 4 representative cells are shown. Time interval between two frames was 5.4 seconds.

Individual segment intensity distribution in every frame showed an increasing trend (n = 10). These results, with those from figure 22.B and 22.C suggest that except that number of segments increases, the intensity of individual segments also increases in time (**Figure 23**).
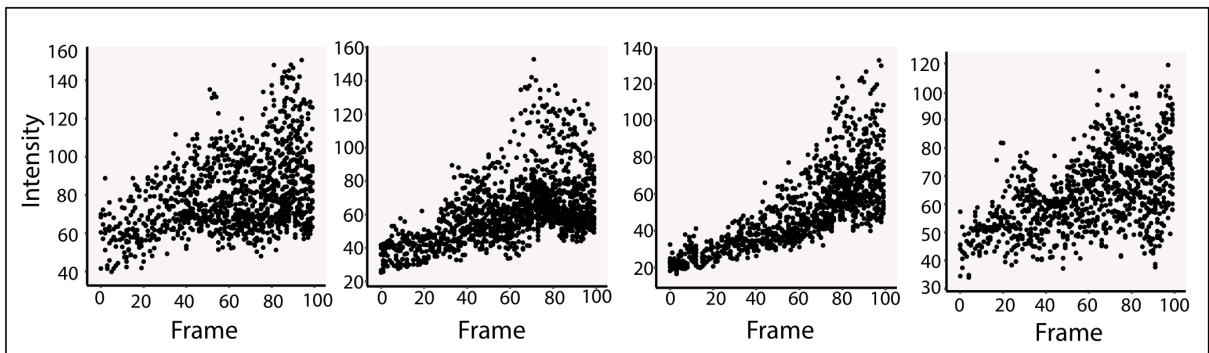
Figure 23. Number of segments and their intensities increase in time. Time interval between two frames was 5.4 seconds. Four representative cells are shown.

Furthermore, data shows that segments of lower intensity at the beginning of time lapse were larger in size (**Figure 24**). In the first part of the plot large segments are prevalent while in the last frames all the segments are smaller in size and higher in intensity.
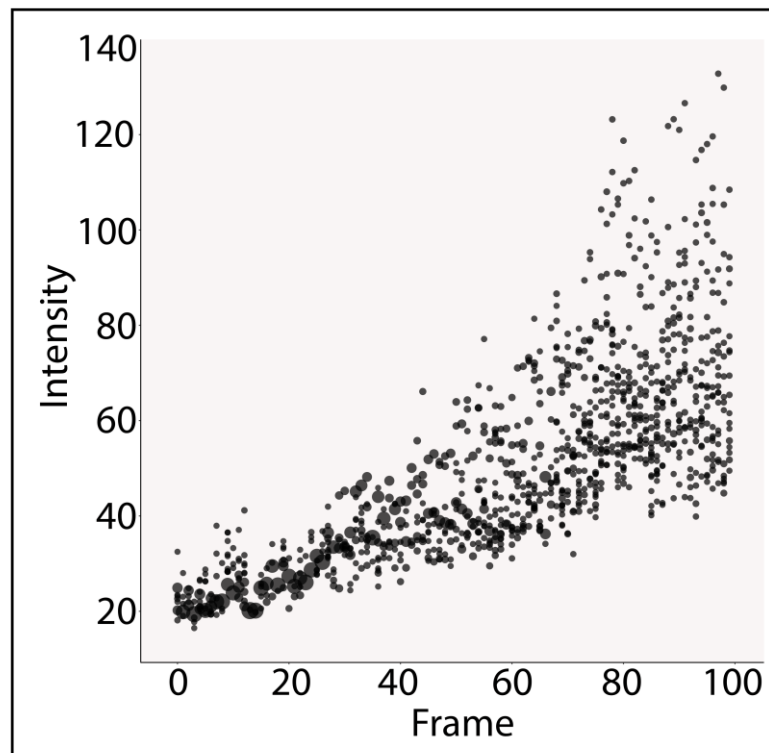
Figure 24. Intensity of individual segments is increasing in time, showing segments of smallest intensity in the first frame and segments of highest intensity in the last frame. In the first frames segments are larger. Number of segments visibly increases in time and they are smaller in size. Plot shows one representative cell. Time interval between two frames was 5.4 seconds.

To confirm the reliability of the method, manual validation was performed. The manual validation was performed on one middle plane of the vertical spindle on 60 frames, as the squash analysis. Mean intensity of the object intensities in every frame, number of object, mean size and mean perimeter match to a satisfactory level. Mean intensity starts with the value 45.377 in the first frame for squash analysis while manually this value is 34.834, but the trend of intensity growth is evident. The same thing also applies to other parameters; number of objects (first frame: squash 4, manual 3, last frame: squash 16 and manual 16), mean size (first frame: squash 526.805, manual 820.333, last frame: squash 72.944, manual 116.813) and mean perimeter (first frame: squash 144.750, manual 169.000, last frame: squash 41.984, manual 45.390). Individual scatter plot of the object size, perimeter and mean object intensity

also shows some differences, but for the purposes of showing a decreasing trend and growth of a parameter, the squash analysis showed satisfactory results (**Figure 25**).

Figure 25. A Mean intensity, **B** Number of objects, **C** Mean size and **D** Mean perimeter show the same trend using squash analysis (blue line) and manual analysis (orange line). Scatter plots of Object size, Object perimeter and Mean object intensity show the same trend and are on same size scale using manual (**E**) and squash (**F**) analysis. Time interval between two frames was 5.4 seconds.

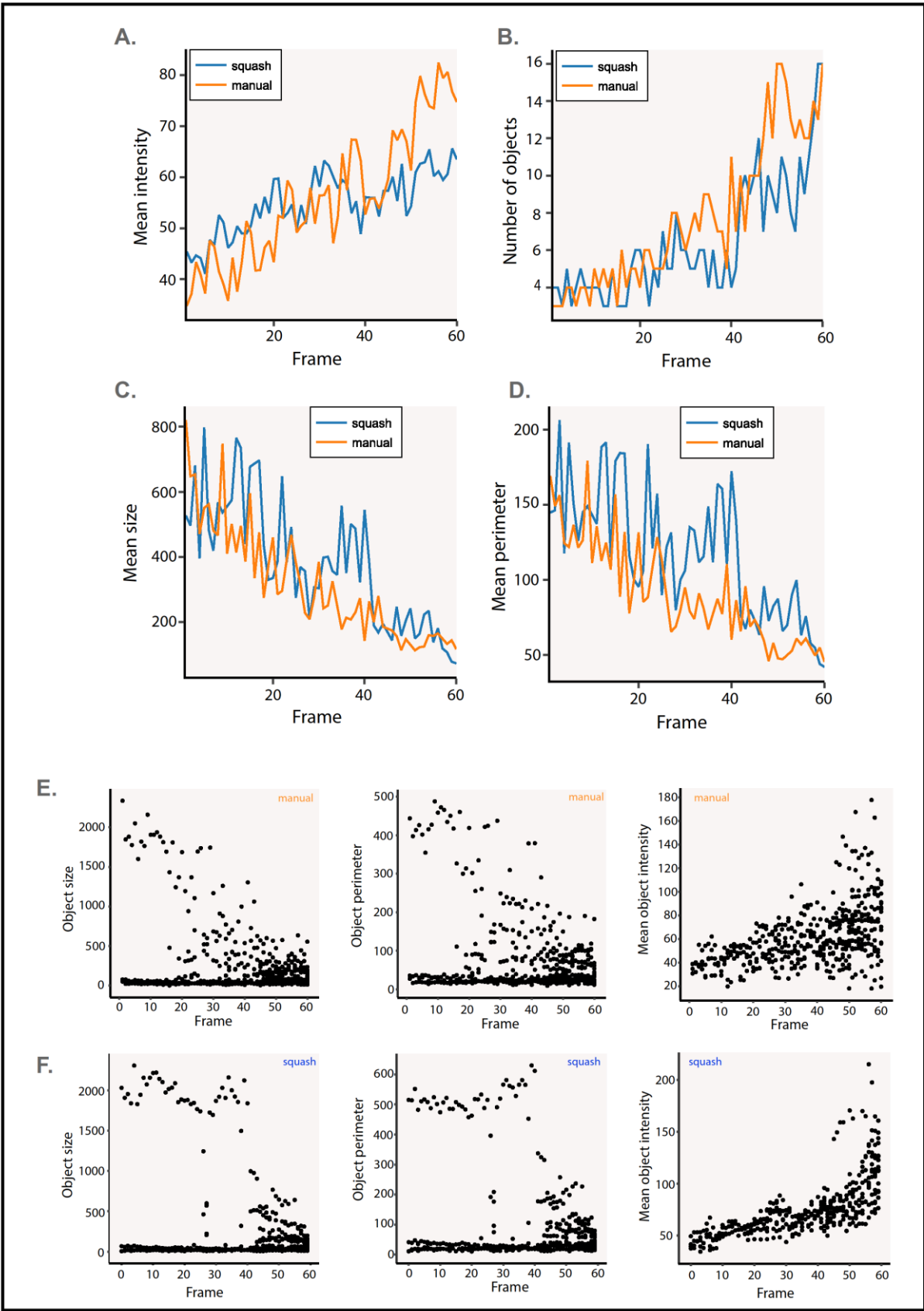Intensity analysis on the middle plane of the vertical prometaphase spindle (**Figure 26 A**) showed that both mean and maximum intensity of the spindle territory is increasing in time. Mean intensity increases slightly, but not significantly; from 11.234 ± 1.226 (n = 12) in first frame to 14.463 ± 1.651 (n = 10) in the last frame (p = 0.125) (**Figure 26 B**). Maximum intensity increases significantly from $217{,}681 \pm 29{,}191$ (n = 12) in the first frame to 375.396 ± 40.049 (p = 0.401×10^{-2}, n = 10). In relation to the first frame, mean intensity increases 1.456 ± 0.080 times (n = 10) and maximum intensity increases 2.033 ± 0.240 (n = 10) times (**Figure 26C**). Frame to frame variations of the maximum intensity are greater than of the mean intensity.

Next, total spindle intensity analysis was performed on the sum of all planes of Z stack in the territory of the spindle, before and after T series was taken (**Figure 26 D**). Mean intensity of the spindle didn't change significantly: 5005.024 ± 173.224 before and 4942.249 ± 117.276 after T series (p = 0.239, n = 17) was taken. Mean intensity of the cytoplasm did significantly drop from 4691.935 ± 69.649 to 4630.895 ± 47.877 (p = 0.688×10^{-2}, n = 17), presumably because of the photo bleaching. After subtraction of the cytoplasm from the spindle intensity, mean intensity of the spindle didn't significantly change before (313.089 ± 127.984) and after (311.354 ± 82.293) the T series was taken (p = 0.946, n = 17) (**Figure 26 F**). However, maximum intensity of the spindle increases significantly from 5954.647 ± 357.679 to 6728.824 ± 735.694 (p = 0.637×10^{-3}, n = 17). Maximum intensity of the cytoplasm also drops from 5012.176 ± 109.605 to 4931.529 ± 83.073 (p = 0.025, n = 17) (**Figure 26 G**). Subtraction of the mean intensity of the cytoplasm from maximum intensity of the spindle results in a significant increase in maximum intensity of the spindle, from 942.471 ± 290.648 to 1797.294 ± 710.871 (p = 9.684×10^{-5}, n = 17) (**Figure 26 H**). These results suggest that there is no net increase in the mean intensity of the spindle and that the signal only redistributes inside the spindle territory. An increase in the maximum intensity suggests that signal concentrates in certain areas of the spindle, antiparallel bundles. However, increase in mean intensity of the middle plane of the spindle is suggesting that there is relocation of signal from other part of the spindle into the middle plane.
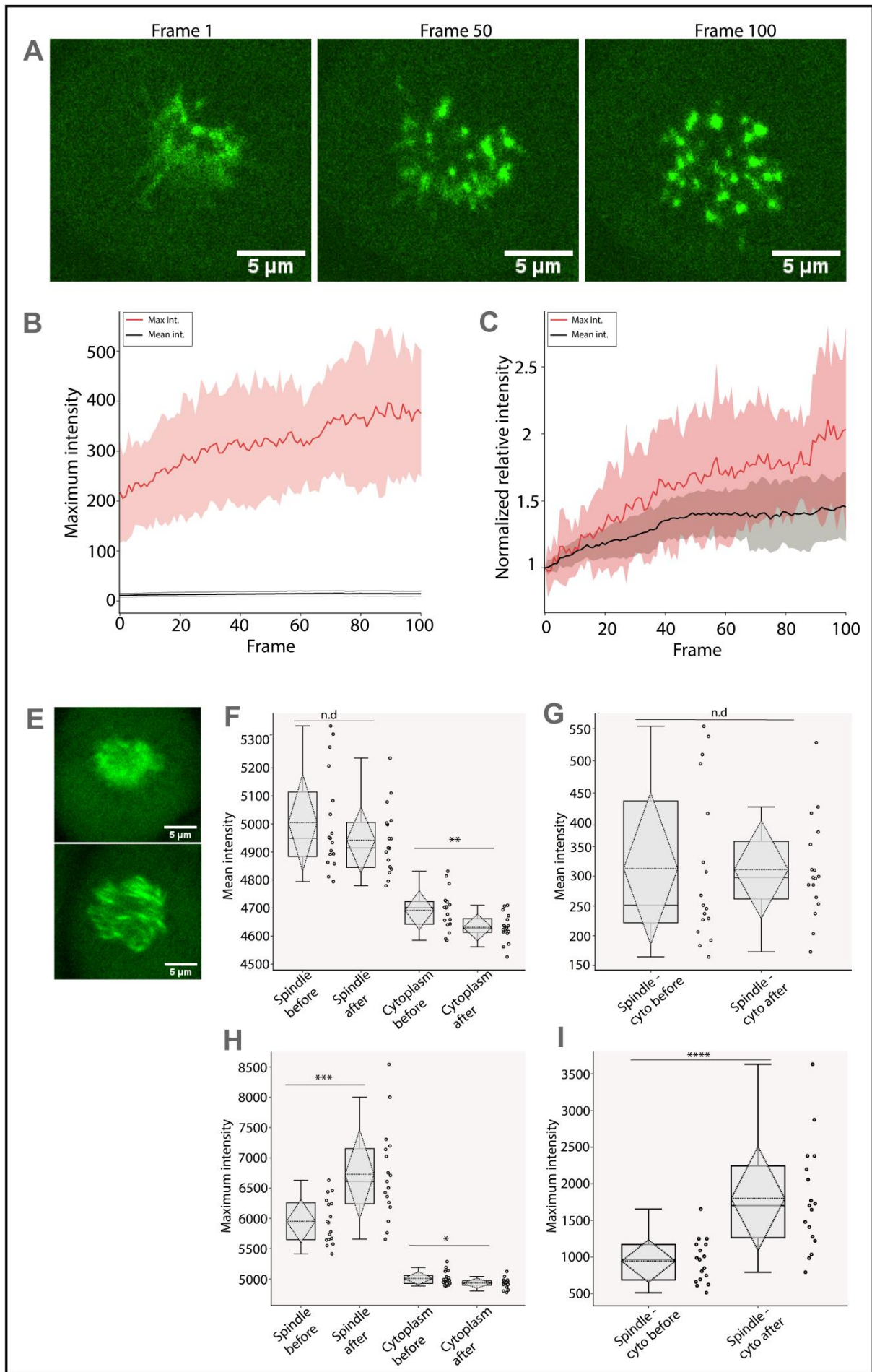
Figure 26. **A.** Redistribution of the signal in time lapse images of one middle plane of the vertical prometaphase spindle in time frames: 1, 50 and 100. **B.** Maximum intensity (red line) and mean intensity (black line) growth in the territory of the spindle in time. Red and gray surfaces around red and black lines represent standard deviation, while red and black line represent mean value. **C.** Normalized relative maximum (red line) and normalized relative mean (black line) intensity growth in time in the territory of the spindle. Growth comparison of mean and maximum intensity shows that maximum intensity grows more than mean intensity. **D.** Sum of the intensity of 41 slices of Z stack prometaphase vertical spindle taken before (upper image) and after T series (bottom image). **E.** Mean intensity of the whole spindle before and after T series is taken does not change, while mean intensity of the cytoplasm drops. **F.** Mean intensity of the spindle after substraction of the mean intensity of the cytoplasm shows no change before and after T series. **G.** Maximum intensity of the spindle grows signiffincantlly, while maximum intensity of the cytoplasm drops in value. **H.** After substracting the maximum intensity of cytoplasm from the maximum intensity of the spindle, maximum intensity of the spindle increases even more. Time interval between two frames was 5.4 seconds.

To study antiparalel microtubule bundle formation in greater detayl in HeLa PRC1-GFP cell line, intensity analysis of individual bundles was conducted. Most of the bundles labelled with PRC1 form in the homogenius area of the spindle, called the mist of PRC1, in time (**Figure 9 A**). Mesuring the mean intensity only in the small area of bundle formation (**Figure 27 A**) showed dramatic growth of intesnity in all 7 inspected bundles of the same spindle (**Figure 9 B**). Mean intensity of the bundle increases from 23.002 ± 2.465 to 87.537 ± 6.857 (p = 0.132 x 10^{-7}, n = 7). Mesuring the mean intensity in the small area immediatelly next to the inspected bundle showed intensity drop in time for all 7 analysed bundles of the same spindle. Mean intensity drops from 24.883 ± 2.699 to 5.534 ± 0.737 (p = 0.282 x 10^{-3}, n = 7) (**Figure 27 C**). That means that the mean intensity in the area of the bundle formation increased 4.145 ± 0.646 times, while the intensity in the area immediatelly next to the forming bundle droped to 0.209 ± 0.046 of the initial value (n = 6) (**Figure 27 D**). The correction on photobleaching was conducted by substracting the mean intensity of cytoplasm away from the intensities mesured in the spindle teritorry. These results suggest that the intensity growth in the area of bundle formation increased by gathering intensity around the area of bundle formation resulting in a drop of intensity. I called this fenomenum "bundle focusing". Also, mean intensity of the bundle started to grow just from the 25th frame, after the growth of intensity was rapid (**Figure 27 D**). Then followed the phase of a constant intensity, from the 40th to the

65th frame, and then again, intensity started to grow from the 65th to the 100th frame. This sugests that all the bundles of one spindle start to form at the same time point.
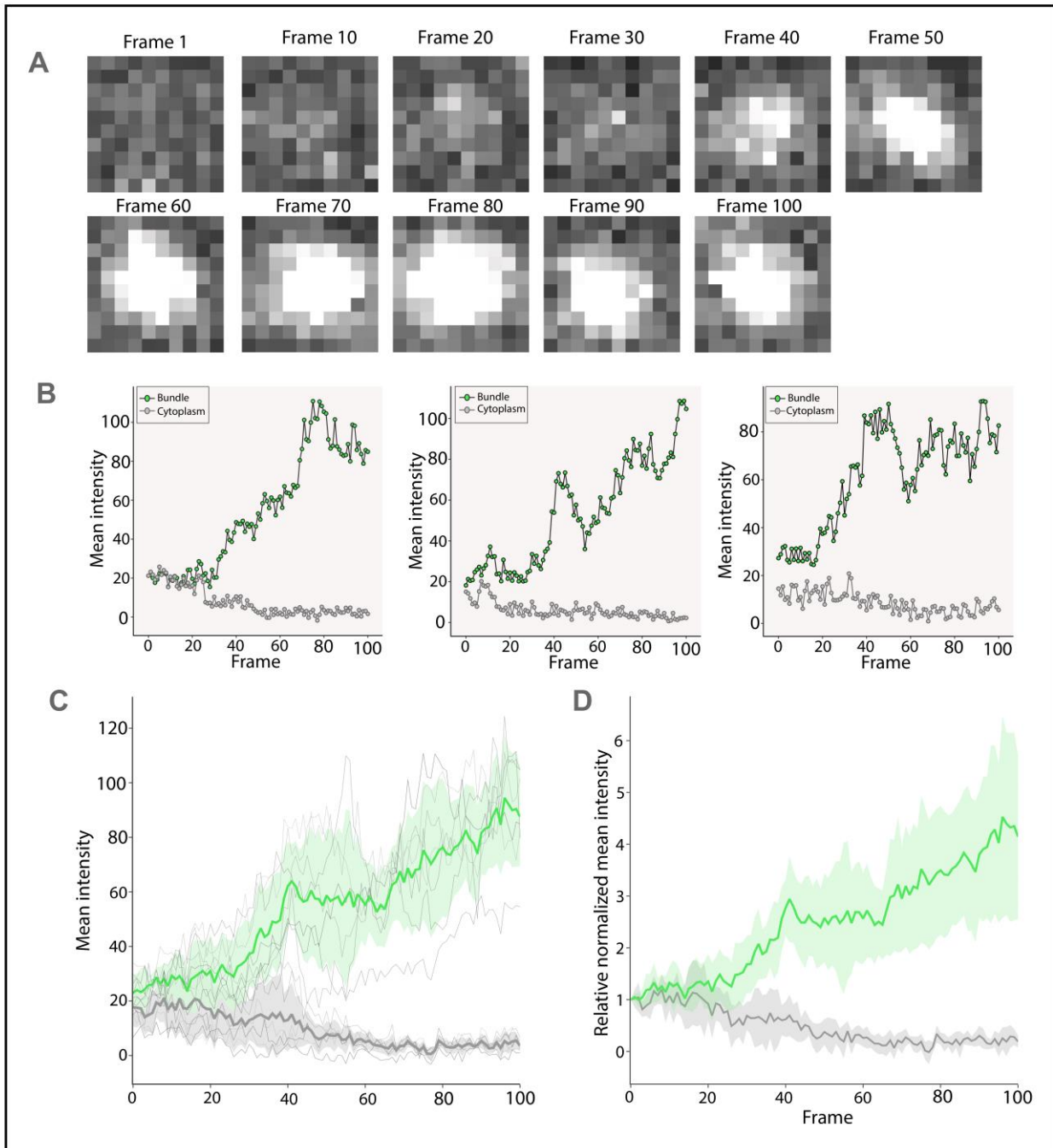
Figure 27. A. Time lapse of the area of individual bundle formation shows gradual increase of intensity (white color) in time. **B.** Mean intensity of the area of bundle formation (green line) and its associated region (grey line) for three individual bundles of the same cell. All three bundles show trend of bundle mean intensity increase and mean intensity drop of associated region. **C.** Plot of all 7 bundles mean intensity (green) and their associated regions (gray). All bundles show increase in the mean intensity while associated region shows a drop in the mean intensity. **D.** Relative normalized mean intensity of the area of bundle formation

and associated area shows the fold increase of four times. Green and gray line represent the mean, while green and gray surfaces represent standard deviation. Time interval between two frames was 5.4 seconds.

To see the intensity distribution inside the cross section of the bundle, line intensity profile analysis was performed. The center of the bundle shows the highest intensity, while the intensity is smaller towards the periphery of the cross section (**Figure 28 A, B**). 3D surface bundle representations suggest that the core of the bundle forms first. Then the bundle forms by intensity growth in the middle of the bundle. Intensity of the bundle cross section shows Gaussian distribution of intensity (**Figure 28 C**).
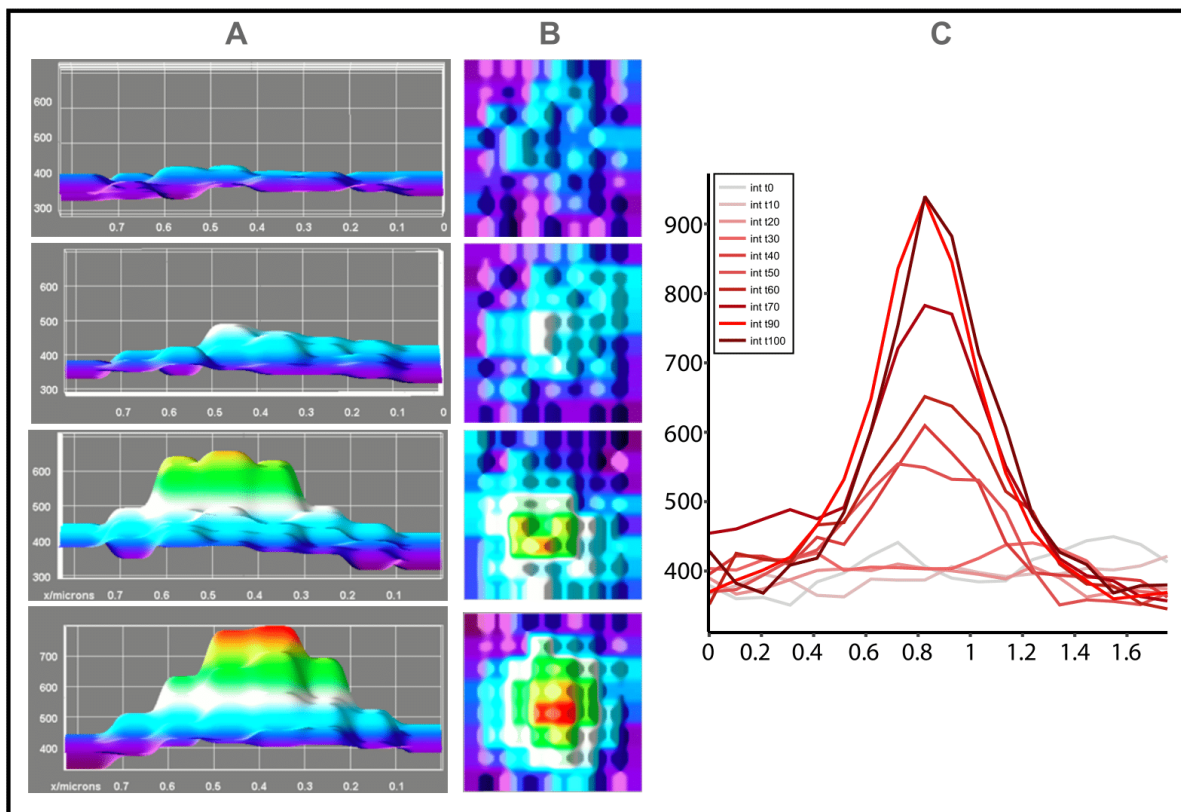
Figure 28. A. 3D surface plot heat map of selected time frames of bundle formation - horizontal view shows that the bundle forms in an uniform region from mist, forming the core first, and then expanding and growing in intensity. **B.** 3D surface plot heat map of selected time frames of bundle formation – vertical view shows the maximum intensity in the middle of the cross section of the bundle (red color). **C.** Line intensity profile of the bundle cross section shows the gradual formation of the bundle in every 10th frame. Line intensity profile shows Gaussian distribution of the intensity in cross section of the bundle. Time interval between two frames was 5.4 seconds.

Except for the bundle focusing *de novo* from the mist, it has been observed that some fully focused PRC1 labeled bundles fuse with each other (**Figure 29 A, B, C**). Sometimes more than 2 bundles fuse to form one larger bundle of higher intensity (**Figure 29 D**). That phenomenon was called bundle fusion. Except for the bundle fusion, it was observed that some bundles form and focus outside the spindle mist and are then retrieved to the territory of the spindle. This phenomenon was called bundle retrieval (**Figure 29 E**). So, three mechanisms were proposed for bundle formation in prometaphase spindle: *de novo* bundle focusing, bundle fusion and bundle retrieval. Next, to determine the frequency of those events, time lapse videos of vertical prometaphase cells were inspected. Frequency of the *de novo* bundle focusing was 1.883 ± 0.184 events per minute. Frequency of bundle fusion was 0.526 ± 0.039 events per minute. Bundle retrieval was the rarest event with frequency of 0.280 ± 0.071 per minute (n = 20) (**Table 1**).

Table 1. Mechanisms of bundle formation and their frequency.

Mechanism of bundle formation	Frequency of events Number of events/min
De novo focusing	1.883 ± 0.184
Bundle fusion	0.526 ± 0.038
Bundle retrieval	0.280 ± 0.071
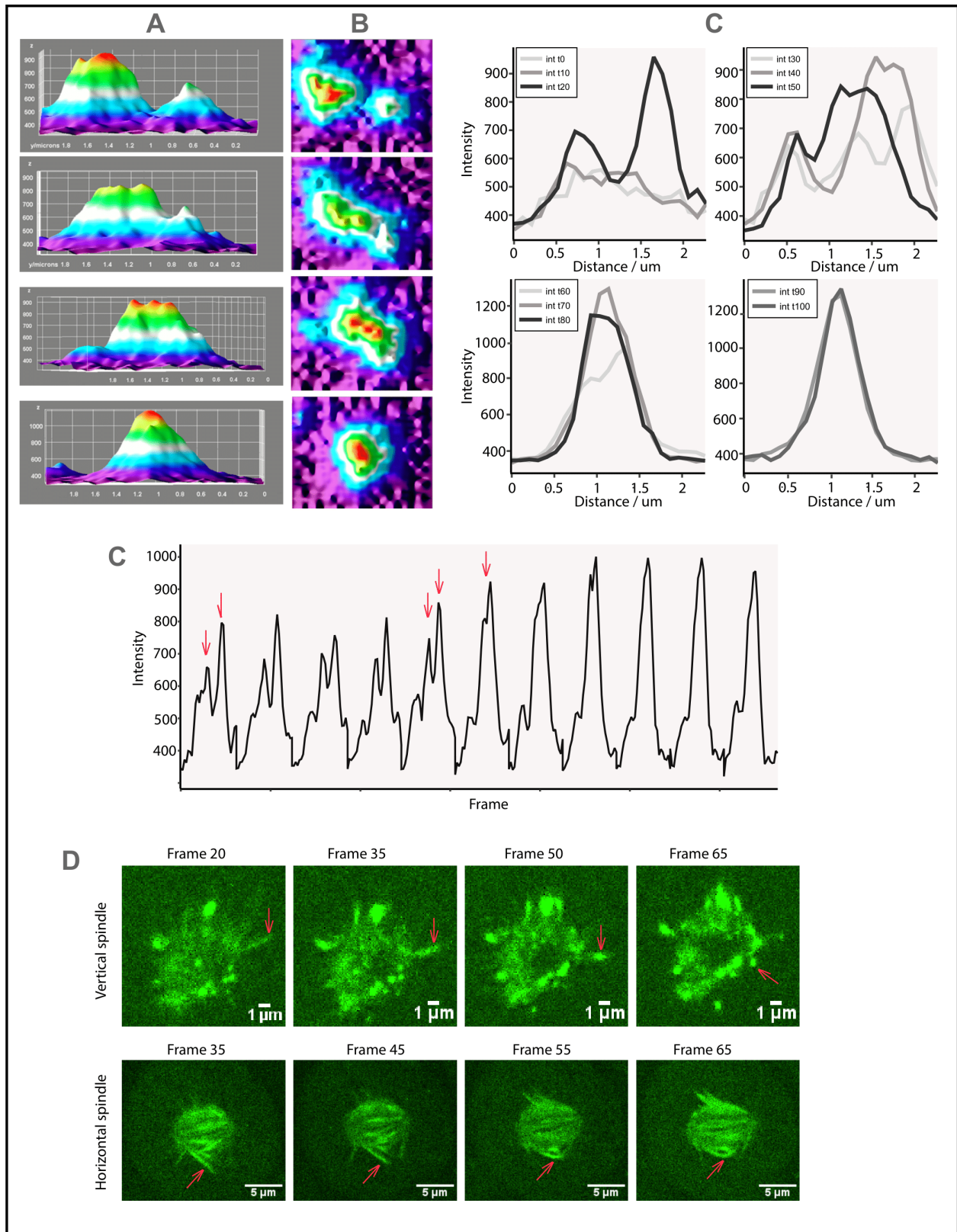
Figure 29. A. 3D surface plot intensity map shows fusion of two focused bundles in horizontal view. **B.** 3D surface plot intensity map shows fusion of two focused bundles from above. **C.** Four line intensity plot profiles shows fusion of the bundles in 100 time frames, every 10th frame. **D.** Close up view of line intensity plot profile shows bundle focusing in every frame in selected time frame. Every minimum separates two different time frames taken

every 5.4 seconds. **E.** Bundle retrieval process of bundle focused outside the spindle territory in selected time frames. Upper image sequence shows process in vertical spindle and image sequence bellow shows a cell with horizontal spindle. Red arrows point at retrieving bundle. Time interval between two frames was 5.4 seconds.

It was observed that not all spindles had the uniform frequency of *de novo* focusing, fusion and retrieval events. Some cells showed small number of fusion events and some didn't show any retrieval event at all. In some cells, bundles formed predominantly by *de novo* focusing, while others had a significant number of fusion or retrieval events while smaller number of *de novo* focusing. It seems that mechanisms of the spindle formation were connected with the number of bundles that protrude outside the spindle territory. I called that "roughness" of the spindle. Therefore, cells were grouped in three groups based on the roughness of the spindle. Group I were cells that had the spindle with most of the bundles protruding outside the spindle territory (**Figure 30 A**). Group III were cells without any protruding bundles. Group II cells showed morphology between Group I and III. Strikingly, group I cell spindles were short in length; 8.071 ± 0.229 μm (n = 7). Group II cell spindles were longer than group I cell spindles; 9.636 ± 0.192 μm (p = 9.216×10^{-5}, n = 11). Group III cell spindle length was 11.429 ± 0.385 μm (n = 14), longer than group I cell spindles (p = 1.221×10^{-5}) and group II cell spindles (p = 0.851×10^{-3}) (**Figure 30 B**). Also, group I, II and III cell spindles showed differences in chromosome coverage. In vertical cross section, chromosomes encircle spindle in an open circle in the early prometaphase and percentage of coverage is differing between these three groups. In Group I cells spindle cross section chromosome coverage was 68.843 ± 1.498 % (n = 7). Group II cell spindles had coverage of 83.367 ± 1.013 % (n = 11), significantly higher than group I cell spindles (p = 3.170×10^{-7}). Group III cell spindles had coverage of 92.109 ± 1.106 (n = 14), higher than group I (p = 1.684×10^{-10}) and group II cell spindles (p = 8.743×10^{-6}) (**Figure 30 C**). There is a positive correlation between the spindle chromosome coverage and spindle length ($R^2 = 0.519$, p = 0.335×10^{-5}). These groups showed different bundle formation mechanism frequency. Group I showed 49.106 ± 2.315% focusing, 25.502 ± 2.592 % retrieval, 25.392 ± 2.672 % (n = 6) fusion events during spindle assembly. Group II showed 67.371 ± 3.767 % focusing, 8.965 ± 3.852 % retrieval, 23.664 ± 4.104 % (n = 6) fusion events during spindle assembly. Group III showed 82.324 ± 2.032 % focusing, 1.661 ± 0.915 % retrieval, 16.016 ± 1.651 % (n = 9) fusion events in the spindle assembly (**Figure 30 E**). In Group I frequency of the events included 1.315 ± 0.148 focusing per minute, 0.685 ± 0.101 retrieval per minute, 0.644 ± 0.034 fusion per minute (n = 6). Group II frequency of events: 1.556 ± 0.269 focusing per minute, 0.178 ± 0.057 retrieval per minute,

0.533 ± 0.096 fusion per minute (n = 5). Group III shows 2.333 ± 0.323 focusing per minute, 0.037 ± 0.023 retrieval per minute, 0.444 ± 0.064 fusion per minute (n = 6).
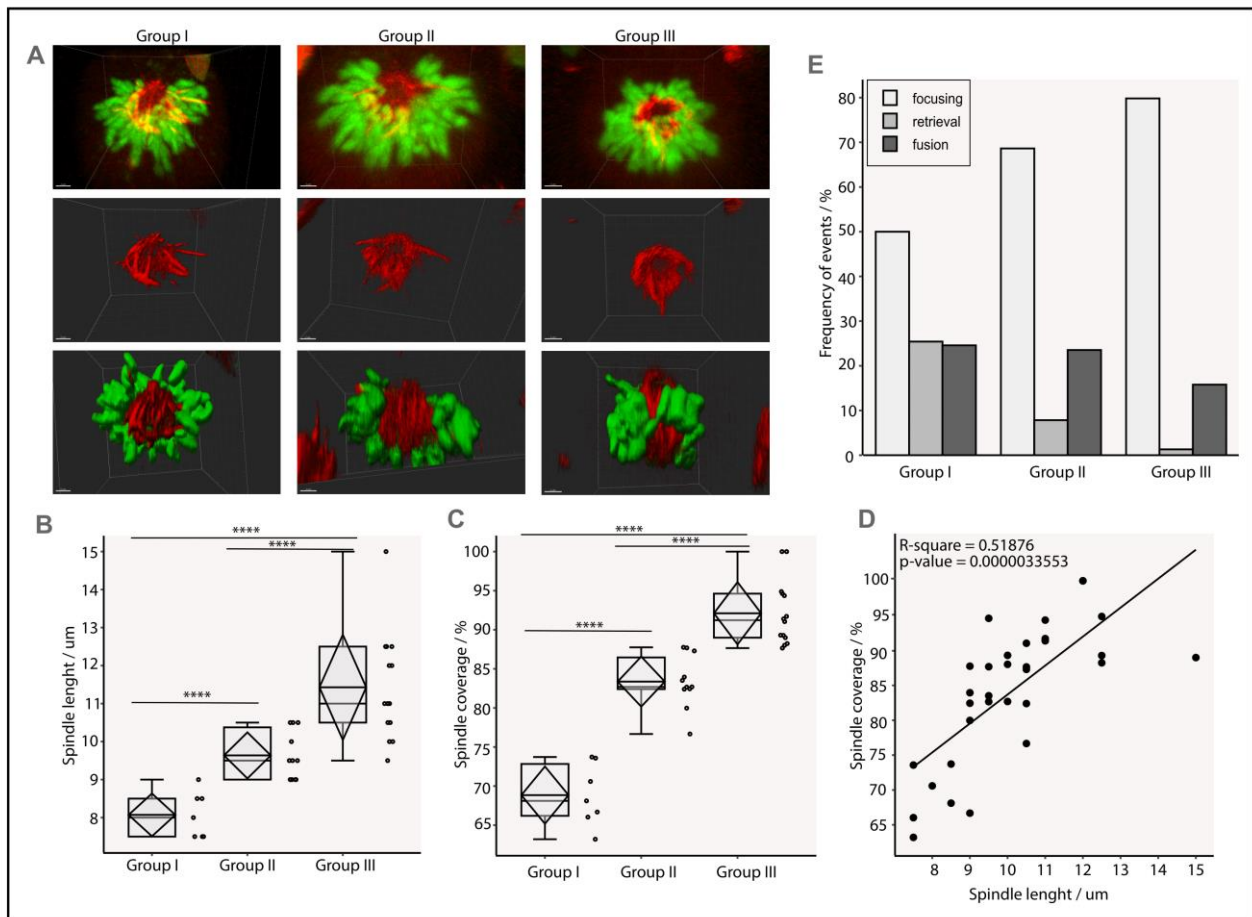
Figure 30. A. 3D images showing 3 groups of cells. First row shows cross section of prometaphase spindle. Second row shows only front view of the spindle, and third row shows upper view of the spindle. Group I shows a lot of protruding bundles in the cross section and a low coverage of the spindle with chromosomes. Group II shows less protruding bundles and more closed chromosome ring, while group three shows no protruding bundles and a closed chromosome ring. **B.** Group I cells have shortest spindles, group II longer and group III cells have the longest spindle. **C.** Spindle coverage is the lowest in group I cells and the highest in group III cells. **D.** Spindle coverage with chromosomes positively correlates with the spindle length. **E.** Three groups of cells show different incidence of bundle forming events.

As the bundles form by one of three mechanism determined above, their number increases in time from 7.211 ± 1.176 to 24.789 ± 1.883 (p = 0.805 x 10^{-10}, n = 19) (**Figure 31 A.**) Most of the cells had few bundles formed in part of the spindle where chromosome ring is open. The other part of the spindle which is encircled by chromosomes shows focusing of the spindle later as time passes. Most of the bundles start to form at the same time (**Figure 31. A, B, C**).
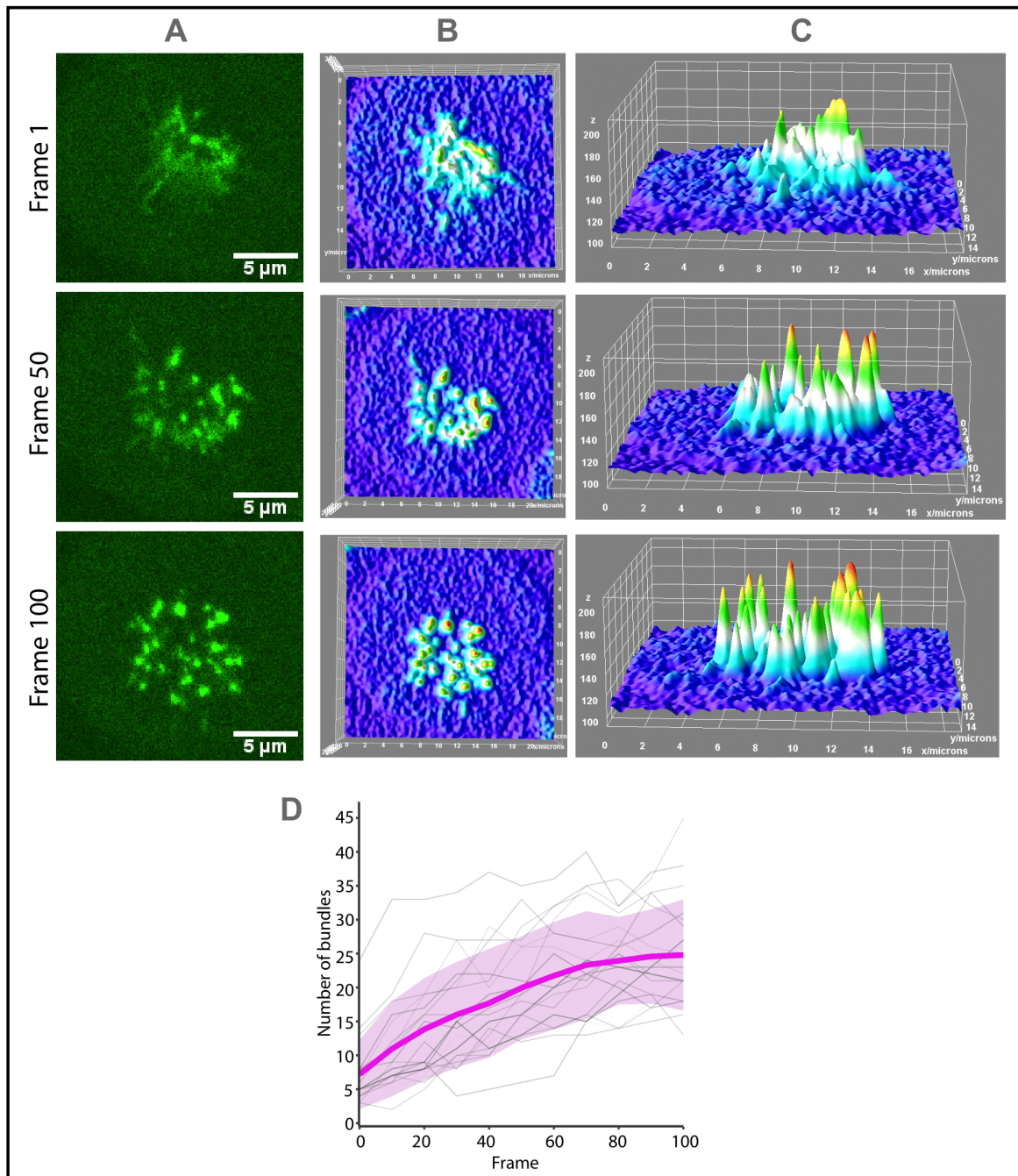
Figure 31. Number of bundles is increasing in time. **A.** Middle plane of the prometaphase spindle shows increasing number of bundles. **B.** Top view of 3D surface plot showing intensity increase of individual bundles and increase in their number in the spindle territory. **C.** Side view of the increase in the number of bundles and their intensity. **D.** Number of bundles increasing in time. Time interval between two frames was 5.4 seconds.

To see what is happening before the bundle starts to focus, intensity profiles of the mist are made. In the time interval before the bundles start to form synchronously, cross section of the prometaphase spindle shows local dynamic changes in intensity. Small peaks of higher intensity arise at one instant and then disappear and appear in another location, showing their

dynamic instability. Then at one instant one of these intensity peaks is stabilized and forms a bundle (**Figure 32**).
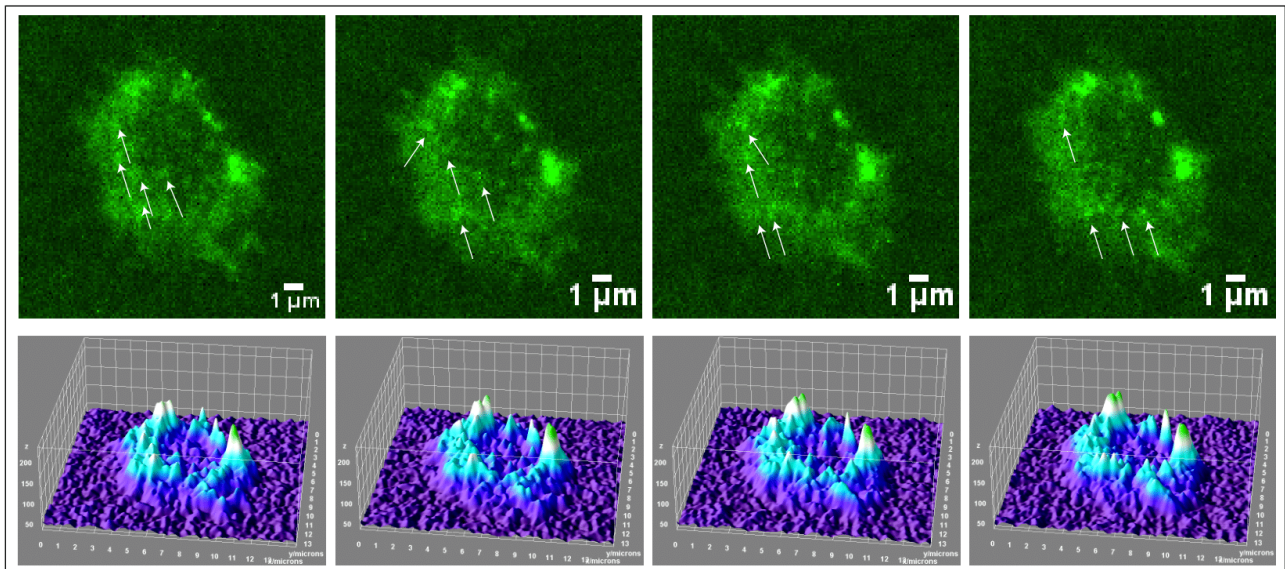
Figure 32. A. The middle plane of the prometaphase spindle in first 4 time frames (from left to right) shows transient formation of small local peaks of higher intensity. **B.** 3D surface plot of frames showed above. White arrows represent small peaks of higher intensity. Time interval between two frames was 5.4 seconds.

4.3 Inhibition of lateral attachment of chromosomes on the prometaphase spindle

To determine whether lateral attachment of kinetochores to the microtubules has any role in antiparallel bundle formation, aurora B kinase was inhibited using specific aurora B inhibitor, Barasertib (AZD1152-HQPA) in 300 nM concentration. When Barasertib was applied acutely (acute inhibition), initial prometaphase spindle was no different in appearance from the wild type. Vertical prometaphase spindles in chronically inhibited aurora B were somewhat different in appearance (**Figure 33 A**). Their intensity was lower in comparison to the cytoplasm and there was less, or no bundles formed. Also, chromosomes were clearly not attached to the spindle. That ring like chromosome collar that appeared unattached to the spindle, but still around the mist of PRC1 protein was one indication that the spindle is vertical in orientation and in the prometaphase. In acute aurora B inhibition, time lapse after inhibitor addition revealed disturbed bundle formation, especially in the bottom part of the spindle that is encircled by the chromosomes (**Figure 33 B**). If the aurora B inhibitor is added half an hour before imaging (chronic inhibition), then there is no bundle formation at all (**Figure 33 B**).
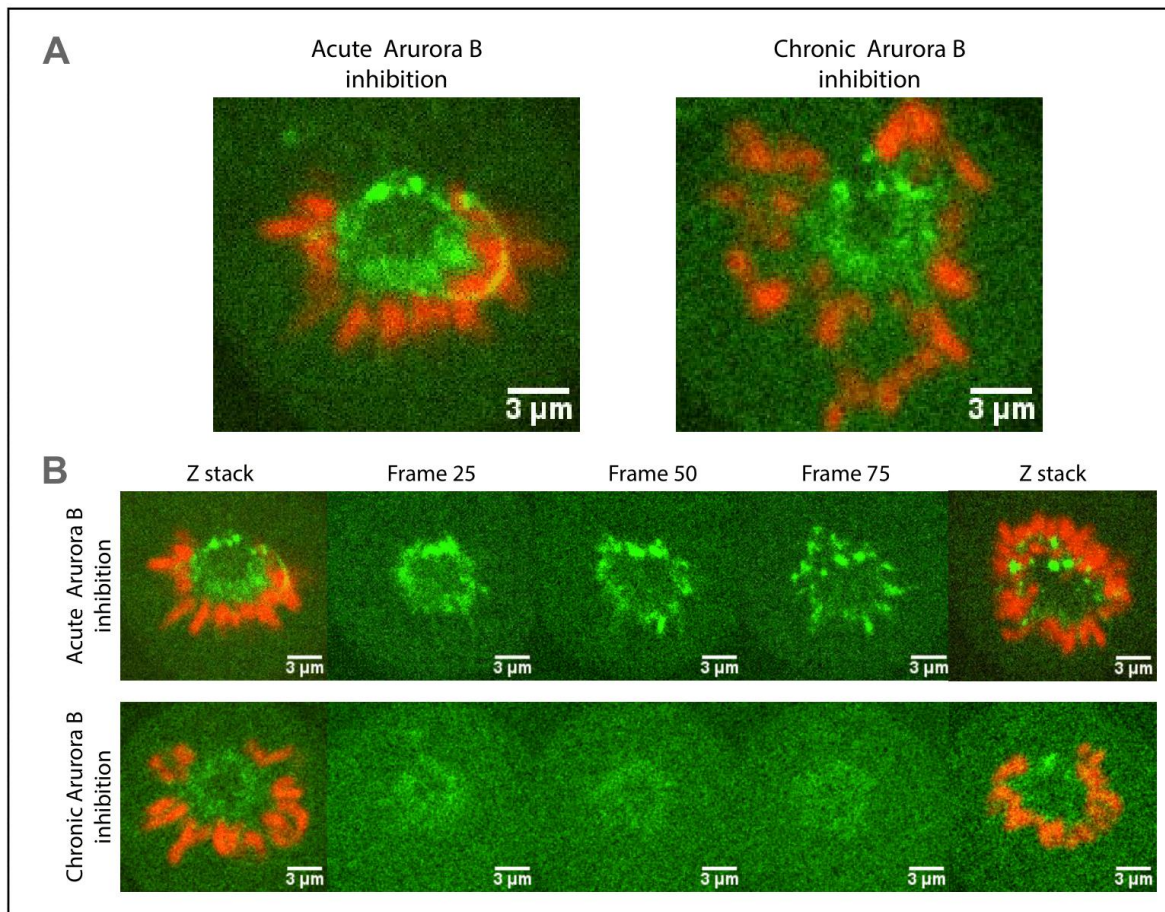
Figure 33. A. Vertical prometaphase spindle in HeLa PRC1-GFP cell line before acute addition of aurora B inhibitor (left), and vertical prometaphase spindle formed when aurora B is chronically inhibited (right). Chromosomes are not attached to the spindle in chronically inhibited aurora B kinase. **B.** Time lapse of the bundle formation in vertical prometaphase spindle in acute inhibition of aurora B (upper image sequence) and in chronic inhibition of the aurora B (bottom image sequence). In acute inhibition there is disturbed bundle formation, while in chronic inhibition there is no bundle formation. Time interval between two frames was 5.4 seconds.

HeLa PRC-GFP cells in which aurora B is chronically inhibited, imaged from the nuclear envelope breakdown, show that spindle has difficulty forming antiparallel bundles. There is total absence of antiparallel bundle formation and spindle seems stalled in the phase before nuclear envelope breakdown. In vertical orientation it seems that spindle does not show any changes in the formation before and after NEBD. Chromosomes are arranged around the spindle and it seems that there is no extensive lateral attachment to the spindle, while in the wild type, chromosomes are tightly bound to the spindle and bundles extensively focus. Focusing of the bundles is even more evident on vertically oriented spindle where the formation of the mist of PRC1 after NEBD is evident (**Figure 34**).
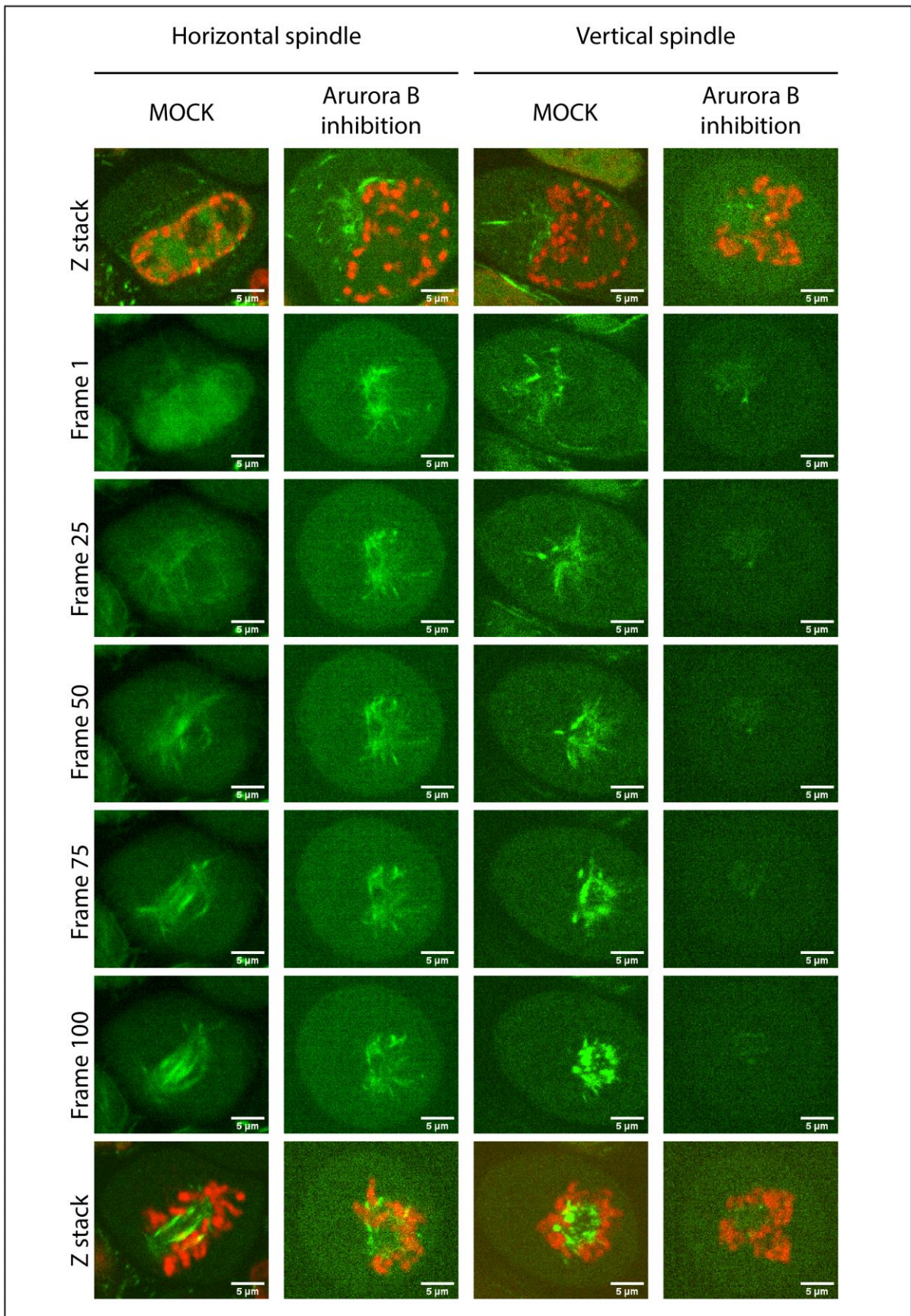
Figure 34. Spindle formation in HeLa PRC1-GFP cell line. Image sequences from the nuclear envelope breakdown to the late prometaphase in cells treated with aurora B inhibitor and non-treated cells (MOCK). Spindle formation in horizontal orientation shows extensive

focusing of antiparallel bundles between poles of the spindle in wild type cells, while formation of bundles is stalled in aurora B treated cells. The same is evident in vertical spindle view. There is formation of the mist of PRC1 and bundles in wild type cells, but not in aurora B inhibitor treated cells. PRC1-GFP protein is colored green and DNA is colored red with SiR-DNA dye. Time interval between two frames was 10 seconds.

The squash analysis showed that in cells in which aurora B is inhibited acutely, number of segmented surfaces still grows (**Figure 36 A**) from 4.75 ± 0.94 in the first frame to 12 ± 1.45 in the last frame ($p = 0.9 \times 10^{-3}$, n = 8) (**Figure 36 C**) (in wild type from 5.300 ± 0.760 (n=10) in the first frame to 17.000 ± 1.461 (n=6) in the last frame) indicating that there is a certain degree of segmentation as in the wild type. In chronic aurora B inhibition number of segments goes from 6.857 ± 1.292 (n = 14) in the first frame to the 6.231 ± 1.302 ($p = 0.736$, n = 13) (**Figure 36 D**) in the last frame, so there is no change in the number of segments (**Figure 36 B**).
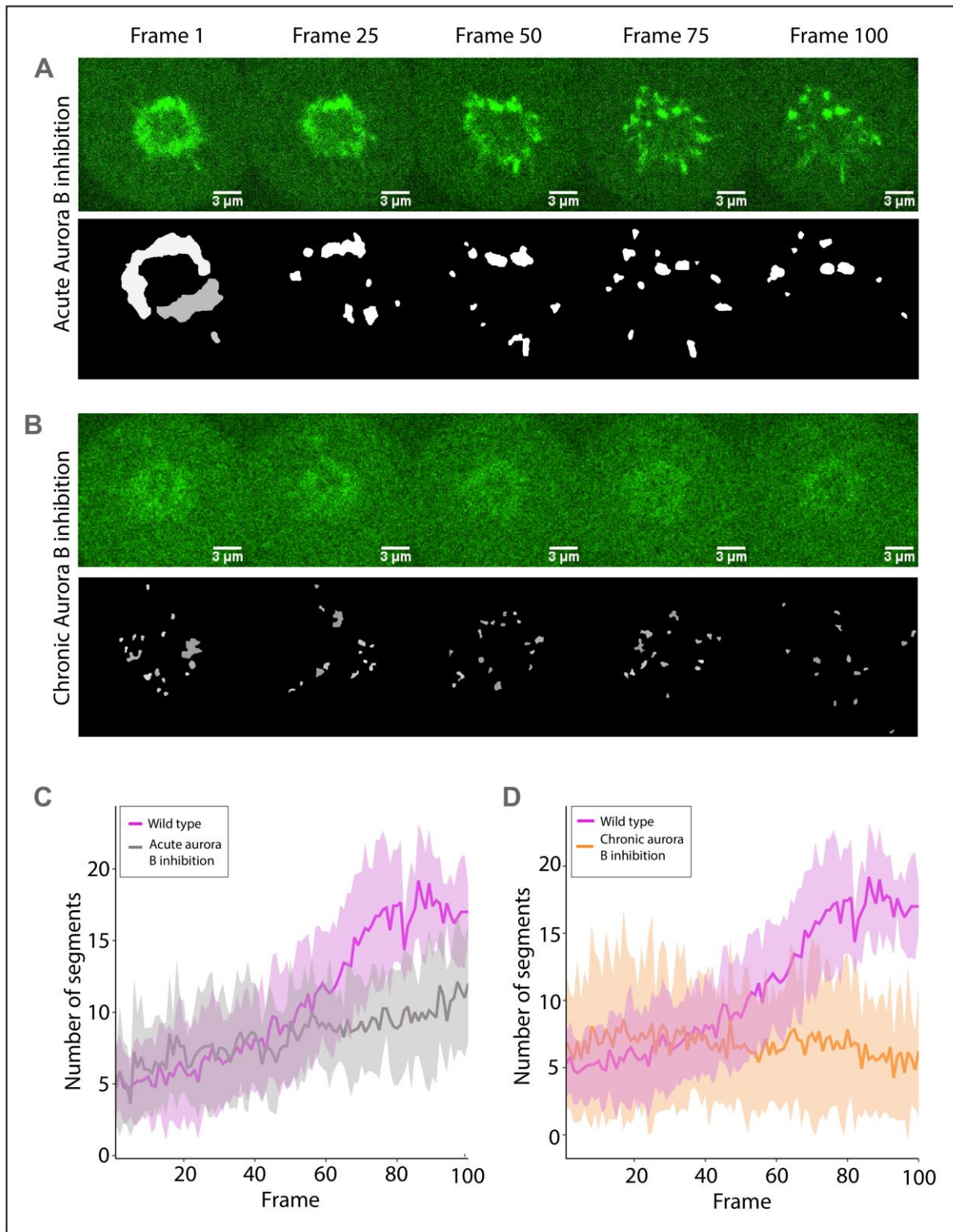
Figure 35. A. Squash analysis of aurora B acute inhibition. Number of segments increases because there is a certain degree of segmentation. **B.** Squash analysis of aurora B chronic inhibition. It seems that the number of segments does not change in time. Also the size of the surfaces does not seem to change and is smaller than in the wild type and acute aurora B inhibition. **C.** Plot of increasing number of segments for acute aurora B inhibition shows increasing number of segments in time, but the final number of segments is smaller than in the

wild type. **D.** Plot of the number of segments changes in time for chronic aurora B inhibition and shows no increase in the number of segments. Number of segments starts the same as for the wild type, but then it is not changing in time. Time period between two frames is 5.4 seconds. Line represents mean and surface around is the standard deviation.

In acute aurora B inhibition, the size of the segments drops from 499.004 ± 155.099 pixels to 68.781 ± 9.138 pixels (p = 0.015, n = 8), closely resembling the wild type (460.089 ± 151.375 pixels (n = 10) to $51.943 \pm 12,056$ pixels (n = 6)) (**Figure 36 A**). On the other hand, mean size of segments in cells with chronically inhibited aurora B is smaller than in the wild type but the drop of value in time is not significant. Size starts with 150.665 ± 53.735 pixels (n = 14) in the first frame and slightly drops to 76.152 ± 24.669 pixels (p = 0.231, n = 13) (**Figure 36 B**).

Mean intensity of the segments in acutely inhibited Aurora B is lower already in the start in regards to the wild type: 18.467 ± 2.817 (n = 8) versus 25.549 ± 4.148 (p = 0.946×10^{-3}, n = 10), and grows slightly, but not significantly, 21.639 ± 3.856 (p = 0.821, n = 8) in the last frame, while in wild type intensity grows (52.402 ± 2.963 in the last frame) (p = 0.233×10^{-8}, n = 6) (**Figure 36 C**). At the end of imaging, mean intensity of segments in the last frame is significantly lower in acute aurora B inhibition regarding the wild type (p = 0.212×10^{-8}). Mean intensity of the segments in chronically inhibited aurora B is also lower in start in regard to the wild type (p = 0.917×10^{-8}). Mean intensity of segments does not change significantly; from 15.601 ± 0.809 in the first frame to 16.279 ± 1.119 (p = 0.621, n = 11) in the last frame (**Figure 36 D**). This indicates that there is no growth of segment intensity in time in cells in which aurora B is inhibited half an hour before the spindle formation.
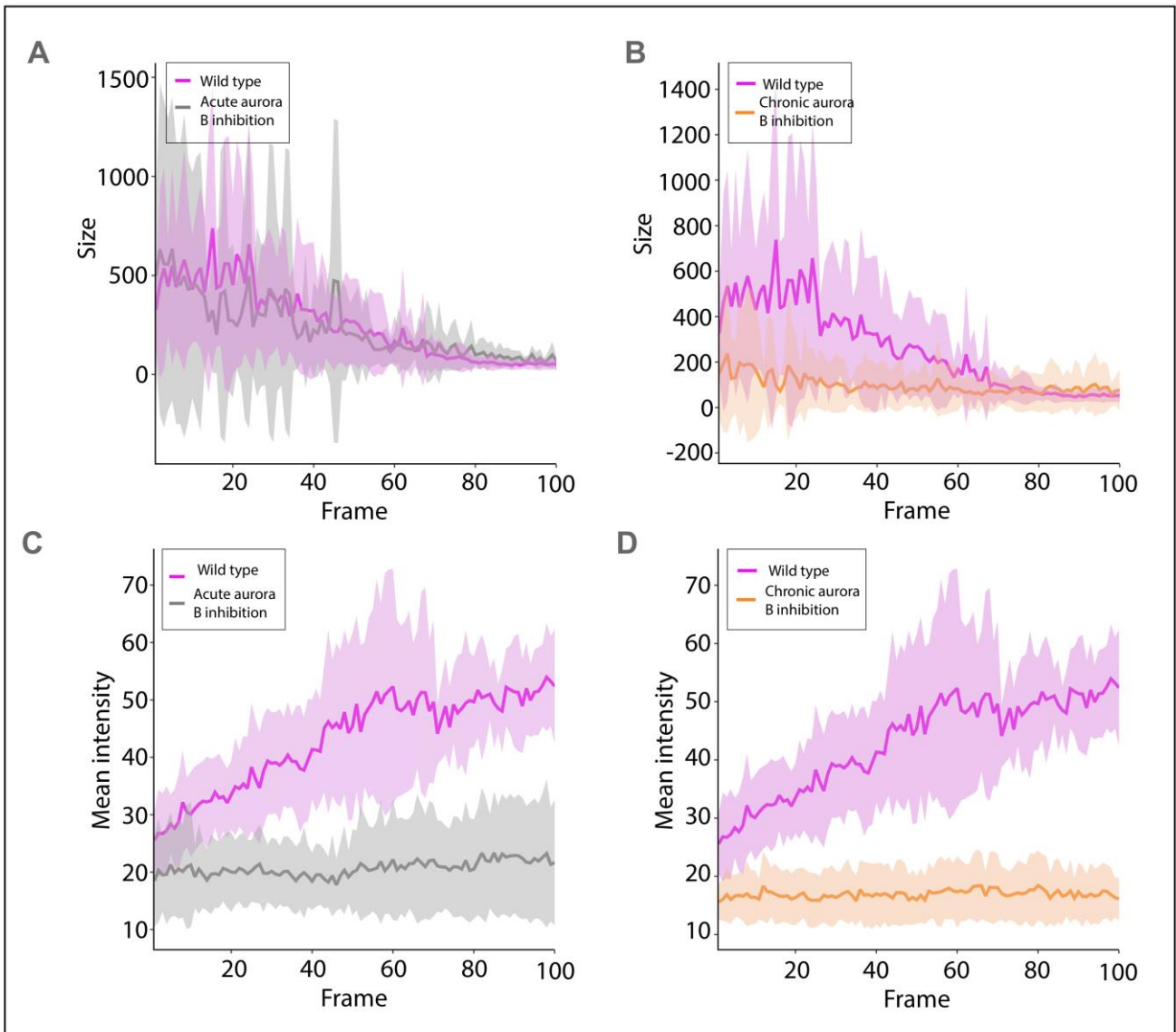
Figure 36. Line plot showing mean size and mean intensity of segments after squash analysis in HeLa PRC1-GFP cell line. **A.** Line plot showing mean size of the segments in every time frame in acutely inhibited aurora B cells and wild type. Size of the segments in acutely inhibited aurora B cells drops in time similar like in wild type cells. **B.** Line plot showing mean size of segments in every time frame in chronically inhibited aurora B cells and wild type. Size of the segments in chronically inhibited aurora B cells is smaller than in wild type and drops only slightly in time. **C.** Line plot showing mean intensity of segments every time frame in acutely inhibited aurora B cells and in wild type. Intensity of segments is smaller in regard to the wild type and increases only slightly in time. **D.** The same line plot for chronically inhibited aurora B cells shows smaller intensity segments and no growth of intensity in time. Time period between two frames is 5.2 seconds. Line represents mean and surface around is the standard deviation.

In cells in which aurora B is inhibited acutely, size distribution of segments shows a population of large segments that fragments in segments of smaller size in time (n = 8). In comparison to the wild type, size drop of the largest segments seems to be linear, while in wild type it looked like reverse sigmoid curve (**Figure 37 A**). On the other hand, size distribution in time for chronically inhibited aurora B cells shows uniform distribution of sizes in time, indicating that no classical segmentation characteristic for wild type is present (n = 12) (**Figure 37 B**).
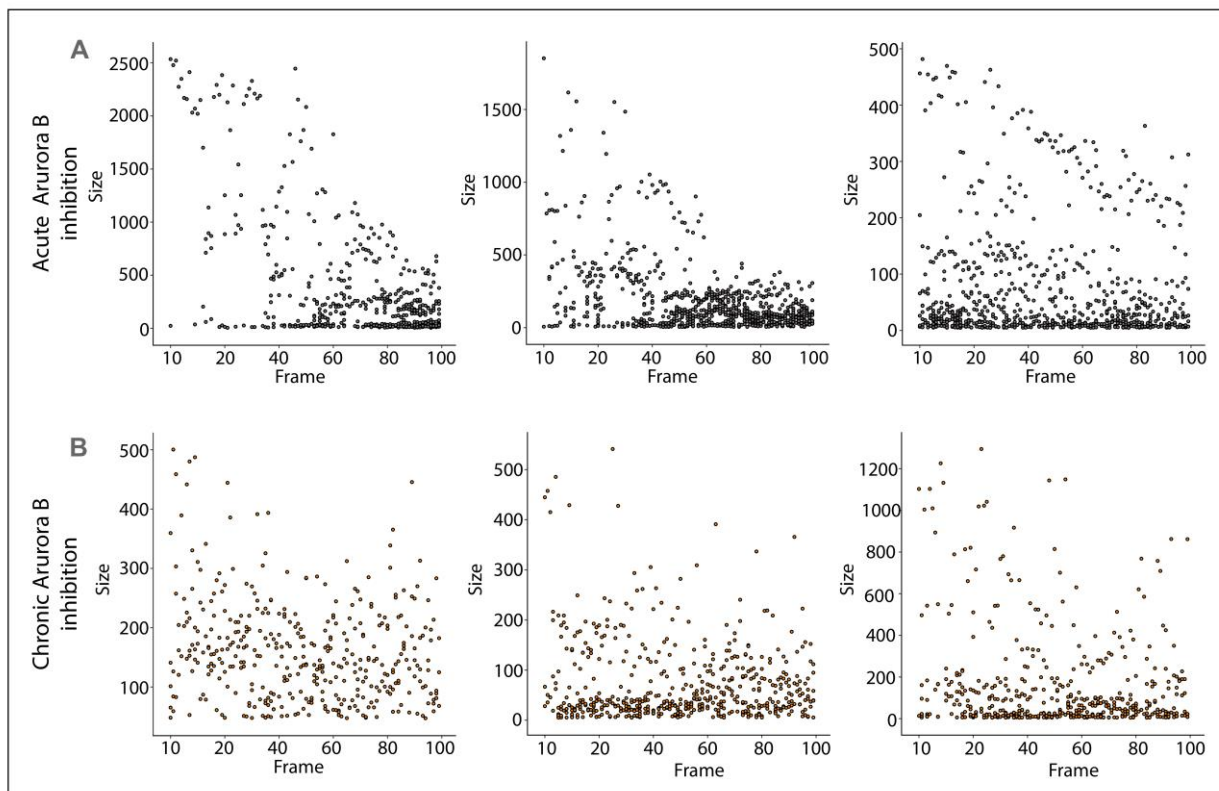
Figure 37. A. Scatter plot of 3 representative cells with acutely inhibited aurora B. Size of largest segments drops in time linearly. **B.** Scatter plot of 3 representative cells with chronically inhibited aurora B. Size of segments shows uniform distribution in all time frames. Time period between two frames is 5.2 seconds.

Segment intensity distribution in time shows a slight growth in the cells with acutely inhibited aurora B, but much smaller than for the wild type (**Figure 38 A**). In cells with chronically inhibited aurora B there is no change. In some cells there is even a slight drop of segment intensity in time (**Figure 38 B**).
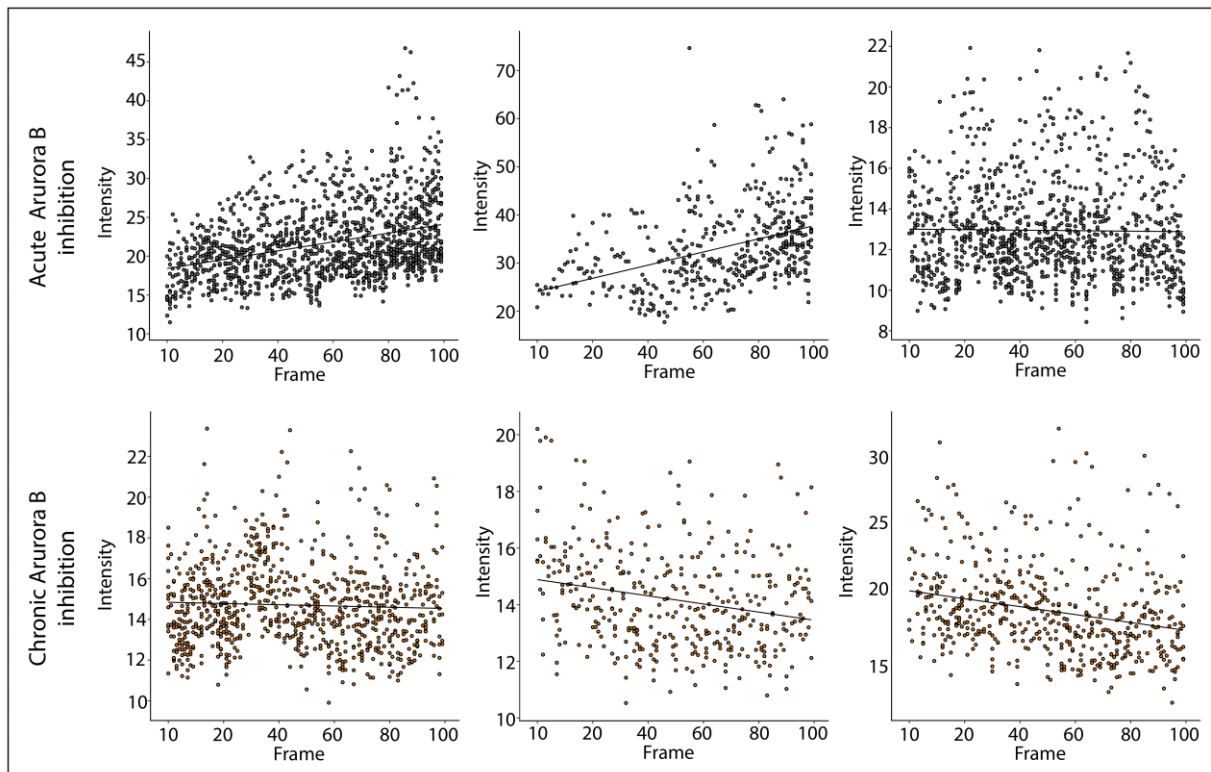
Figure 38. A. Scatter plots of 3 representative cells with acutely inhibited aurora B. Mean intensity of segments slightly increases in most cells with acutely inhibited aurora B. **B.** Scatter plots of 3 representative cells with chronically inhibited aurora B. Mean intensity of segments slightly decreases in most cells. Time period between two frames is 5.2 seconds.

Measuring intensity of the middle slice of vertical prometaphase spindle territory showed that mean intensity of acutely inhibited aurora B spindles drops slightly in time from 7.088 ± 0.989 (n = 8) to 5.283 ± 1.526 (p = 0.338, n = 8) (**Figure 39 A**). When the mean intensity is normalized to the first frame, mean intensity drops in time to 0.677 ± 0.084 (n = 8) of the initial value, while in the wild type mean intensity grows (**Figure 39 B**).

Mean intensity of the middle slice of the vertical prometaphase spindle territory in cells with chronically inhibited aurora B is 3.107 times lower (p = 0.163×10^{-6}) than in the wild type from the start of imaging and drops even more, although slightly, in time; from 3.615 ± 0.735 in the first frame (n = 13) to 2.041 ± 0.715 (p = 0.139, n = 12) in the last frame (**Figure 39 C**). When normalized to the first frame, data shows that mean intensity drops to 0.547 ± 0.076 of the initial value (n = 11) (**Figure 39 D**). In both treatments mean intensity drops in time, while in the wild type mean intensity grows, indicating that there is no concentration of signal in middle slice of the spindle territory.

Maximum intensity of the spindle territory in the middle plane in acutely inhibited aurora B cells is 2.187 time lower in the first frame in regards to the wild type and shows no dramatic change in time; from 99.525 ± 21.715 (n = 8) in the first frame to 91.705 ± 25.355 (p = 0.818, n = 8) (**Figure 39 E**). Normalized maximum intensity shows that maximum intensity value at the end of the imaging makes 0.905 ± 0.108 (n = 8) value of initial value, dramatically smaller than in the wild type (2.033 ± 0.240 times higher) (**Figure 39 F**).

Maximum intensity drop is even more dramatic in chronic aurora B inhibition in regards to the wild type: values in the first frame show even smaller maximum intensity values; 51.934 ± 6.934 (4.192 times smaller than in the wild type) (p = 0.777×10^{-12}, n = 13) and slight, but not significant drop to the last frame; 45.661 ± 6.498 (p = 0.518, n = 12) (**Figure 39 G**). So, it is evident that concentration of signal and focusing in Barasertib treated cells is not appearing. Normalized maximum intensity shows that maximum intensity value at the end of the imaging makes 0.855 ± 0.06 (n = 12) value of initial value in cells with chronically inhibited aurora B (**Figure 39 H**).
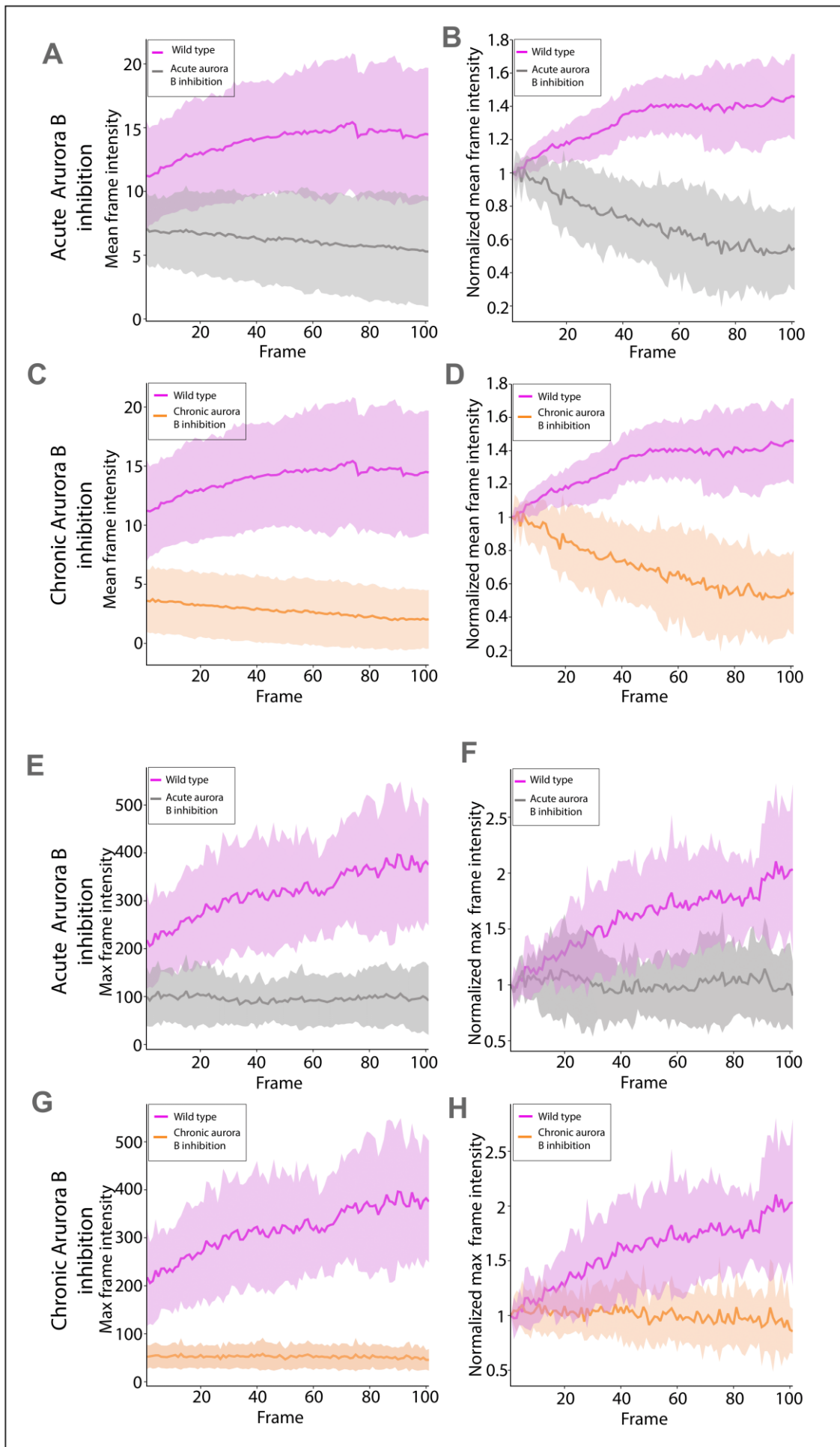
Figure 39. Mean and maximum intensity of the spindle territory in the middle plane in HeLa PRC1-GFP cells. Intensities are measured for PRC1-GFP channel only. Pink line represents mean value of wild type cells, gray lines represent cells with acutely inhibited aurora B and orange lines cells with chronically inhibited aurora B. Surfaces around lines represents standard deviation. **A.** Spindle acutely treated with aurora B inhibitor shows a slight reduction of mean intensity (gray line) of the spindle territory in time, while the mean intensity of the wild type grows (pink line). **B.** Normalized relative mean spindle intensity of acutely treated aurora B spindle (gray) and wild type (pink) shows the relative growth of intensity. **C.** Mean intensity of the chronically inhibited aurora B (orange) drops in time. **D.** Normalized relative mean intensity from plot D shows relative growth of intensity. **E.** Maximum intensity of middle slice of vertical prometaphase spindle acutely treated with aurora B inhibitor shows no change in time (grey line). **F.** Normalized maximum intensity of the middle slice in spindles acutely treated with aurora B inhibitor. **G.** Maximum intensity of the middle slice in spindles chronically treated with aurora B inhibitor slightly decreases over time. **H.** Normalized intensity of maximum intensity from plot G. Time interval between two frames is 5.4 seconds.

Measuring the mean intensity of the whole spindle in HeLa PRC1-GFP, before and after T series showed no changes in the mean intensity in acute or chronic addition of aurora B inhibitor (**Figure 40 A**). In acute inhibition, mean intensity was not significantly changed; 156.019 ± 21.468 before, and 109.152 ± 15.139 after T series was taken (p = 0.059, n = 10). For chronic inhibition, intensity before T series was taken, was 82.067 ± 13.520 (n = 13) and 79.160 ± 15.336 (n = 12) after T series was taken (p = 0.888) which does not make a significant change (**Figure 40 B**). That means that there is no net removal nor addition of PRC1 from and on the spindle territory from the cytoplasm. However, the whole spindle mean intensity before and after T series was lower regarding the wild type. Intensity before the T series for acutely inhibited aurora B was significantly lower; 156.019 ± 21.468 (n = 10) and 313.089 ± 21.468 (p = 0.184×10^{-2}, n = 10), 2.007 times lower. Also, the mean intensity of the spindle in cells treated chronically with aurora B inhibitor was even lower than in the wild type, 3.815 times lower; 82.067 ± 13.520 versus 313.089 ± 21.468, respectively (p = 3.706×10^{-6}, n = 10), but also 1,901 times lower than in cells acutely treated with aurora B inhibitor; 82.067 ± 13.520 versus 156.019 ± 21.468 respectively (p = 0.683×10^{-2}). Maximum intensity of the spindle also didn't change neither in acutely; from 682.218 ± 81.819 to 706.291 ± 189.198 (p = 0.911), nor chronically treated cells; from 682.218 ± 50.214

to 706.291 ± 54.867 (p = 0.382) on the opposite to the wild type (**Figure 40 C**). This suggests that in cells with inhibited aurora B there is no bundle focusing and PRC1 concentration.
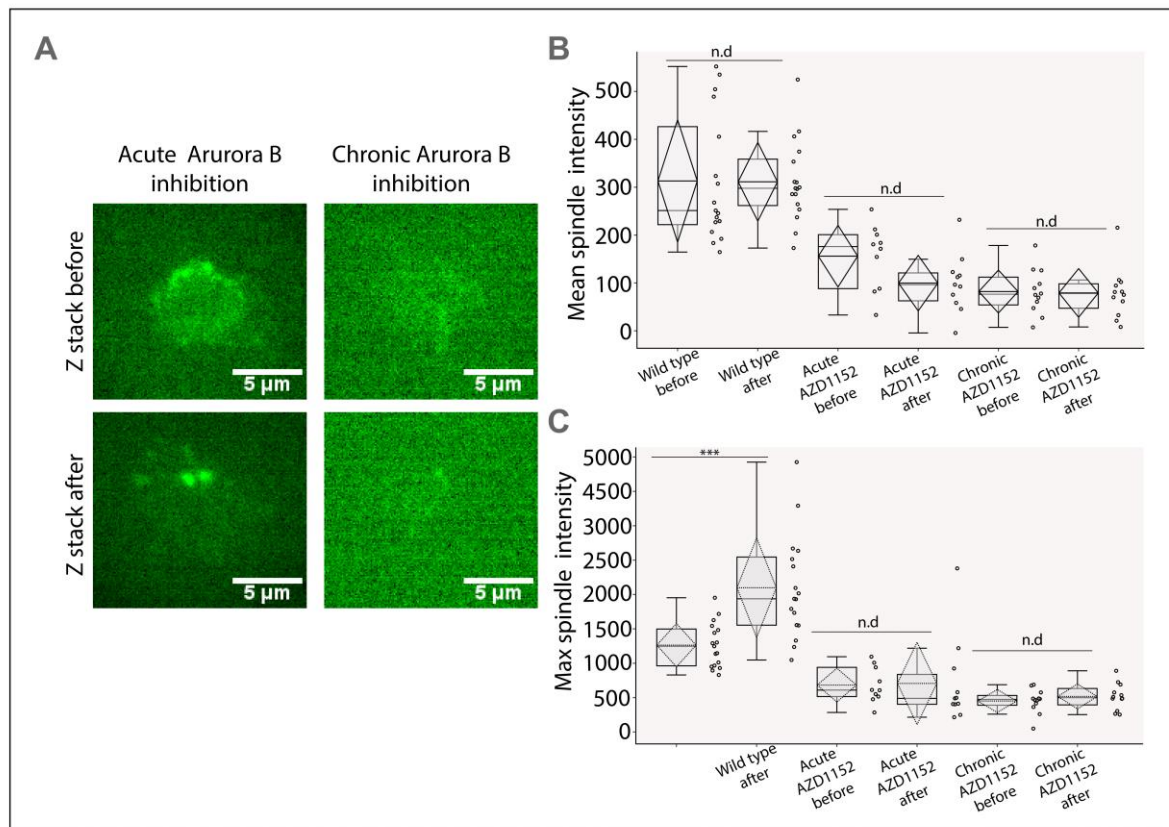
Figure 40. A. Sum of the intensity of all planes in Z stack of the spindle before and after T series was taken in HeLa PRC1-GFP cell line. Images represent acute aurora B inhibition (left) and chronic aurora B inhibition (right). **B.** Mean intensity of the whole spindle. Mean intensity does not change significantly before and after T series was taken, indicating that there is no removal or addition of PRC1 of and to the spindle. **C.** Maximum intensity in the whole spindle before and after T series was taken. On the opposite of the wild type where maximum intensity grows after T series was taken, in both acute and chronic aurora B inhibition there is no change in the maximum intensity.

To see whether end-on attachment of microtubule bundles also affects the formation of the bundles, Ndc80 was silenced using siRNA technique. After 24 hours almost all the cells in the dish were stalled in chromosome ring configuration due to absence of end-on attachment and mitotic spindle checkpoint activation. That was one indication that Ndc80 was successfully silenced. Insight into the metaphase spindle showed that there were changes in the morphology, but all the cells had normal antiparallel bundles formed indicating that end on attachment is not essential for antiparallel bundle formation (**Figure 41**).

Spindly, protein localized to the kinetochore complex in time when kinetochores are laterally attached to the spindle, was silenced to see whether Spindly has any role in the bundle formation. Because of the similar phenotype as in the Ndc80 silenced cells, only cells stalled in the metaphase were acquired. Also, except for some changes in morphology, all cells had fully formed antiparallel bundles (**Figure 41**). Full dish of cells stalled in the metaphase indicates that Spindly was successfully silenced.
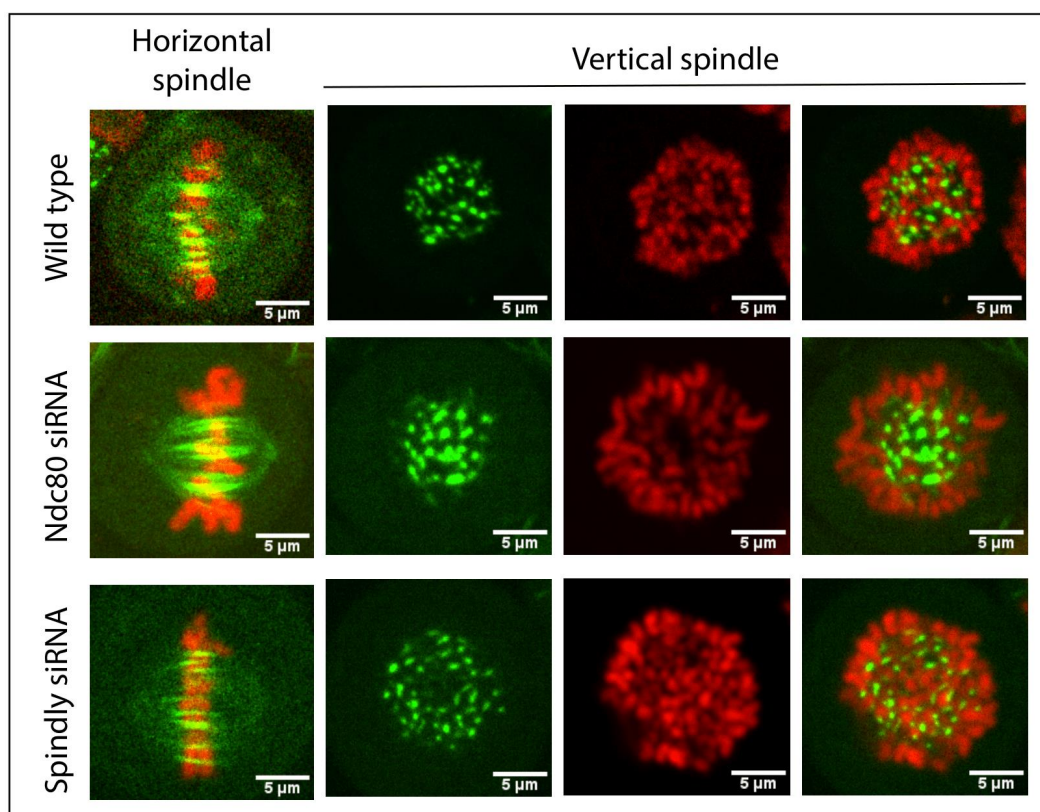
Figure 41. Silencing of Ndc80 protein, responsible for end-on attachment of microtubules to the kinetochores, and Spindly protein, present in kinetochore complex during lateral attachment, in HeLa PRC1-GFP cell line using siRNA. Ndc80 silencing resulted in chromosome ring configuration, but normal antiparallel bundle formation. Silencing of Spindly protein also doesn't affect the antiparallel bundle formation. PRC1 is colored greed. DNA is labeled with SiR-DNA dye and colored red.

To determine whether spindly and Ndc80 proteins were silenced successfully by siRNA, immunoflourescence staining was performed. Data showed that 40.413% of Ndc80 was depleted in the HeLa PRC1-GFP cell line 24 hours after transfection ($p = 0.134 \times 10^{-8}$). Spindly protein was depleted for 90.059% ($p = 0.179 \times 10^{-11}$) 48 hours after transfection. Both Ndc80 and Spidnly silencing of showed satisfying depletion of protein from the cell, considering that in both treatments cells were staled before metaphase. Control was treatment with control siRNA.
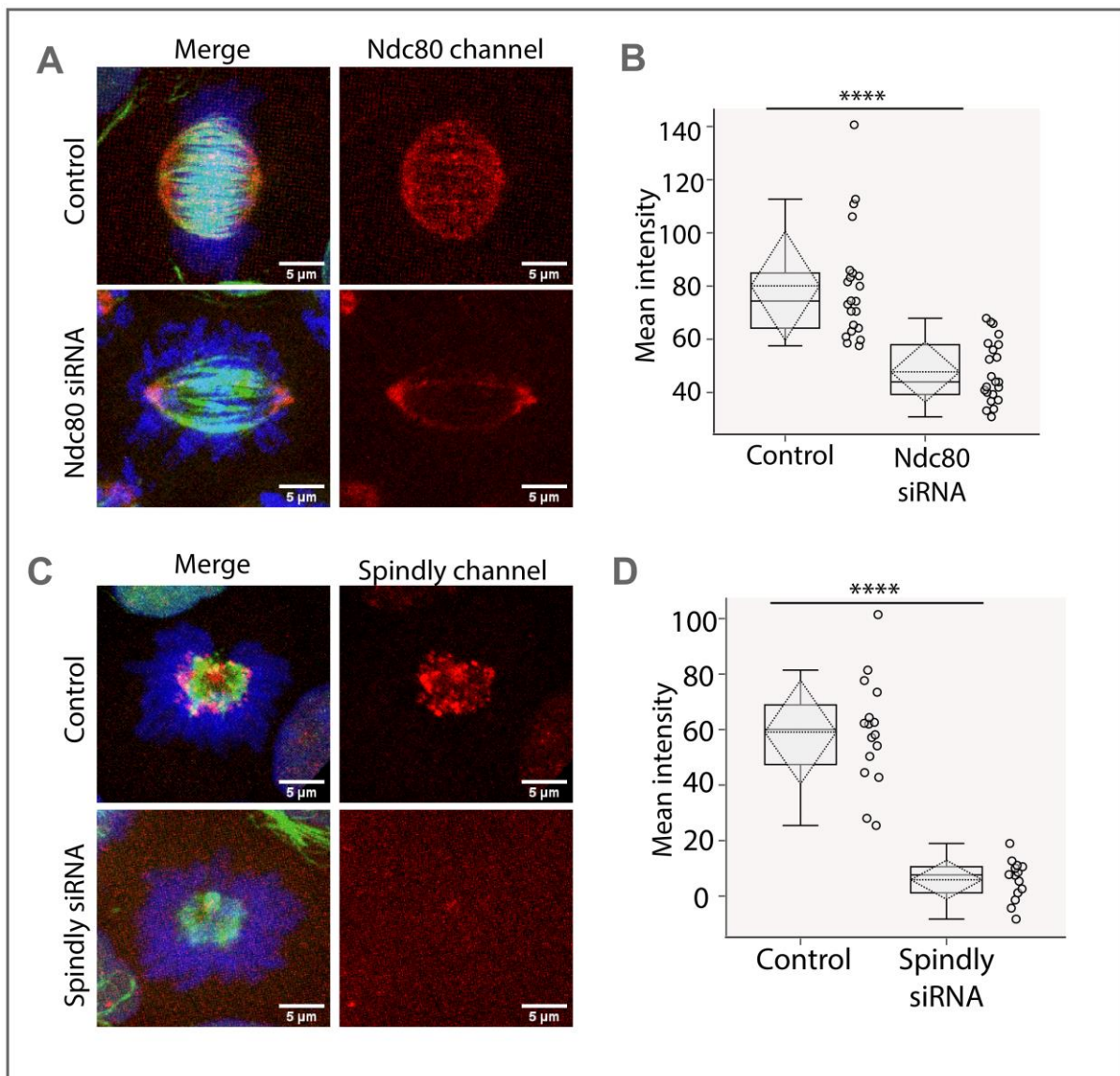
Figure 42. A. Immunoflourescence staining of HeLa PRC1-GFP cell with silenced Ndc80 (Hec1 protein) and control. PRC1 is colored greed (GFP channel), DNA is colored blue (DAPI) and Ndc80 red (secondary antibody Alexa Fluor 594). Maximum intensity projections are shown. **B.** Mean intensity of spindle in Ndc80 channel showed 40% decrease of Ndc80 protein 24 hours after transfection. **C.** Immunoflourescence staining of vertical prometaphase HeLa PRC1-GFP cell with silenced Spindly protein and control. PRC1 is colored greed (GFP channel), DNA is colored blue (DAPI) and Spindly red (secondary antibody Alexa Fluor 594). Maximum intensity projections are shown. **D.** Mean intensity of spindle in Spindly channel showed 90% decrease of Spindly protein 48 hours after transfection.

Considering that a few bundles on the top of the spindle were focused first and are not in contact with kinetochores, main motor protein that localizes in bundles between centrosomes in the early prometaphase was inhibited to see its effect on other bundle formation. After acute addition of STLC in 200 nM concentration, it seems that the mist forms bundles, but they protrude outward of the spindle axis. Also, as Eg5 promotes pole separation by antiparallel bundle sliding, addition of STLC stopped the spindle elongation, but focusing of antiparallel bundles was evident (**Figure 43**).
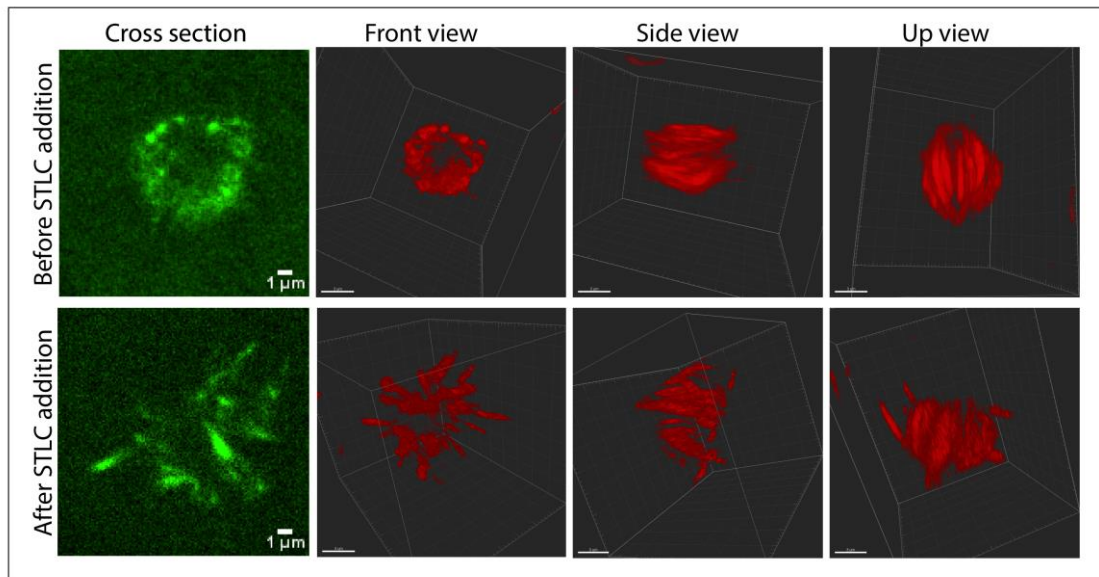
Figure 43. Addition of STLC in the prometaphase mist in HeLa PRC1-GFP cells showed reduction of pole separation, but normal antiparallel bundle formation. As bundles form they protrude outward of spindle axis. Only Z stack was acquired before and after the T series. T series between was also acquired, but is not showed here. Time interval between two frames was 5.4 seconds. 3D representations are made in Imaris 3D viewer (red).

4.4 Inhibition of prometaphase mist formation

To see how the mist of PRC1 forms in HeLa PRC1-GFP cells, Haus6, protein of augmin complex, was silenced using siRNA. Strikingly, in cells with silenced Haus6 protein, the mist of PRC1 in the early prometaphase spindle was never found. All early vertical prometaphase cells recognized on the basis of semicircular chromosome collar had already formed certain amount of bundles and there was no amorphous mist of PRC1 protein surrounding them (**Figure 44 A**). Time series imaging showed that there is no classical focusing of microtubules from the mist as in the wild type cells (**Figure 44 B**). Most of the bundles present in the first

frame are present and easy trackable to the last frame. Also, space between the bundles is homogeneous with cytoplasm in PRC1-GFP channel.
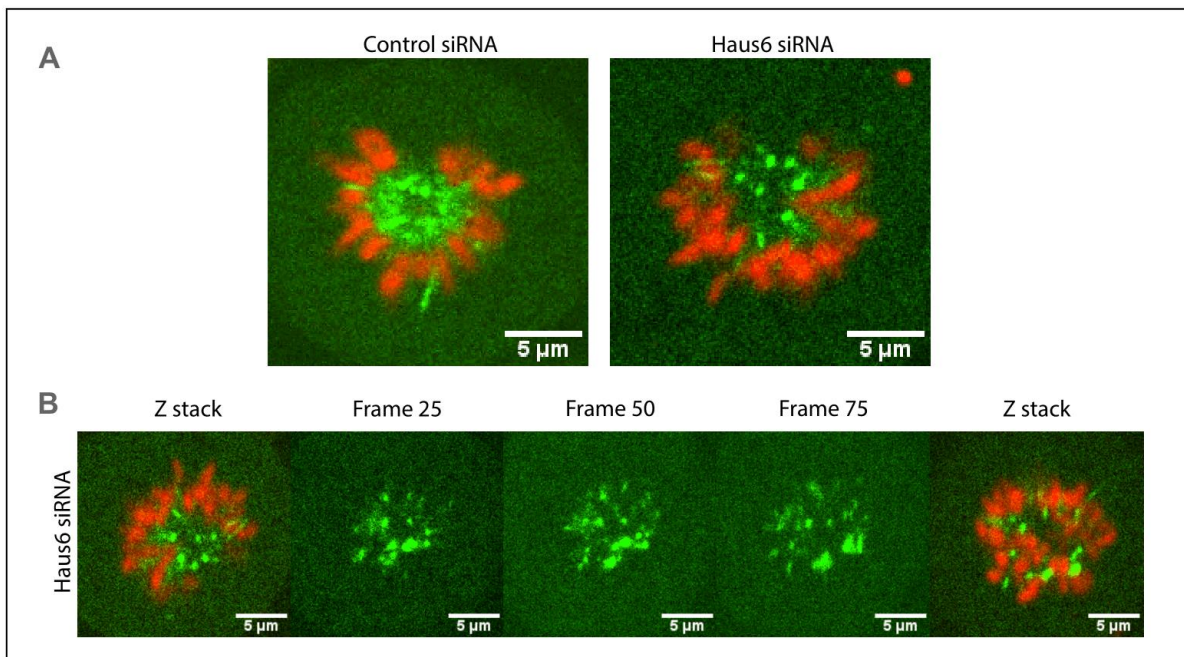
Figure 44. A. Middle plane of an early vertical prometaphase spindle in HeLa PRC1 – GFP cell line treated with control siRNA and Haus6 siRNA 48 hours after transfection. In cells with silenced Haus6 protein, no mist of PRC1 was noticed. **B.** Time lapse movie of vertical prometaphase spindle in Haus6 depleted cells shows no antiparallel bundle focusing. PRC1 is colored green. DNA is labeled with SiR-DNA dye and colored red. Time interval between two frames was 5.4 seconds.

Squash analysis showed that there is no classical segmentation of the mist of PRC1 like in the wild type cells. Most of the bundles that are seen in the last frame are already present and formed in the first frame. Only their arrangement is changed due to their dynamics during prometaphase (**Figure 45 A**). This observation is supported by data of Squash analysis. Squash analysis showed that the number of bundles is not growing in time; from 7.500 ± 0.946 (n = 10) in first frame, to 6.667 ± 0.667 (n = 9) in the last frame (p = 0.490) (**Figure 45 B**). Also, there is no growth of segments in size in time; from 63.083 ± 6.588 pixels (n = 10) to 60.155 pixels (p = 0.802, n = 9), which is consistent with the observation that there is no segmentation of new bundles from larger patches of signal and that fully formed bundles are present from the first frame (**Figure 45 C**). Curve of the intensity growth follows the curve of wild type; mean intensity of the objects grows from 41.154 ± 3.949 (n = 10) to the 61.151 ± 9.602 (p = 0.005, n = 9) indicating that the certain amount of focusing was present and took place in already existing bundles (**Figure 45 D**).
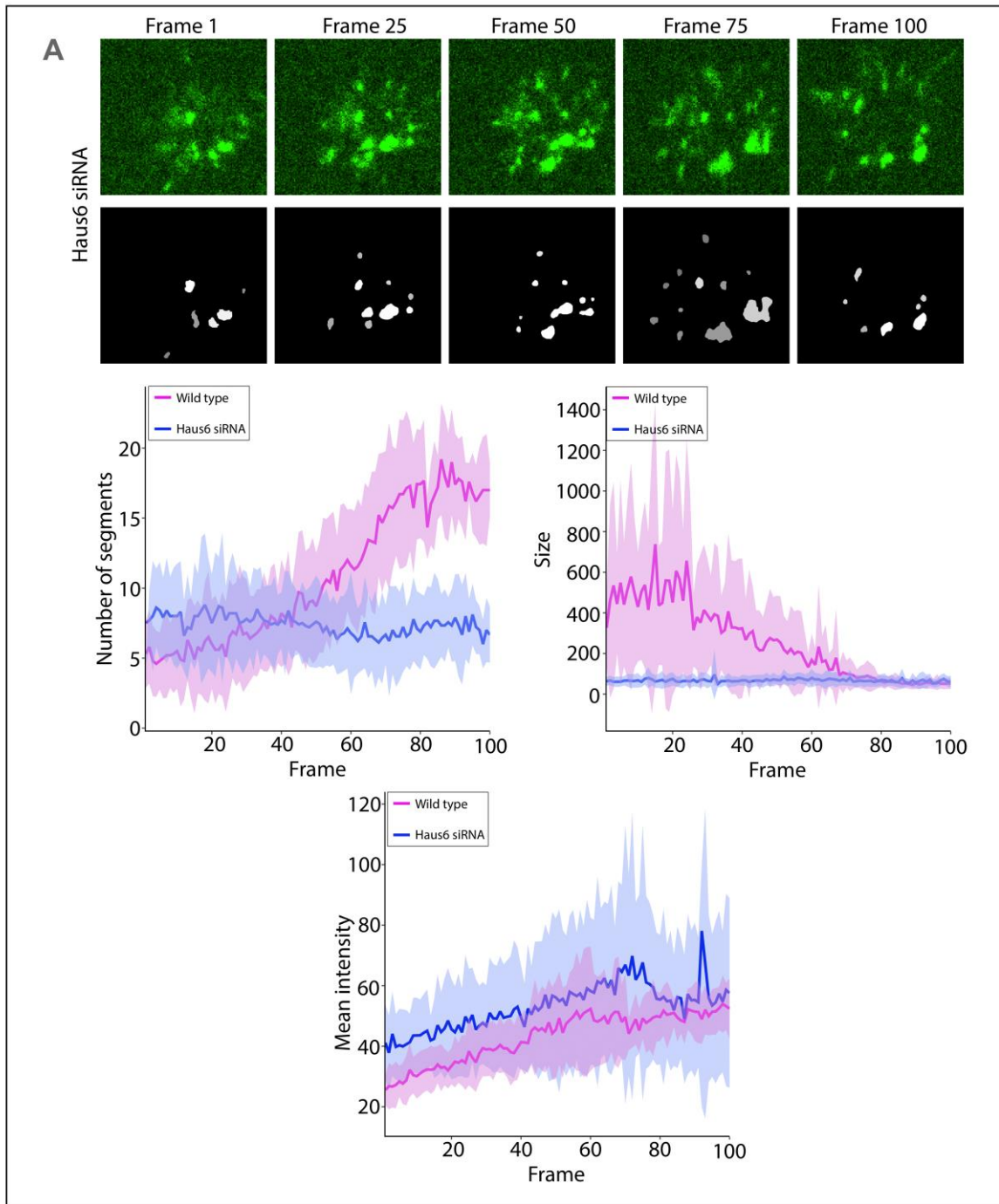
Figure 45. A. Squash segmentation analysis in Haus6 siRNA targeting in HeLa PRC1-GFP cell line. **A.** Upper row represents time lapse of middle plane in prometaphase and second row represents intensity output of squash analysis. **B.** Number of segments does not increase in time. **C.** Size of the segments does not decrease in time. **D.** Mean intensity of objects increases in time, but mean intensity of objects is higher than in the wild type in all time frames. Pink line represents wild type and blue line represents cells treated with Haus6 siRNA. Surface represents standard deviation.

Size distribution of segments didn't show any trend of increase or decrease in time, but it seems that few categories of segments are present (**Figure 46 A**). This categorization is even more evident in segment intensity distribution in time showing that in most cells (8 out of 10 analyzed cells) segments split into 2 populations differing in the intensity (**Figure 46 B**). Segment intensity of both groups shows increase in time.
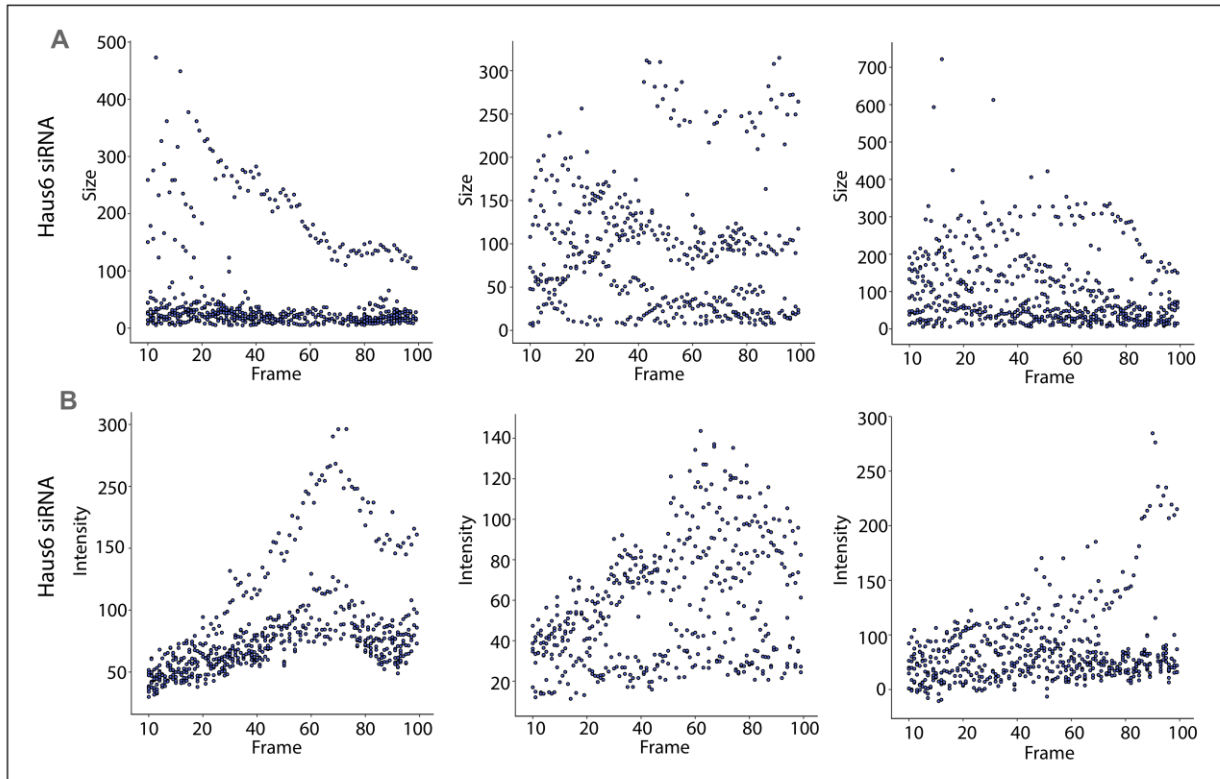
Figure 46. A. Scatter plots of 3 representative cells showing segments size distribution in time. Few populations of segments based on the size can be seen. **B.** Scatter plots of 3 representative cells showing segments intensity distribution in time. In 8 out of 10 cells, segments split into two populations of different intensity. Time interval between two frames is 5.4 seconds.

Measuring intensity of the spindle territory in one middle plane of the vertical prometaphase spindle treated with Haus6 siRNA showed that mean intensity of the spindle increases in time; from 5.215 ± 0.875 (n = 10) to 8.537 ± 1.302 (p = 0.045, n = 8) (**Figure 47 A**) making an increase of 1.392 ± 0.202 times of the initial value, similar to the 1.456 ± 0.080 times increase in the wild type (**Figure 47 B**). From start, mean intensity of the spindle in Haus6 siRNA treated cells is lower in intensity; 5.215 ± 0.875 (n = 10) in regard to 11.234 ± 1.226 (n = 12) in the wild type spindle (p = 0.101×10^{-2}). This makes an intensity of the wild type 2.154 times higher (p = 0.02). At the end of the T series mean intensity is still lower in regard

to the wild type; 8.537 ± 1.302 (n = 8) versus 14.463 ± 1.651 (n = 10) respectively, 1.69415 time lower than in wild type (p = 0.377 x 10^{-2}).

Maximum intensity also increases from 164.582 ± 19.415 (n = 10) to 287.666 ± 51.342 (p = 0.028, n = 8) (**Figure 47 C**) which makes an increase of 1.738 ± 0.194 times, similar as the increase of the maximum intensity in wild type cells 2.033 ± 0.240 times increase (n = 10) (**Figure 47 D**).

There is no significant difference in maximum intensity of the Haus6 siRNA treated spindle and wild type; 164.582 ± 19.415 (n = 10) in regard to 217.681 ± 29.191 (n = 12) in the wild type spindle (p = 0.163). At the end of the T series there is still no significant difference; 287.666 ± 51.342 (n = 10) versus 375.396 ± 40.0499 (n = 10) in the wild type spindle (p = 0.195).
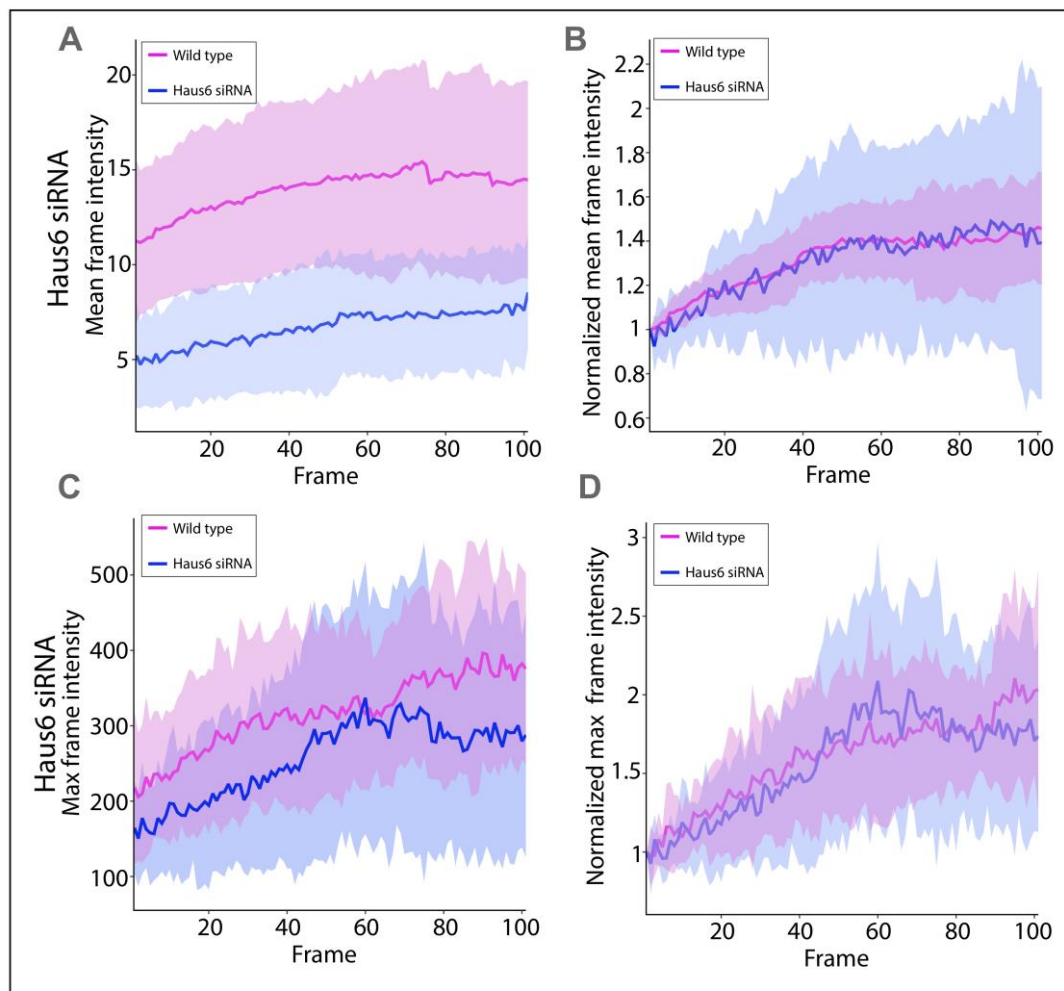
Figure 47. Mean and maximum intensity of the spindle territory in the middle plane of the vertical prometaphase spindle in time. **A.** Mean intensity of the spindle in Haus6 targeting cells is lower than in the wild type, but increases in time. **B.** Normalized mean intensity of cross section of prometaphase spindle of Haus6 targeting and wild type cells shows similar

growth curve. **C.** Maximum intensity of the Haus6 targeting and the wild type shows similar values and growth in time. **D.** Normalized maximum intensity of cross section of prometaphase spindle in targeting shows similar growth curve as in the wild type. Time interval between two frames is 5.4 seconds.

There is no significant change in the mean intensity of the whole spindle before and after time series; 88.548 ± 8.172 before T series and 83.279 ± 10.708 after ($p = 0.464$) (**Figure 48 B**). Also, maximum intensity of the whole spindle doesn't change significantly in time; 546.004 ± 63.445 before T series and 666.525 ± 98.029 ($p = 0.312$) after (**Figure 48 C**).
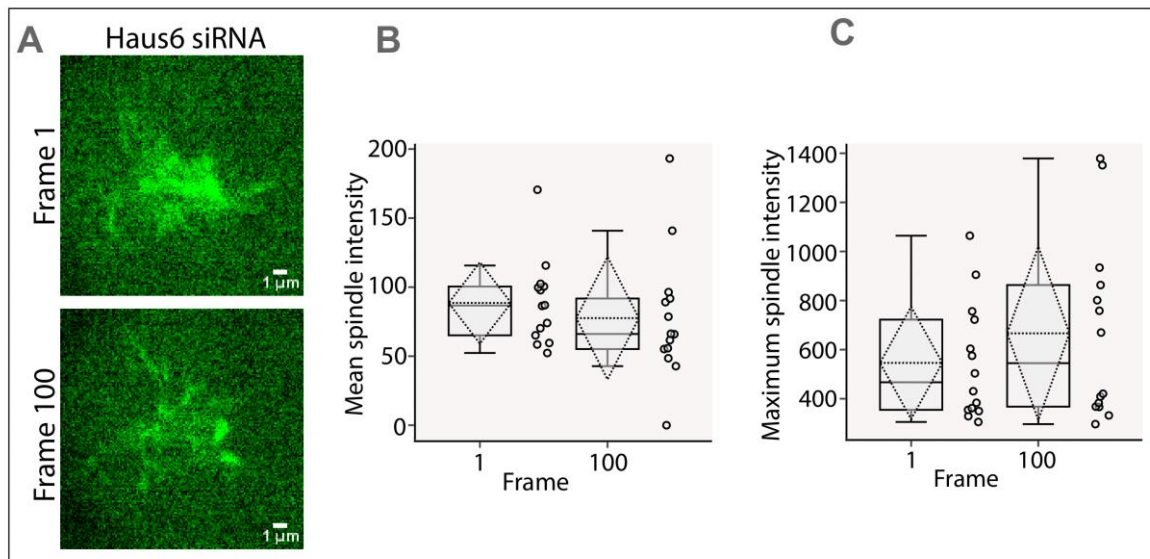
Figure 48. A. Sum of the intensity of Z stack in PRC1-GFP channel of vertical prometaphase spindle in HeLa PRC1-GFP cell line treated with Haus6 siRNA before and after T series was acquired. **B.** Mean intensity of the whole spindle before and after T series doesn't change significantly. **C.** Maximum intensity of the whole spindle before and after T series also doesn't change significantly.

To determine how the antiparallel bundles in Haus6 targeting HeLa PRC1-GFP cell line form, cells were imaged from the nuclear envelope breakdown (**Figure 49**). In the prometaphase pathway of mitosis, in the wild type, most of the antiparallel bundles form between two poles of the spindle from the amorphous mist of PRC1 protein. Those *de novo* formed bundles are all localized between two poles in the region of the spindle. In contrast, imaging of Haus6 targeting cells showed that a great majority of antiparallel bundles are recycled and retrieved from the cytoplasm. These cytoplasmatic bundles were already present in the cell during the interphase. They are recruited and organized in the mitotic spindle upon the nuclear envelope breakdown, while *de novo* formation of the bundles is much less represented comparing to the

wild type. The same phenomenon was observed in prophase pathway of mitosis. However, a certain population of cytoplasmatic antiparallel bundles localized around the nucleus is recycled and incorporated into the mitotic spindle just before the nuclear envelope breaks, even in the wild type. Still, a great portion of the newly formed bundles exist between two poles by focusing from the mist. In Haus6 targeting cells, almost all bundles come from the already present bundles in the cytoplasm and around the nucleus, while only a small amount of the focusing is observed.

	Promethaphase pathway		Prophase pathway	
	Wild type	Haus6 siRNA	Wild type	Haus6 siRNA
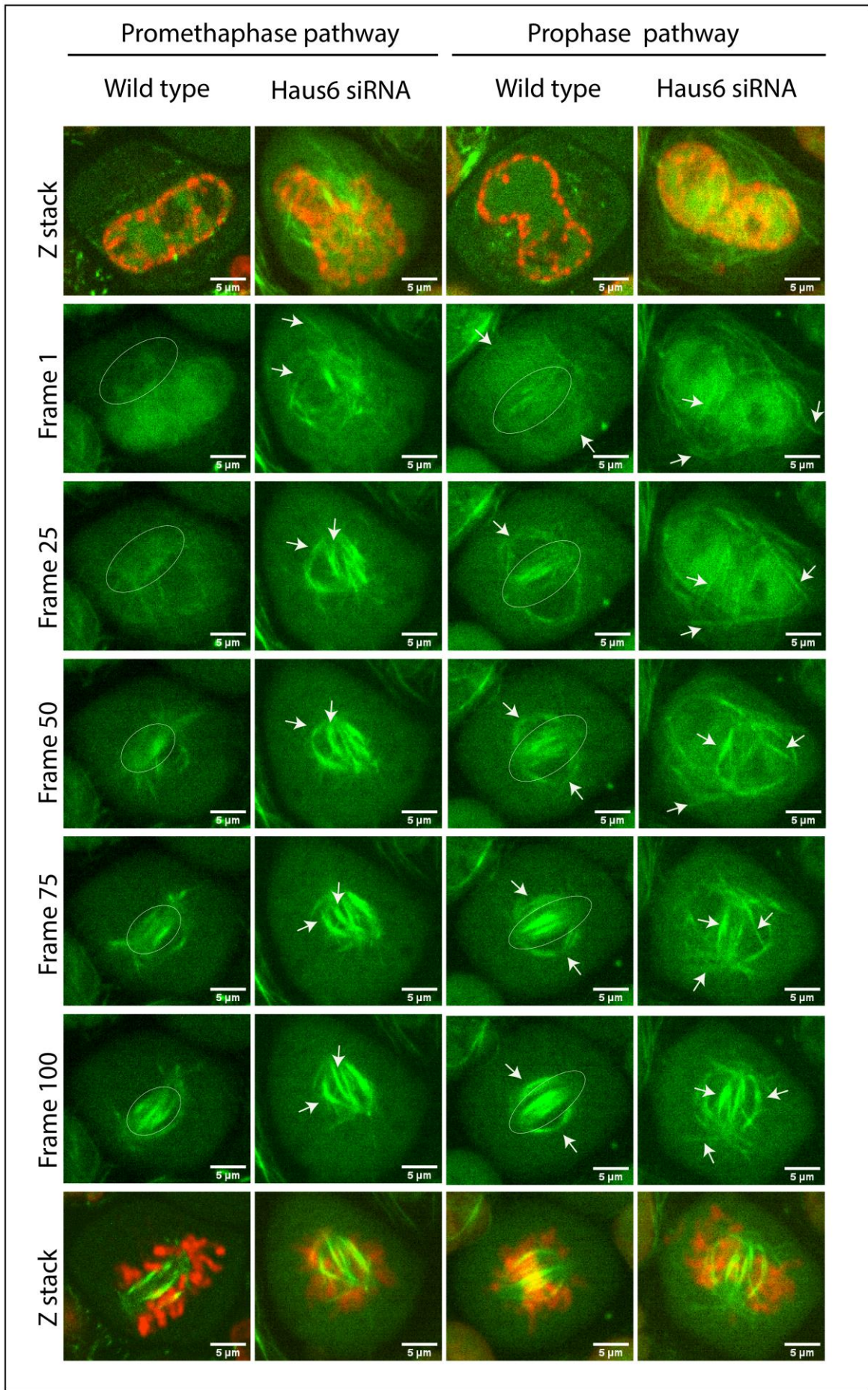
Figure 49. Prometaphase and prophase pathway of mitosis in the wild type and Haus6 targeting in HeLa PRC1-GFP cell line. White arrows represent cytoplasmatic bundles that are reused for the spindle assembly. White eclipse represents the region between two spindle poles in which antiparallel bundle focus from the mist of PRC1. PRC1 protein is colored green. DNA is labeled with SiR-DNA and colored red. Haus6 targeting shows extensive retrieval of interphase bundles from cytoplasm for spindle assembly. In wild type, focusing is predominant way of bundle formation. Every image is represented as a sum of 15 slices with spacing of 1 μm. Time between two time frames is 10 seconds.

Detailed inspection of metaphase spindle of HeLa PRC1-GFP cell line in 3D space revealed two populations of antiparallel bundles in Haus6 targeting cells. Large thick antiparallel bundles are positioned externally. They give the shape of the Haus6 targeting spindle. Inside the spindle, beneath of the large bundles, small thin bundles of smaller intensity are present (**Figure 50**). Large bundles originate from the cytoplasmatic interphase bundles that are retrieved from the cytoplasm during spindle formation.
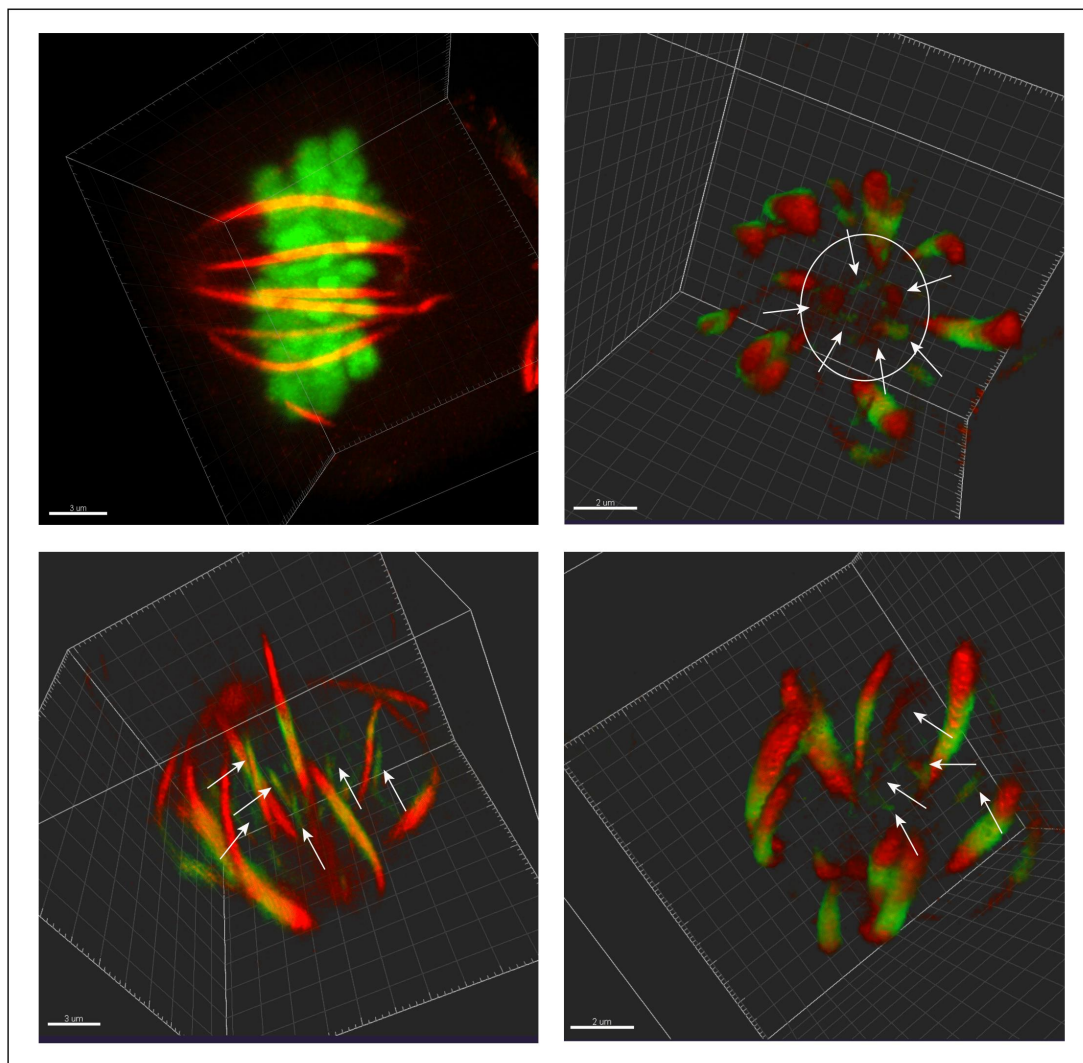
Figure 50. 3D presentations of Haus6 targeting metaphase spindle in HeLa PRC1 – GFP. Metaphase spindle shows 2 populations of antiparallel bundles: external, large and thick bundles and internal thin bundles. Antiparallel bundles are colored red and chromosomes green. Images are made in Imaris 3D viewer.

To see whether the spindle formation differs in Haus6 targeting and non-targeting in other cell lines, non-tumor immortalized RPE1 CenpA – GFP, Centrin – GFP cell line was used. Microtubule bundles were visualized with SiR – tubulin dye and represent general bundles in the cell. In wild type cells spindle showed an extensive incorporation of interphase bundles in spindle during the formation, but it seems that intensity of the spindle was much higher in regard to the wild type. Mesh of microtubules forming between two poles seemed thicker than in Haus6 targeting. Also, a certain part of the interphase bundles was retained in cytoplasm and membrane. On the other hand, spindles formed in Haus6 targeting appeared morphologically less organized. Also, the thickness of the spindle territory seems lower. Mesh of microtubules seems less dense and all the cortical bundles were retrieved and incorporated in the spindle (**Figure 51 A**). Methaphase spindles also showed different morphology. The most striking is the mesh of bundles on the bottom and above the mitotic spindle. Also, the spindle was flattened and attached to the bottom membrane of the cell. In the wild type cells the spindle was round and compact. Also, wild type spindle seems much thicker. Furthermore, there are no cortical microtubule bundles under and above the spindle. Spindle was not attached to the bottom membrane of the cell (**Figure 51 B, C**).

A Spindle formation

	RPE1 Haus6	RPE1 Wild type
Frame 1		
Frame 10		
Frame 20		
Frame 30		
Frame 40		
Frame 50		

B Methaphase spindle

	RPE1 Haus6 siRNA	RPE1 Wild type
Sum of Z stack		
Upper plane		
Middle plane		
Bottom plane		

C

Side view RPE1 wild type

Side view RPE1 Haus6 siRNA
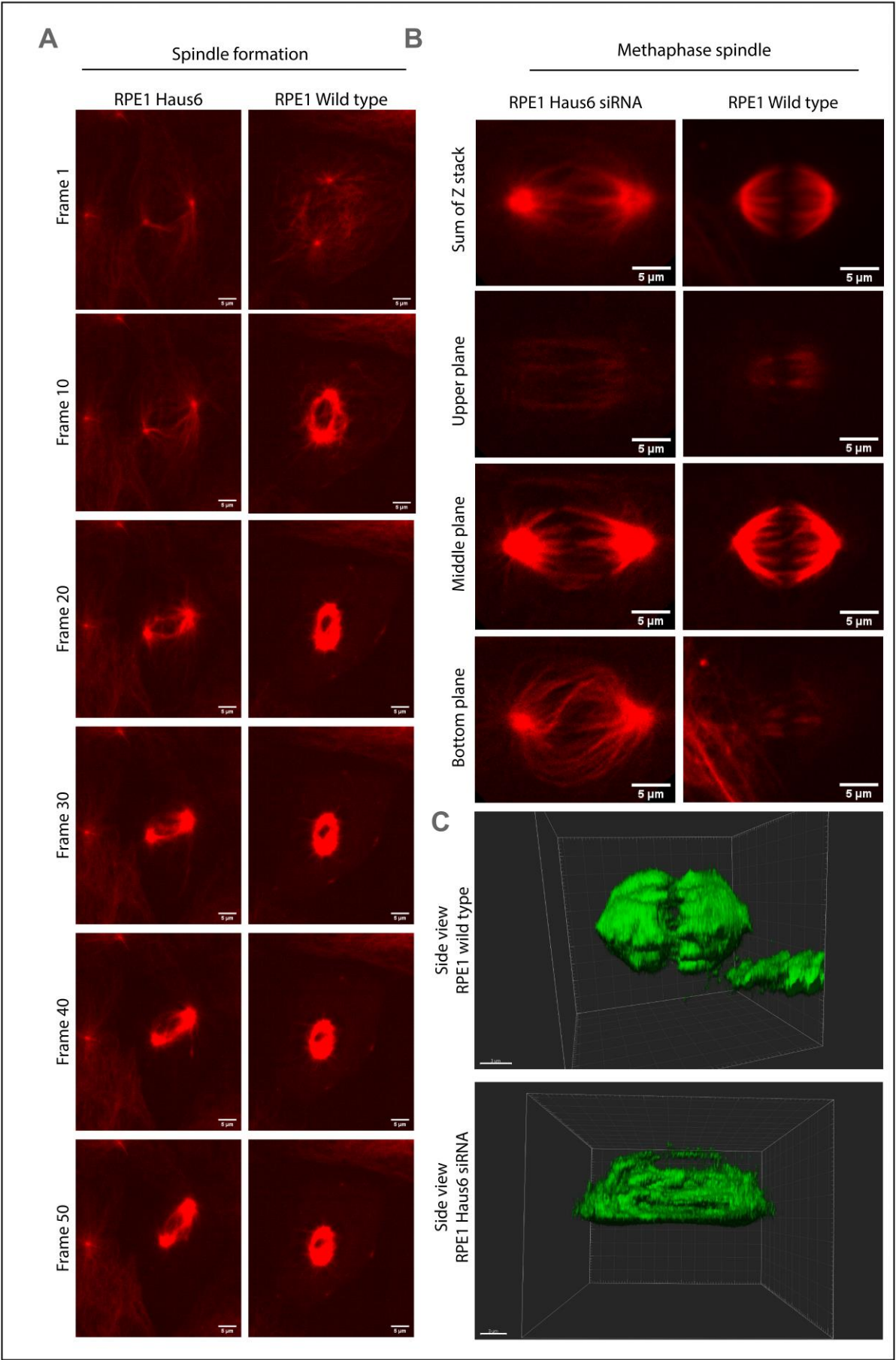
Figure 51. A. Spindle formation in RPE1 CenpA-GFP, Centrin1-GFP cell line from the nuclear envelope breakdown in Haus6 targeting and non-targeting cells. Only channel with microtubules is presented. Microtubules are labeled with SiR-Tubulin dye. All images are a sum of 15 slices. Time between two frames was 20 seconds. White arrows represent interphase and cortical bundles. Spindle in targeting shows higher degree of bundle retrieval from cytoplasm. **B.** Metaphase cells in Haus6 targeting and non-targeting. First row represents sum of slices, second row upper slice of the spindle, third row middle, and fourth row bottom slice of the spindle. First row shows different morphology of targeting and non-targeting metaphase spindle. Upper and bottom slice of the metaphase spindle show extensive cortical bundles in Haus6 targeting. **C.** 3D illustrations made in Imaris 3D viewer software show side view of non-targeting and Haus6 targeting metaphase spindle. Haus6 metaphase spindle is attached to the bottom membrane of the spindle by bottom cortical bundles shown in B. Spindle is flattered regarding the wild type.

To determine whether the siRNA silencing of Haus6 protein successfully depleted the protein, immunofluorescence staining was performed. Data showed 74.93 % depletion of Haus6 72 hours after transfection (p = 0.175 x 10^{-9}).
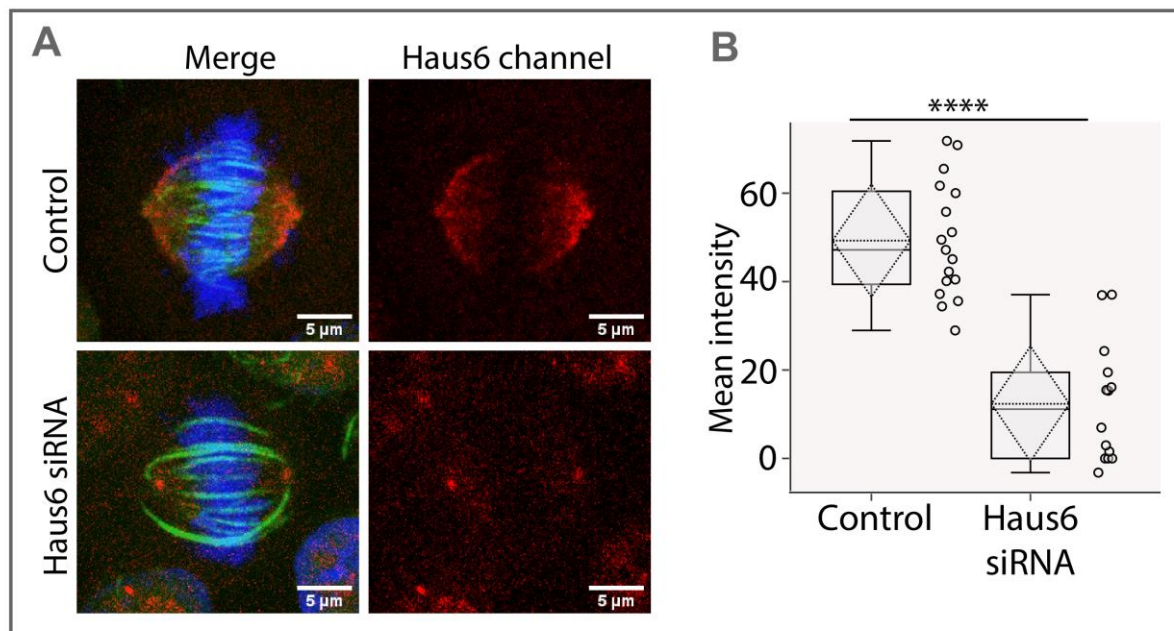
Figure 52. Immunoflourescence staining of HeLa PRC1-GFP cell with silenced Haus6 protein and control. PRC1 is colored greed (GFP channel), DNA is colored blue (DAPI) and Haus6 red (secondary antibody Alexa Fluor 594). Maximum intensity projections are shown. **B.** Mean intensity of spindle in Haus6 channel showed 74 % decrease of Haus6 protein 72 hours after transfection.

Number of the bundles grows in time from 9.182 ± 0.501 to 17.909 ± 1.099 in Haus6 targeting ($p = 0.334 \times 10^{-7}$, $n = 11$). In acute aurora B inhibition number of bundles grows from 4.625 ± 0.497 to 12.875 ± 2.875 ($p = 0.013$, $n = 8$), while in chronic aurora B inhibition, there is no increase in the number of bundles: 3.056 ± 0.545 before and 4.500 ± 0.706 after T series ($p = 0.146$, $n = 18$) (**Figure 53 B**). Also, the number of bundles in metaphase cells differs from treatment to treatment (**Figure 53 A**). Mean number of bundles in HeLa wild type is 27.424 ± 0.892 ($n = 33$). When aurora B is inhibited there is a 37.039 % decrease in the number of bundles in regard to the wild type; 17.267 ± 0.808 ($n = 15$, $p = 0.696 \times 10^{-10}$). There is an even more dramatic decrease in the number of bundles, of 50.976 %, in Haus6 targeting regarding the wild type (13.444 ± 0.807) ($n = 18$, $p = 0.280 \times 10^{-14}$). Moreover, Ndc80 targeting shows 26.160 % lower number of bundles than the wild type; 20.250 ± 0.625 ($n = 28$, $p = 0.318 \times 10^{-8}$). On the other hand, in Spindly targeting, the number of bundles is higher; 34.259 ± 1.198, for 19.951 % in the wild type ($n = 27$, $p = 0.186 \times 10^{-6}$) (**Figure 53 C**).
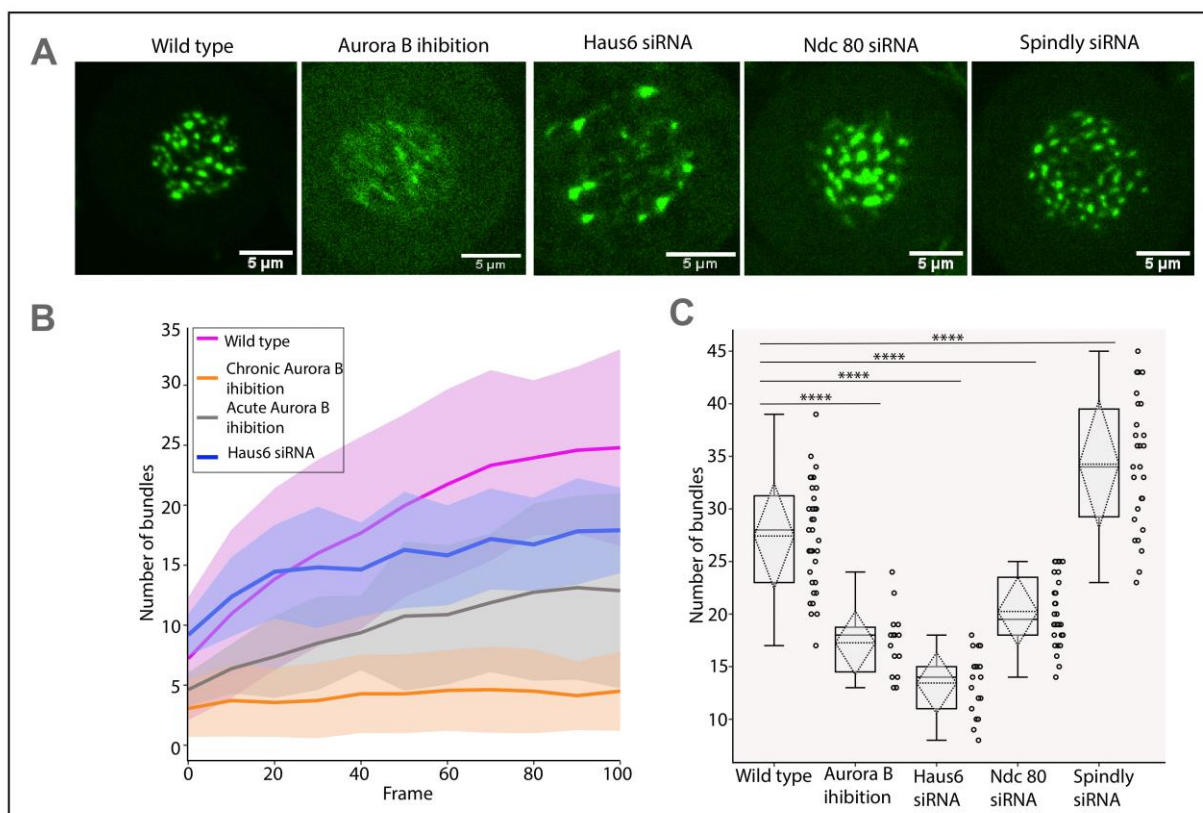
Figure 53. A. Cross sections of metaphase cells in the wild type, aurora B inhibited cells, Haus6 targeting, Ndc80 targeting and Spindly targeting show different number of bundles. **B.** Number of bundles increases in time in the wild type, Haus6 targeting and acutely inhibited

aurora B cells, while in the chronically inhibited aurora B, there is no increase in the number of bundles. **D.** Number of bundles in metaphase cells in aurora B inhibition, Haus6 targeting and Ndc80 targeting cells shows lower number of bundles in respect to the wild type. Spindly targeting, on the other hand, shows increased number of bundles in metaphase cells in regard to the wild type.

4.5 Antiparallel bundle dynamics

During and after the formation of bundles it was seen that all cells show a similar pattern of bundle movement during prometaphase in HeLa PRC1-GFP cell line. All spindle cross section had some common characteristics; two fully focused bundles at the top of the prometaphase spindle cross section. Those two bundles were not covered with chromosomes and I called them "central bundles". The rest of the cross section was made of mist of PRC1 encircled with chromosomes. Cross section of vertical prometaphase spindle is rotated so that all cross sections were in the same orientation, with central bundles aligned. Mist of PRC1 then focuses in time and all bundles that formed from the mist I called "newly formed bundles". During and after the formation of bundles, two central bundles on the top of the spindle showed downward movement (in the plus direction in Fiji image), while the rest of the bundles mostly moved in the opposite direction – upwards (in the minus direction in Fiji image) (**Figure 54 A, C**). To correct the image sequence for lateral movement of the whole spindle, all images were corrected in a way that half axis connecting two large fully focused bundles without chromosomes were placed in the origin of the coordinate system (0, 0). That way, movement of all other bundles was recorded relative to the central bundles (**Figure 54 B, D**). In inspected cells mean y starting position of the bundles was 13.830 ± 5.885 μm (n = 11) and mean final y position at the end of T series was 3.452 ± 5.287 μm (n = 23), making a mean distance of 10.378 μm (**Figure 54 E**). Mean bundle position change for all cells was ranging from: 25.38 ± 1.556 to 14.191 ± 2.567 (n = 9), making an 11.189 μm shift in y coordinate (**Figure 54 F**).
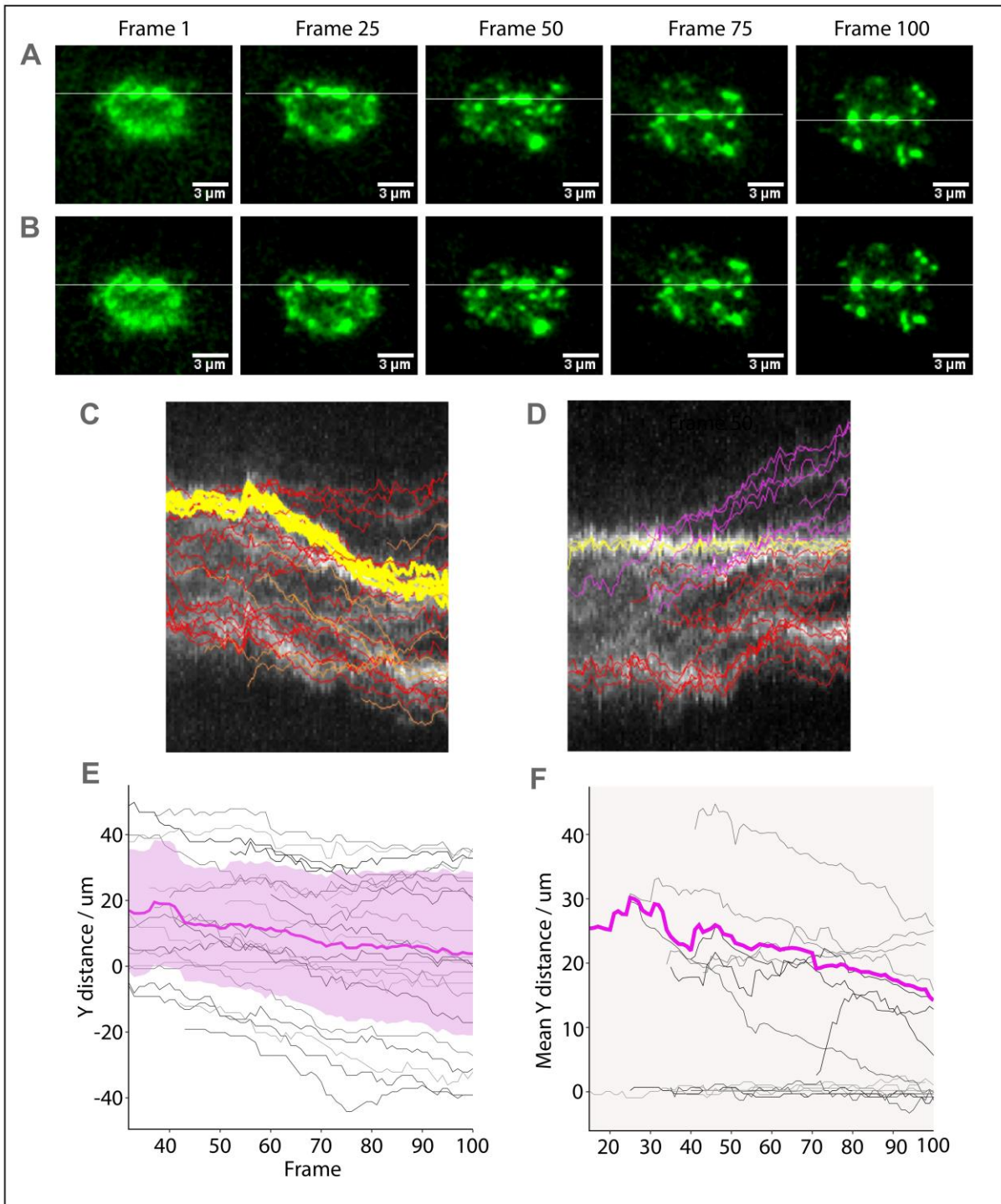
Figure 54. Bundle dynamics in HeLa PRC1-GFP cells. **A.** Two central bundles moved in the plus direction (downwards on the image) while other bundles moved in the opposite direction. **B.** Relative movement of the bundles in the minus direction. **C.** Y kymograph of the bundle movement shows dynamics of bundles in y coordinate. There is movement of central bundles (yellow) in the plus direction (downwards) and movement of the other bundles (red) in the minus direction (upwards). **D.** Y kymograph of relative bundle movement in the minus direction (red). Two central bundles are placed in the origin of the coordinate system (0, 0) (yellow). **E.** Movement of newly formed bundles of one cell in the minus direction. **F.** Mean

movement of newly formed bundles in 7 cells. Central large bundles are positioned in the origin of the coordinate system. Time interval between two frames is 2.7 seconds.

When tracked in time, newly formed bundles of the prometaphase spindle showed similar movement in all cells. When central bundles positioned in origin of coordinate system, newly formed bundles move synchronously towards and above the central bundles (**Figure 55 A, B, C**). To see the movement of chromosomes in the prometaphase, cells were imaged in both channels (GFP and SiR-DNA channel). All the cells show accompanying movement of chromosomes with bundles in time. Chromosomes show movements towards the upper center of the spindle closing the gap between. That way, open circle of chromosomes closes and they are evenly distributed around the spindle (**Figure 55 D**).
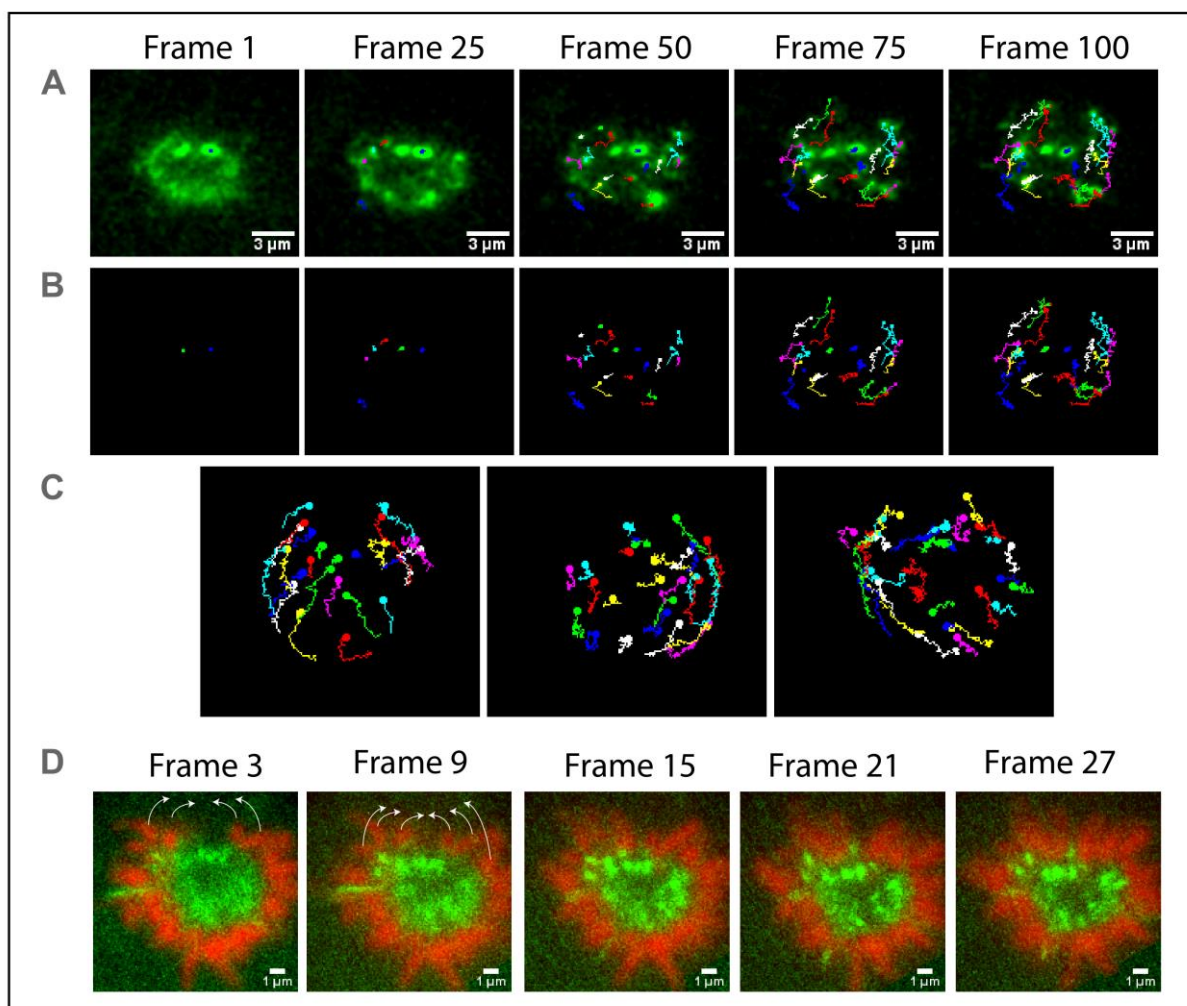
Figure 55. A. Trajectories of bundle dynamics in HeLa PRC1-GFP prometaphase. Alignment of the trajectories with the image shows the way the tracking of bundles was performed. Circle on the end of trajectory shows the position of bundle in last frame. **B.** Trajectories of bundle movement in time. **C.** Trajectories of three representative cells show similar movement pattern. All newly formed bundles move in the minus direction (upwards) towards

the fixed central bundles. **D.** Movement of the chromosomes during prometaphase. Chromosomes are closing the gap in early prometaphase. White arrows represent the direction of the movement. Time interval between two frames is 2.7 seconds.

As the prometaphase advances, movement of the bundles is accompanied by the expansion of the spindle. Spindle expands in time from 51.498 ± 7.373 µm^2 in the first frame (start of the growth) and culminates with 90.884 ± 11.526 µm^2 in the 60th frame (n = 5) (**Figure 56 A**). After 60th frame growth stagnates. In percentage, spindle is grown from abruptly from 60.243 ± 2.591 % of the final size to the final size in 60 time frames (n = 5) (**Figure 56 B**). Measuring the length and height of the spindle cross section revealed that the cross section is elliptical in shape. In all cells, the width of the cross section is larger than the high. As the spindle expands, height of the spindle reaches the length of the spindle width, forming spherical cross section (**Figure 56 C**).
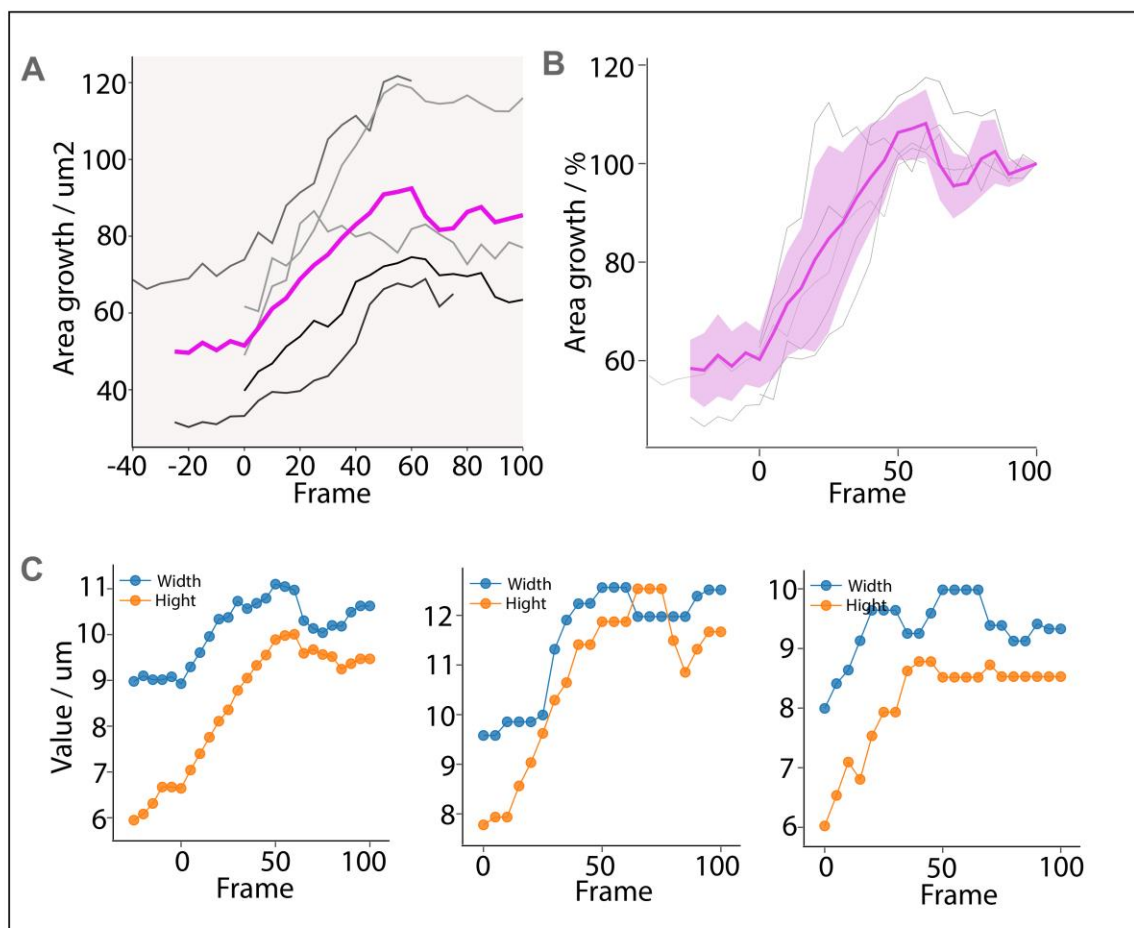
Figure 56. A. Expansion of the spindle cross section in time in HeLa PRC1-GFP cell line. **B.** Expansion of the spindle cross section in percentage shows abrupt growth of spindle area in 60 time frames. **C.** Spindle cross section width and height changes in time. At the end of the

expansion, spindle cross section is spherical. Time interval between two frames is 2.7 seconds.

To determine the cause of bundle dynamics Cenp-E protein responsible for congression of chromosome is inhibited by acute addition of 200 nM GSK inhibitor in the early prometaphase. Cross section showed different pattern of bundle movement in time than in the wild type. It seems that newly formed bundles slightly moved in the opposite direction of the large central bundles (**Figure 57 A, C**).
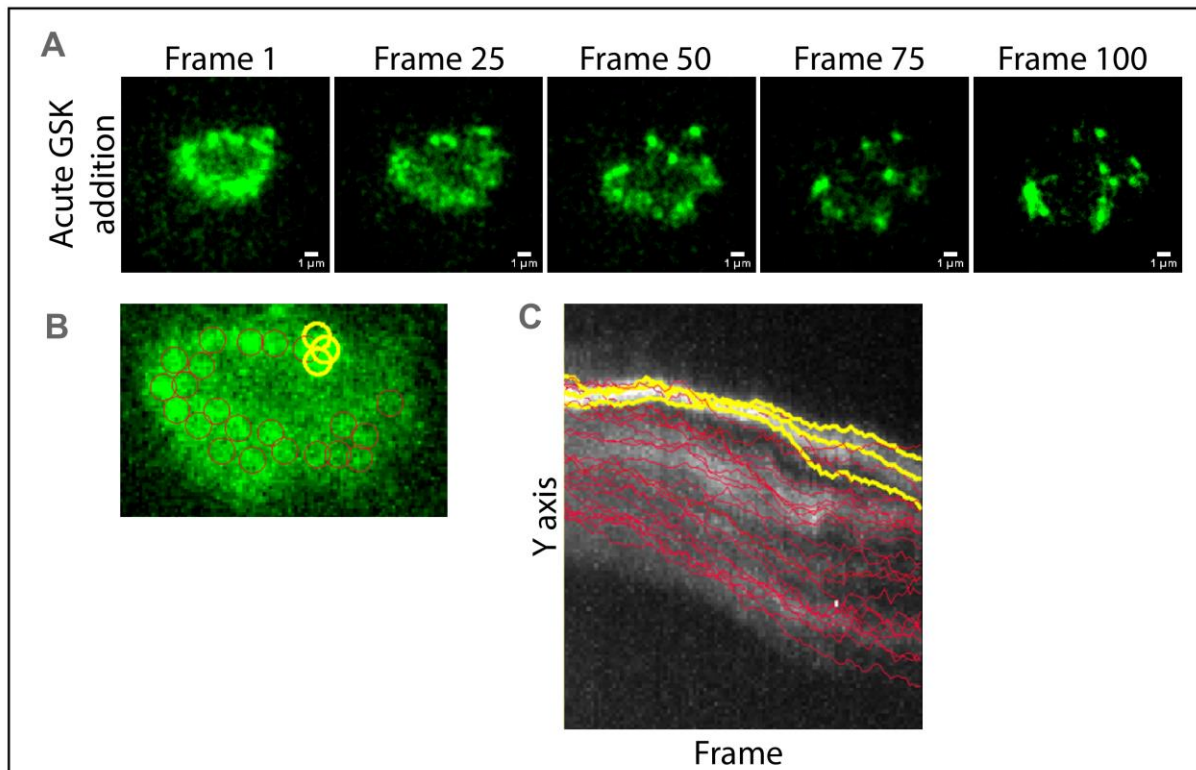
Figure 57. A. Time lapse of early prometaphase in HeLa PRC1 – GFP in which Cenp-E is inhibited, showed different patterns of bundle movement in time than in the wild type. **B.** Cross section of early vertical spindle with central bundles (yellow circles) and newly formed bundles (red circles). **C.** Y kymograph of bundle movement in y direction. Most of the newly formed bundles move in the same direction as the central pair of bundles. Time interval between two frames is 2.7 seconds.

To see whether the chromosome position has any effect on expansion of the spindle and their width, horizontal metaphase cells treated with GSK were inspected. Inhibitor of Cenp-E showed significant decrease of the spindle width in HeLa PRC1-GFP cell line. Spindle width decreases from 10.852 ± 0.259 (n = 28) μm to 8.397 ± 0.277 μm (n = 26, p = 0.425×10^{-10}). Spindle width divided with the spindle length in the wild type was 0.855 ± 0.019 (n = 28). In cells treated with GSK this number was significantly smaller; 0.562 ± 0.108 (n = 26, p =

0.563 x 10^{-25}). In RPE1 Cenp-A-GFP, Centrin1-GFP cells treated with GSK showed significantly smaller width; 7.443 ± 0.149 μm (n = 37) in regard to the wild type; 10.237 ± 0.240 μm (n = 30, p = 0.368 x 10^{-15}). Spindle width divided with the spindle length is significantly smaller in GSK treated cells; 0.518 ± 0.071 (n = 37) in regard to 0.810 ± 0.043 in the wild type (n = 30, p = 0.107 x 10^{-10}).

When DNA is removed from spindle and detached from the kinetochores using caffeine and urea treatment, spindle width drops even more. There is a significant decrease of the spindle width in HeLa PRC1-GFP cell line. Spindle width decreases from 10.852 ± 0.259 μm to 7.548 ± 0.358 μm (p = 0.582 x 10^{-10}). In cells with induced MUG, spindle width divided with the spindle length was 0.394 ± 0.084, significantly smaller than in the wild type (p = 0.657 x 10^{-23}) and in GSK treated cells (p = 0.351 x 10^{-8}). In U2OS tubulin-GFP, Cenp-A-mCherry cell line spindle width drops from 10.596 ± 0.235 μm (n = 16) to 6.508 ± 0.219 (n = 19, p = 0.819 x 10^{-14}) in cells with induced MUG. Spindle width divided with spindle length is also significantly smaller in cells with induced MUG; 0.405 ± 0.091 (n = 16) in regard to wild type; 0.805 ± 0.068 (n = 19, p = 0.298 x 10^{-20}) (**Figure 58**).
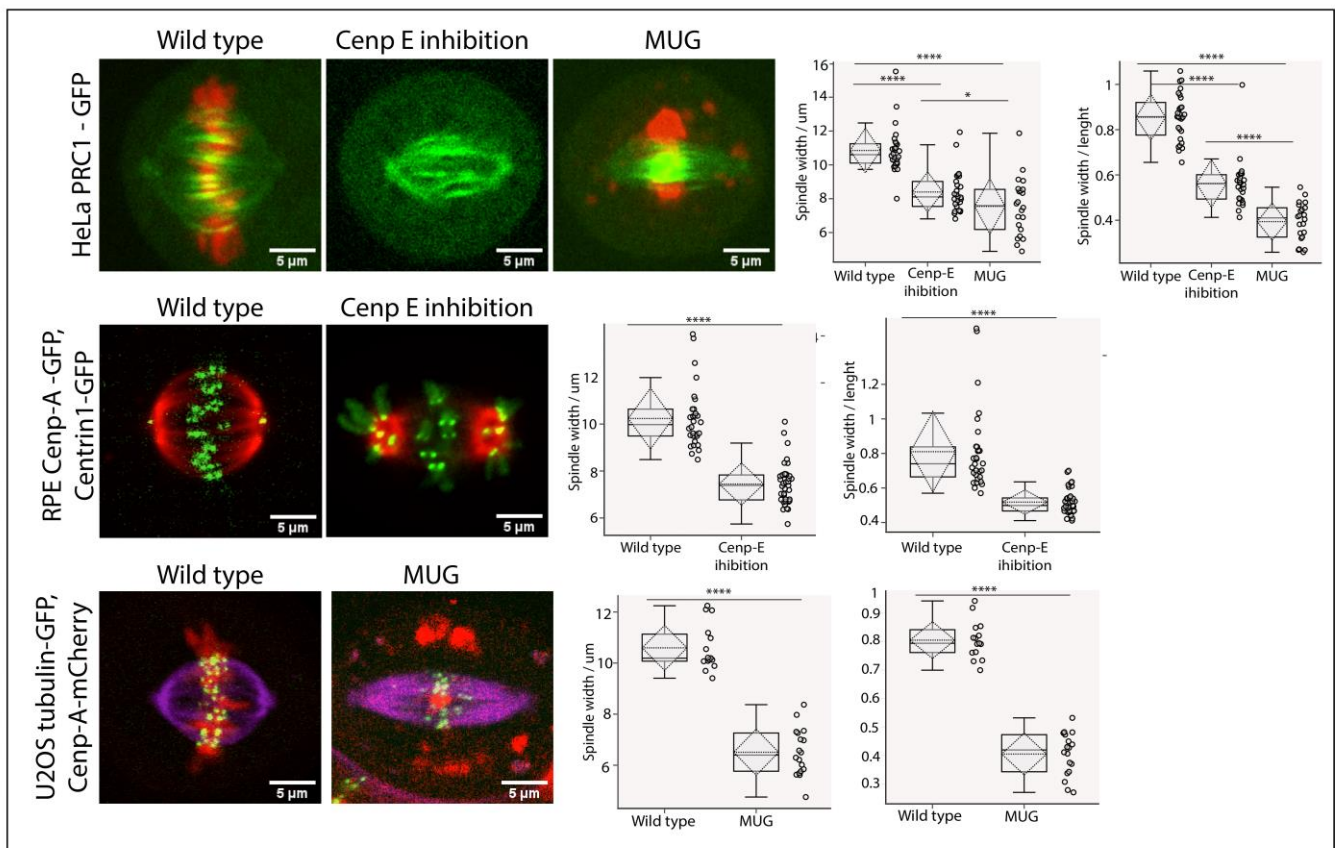
Figure 58. Significant decrease of spindle width in HeLa PRC1-GFP (first row) treated with Cenp-E inhibitor and with induced MUG, RPE1 Cenp-A-GFP, Centrin1-GFP treated with Cenp-E inhibitor (second row) and U2OS tubulin-GFP, Cenp-A-mCherry cell line with

induced MUG (third row). In HeLa PRC1-GFP and U2OS tubulin-GFP, Cenp-A-mCherry cell line DNA is labeled with SiR-DNA dye. In RPE1 Cenp-A-GFP, Centrin1-GFP microtubules are labeled with SiR-tubulin dye.

5. DISCUSSION

As the nuclear envelope breakdown (NEBD) appears, mitotic spindle starts to assemble and chromosomes attach to it. In respect to spindle assembly there are two main pathways of mitosis. In prophase pathway centrosomes migrate to the opposite sides of the nucleus ahead of nuclear envelope breakdown so that when rupture of the nuclear membrane occurs, the bipolarity of the spindle is already set up with the chromosomes between the two poles. In the prometaphase pathway, centrosomes are both on the same side of the nucleus at NEBD and a spindle forms a monopolar structure that subsequently bipolarizes (Kaseda et al., 2012).

5.1 PRC1 protein

This work is mainly focused on the prometaphase pathway of mitosis. Mitotic spindle, as one of the most complex macromolecular structure with essential biological role in all eukaryiotes, lures a big interest in the scientific community. Most scientific papers deal with the onset of mitosis with the emphasis on chromosomes, while research of the mitotic spindle assembly is less represented. Until now, the mitotic spindle was studied mostly in its horizontal orientation. Here, I investigate the process of the spindle assembly from a unique vertical perspective. I mainly focused on the early vertically oriented prometaphase spindle formed in the prometaphase pathway of the mitosis when chromosomes are already tethered on the spindle surface and form a prometaphase rosette. The main stage for all biophysical processes in the spindle, are microtubules. Since individual microtubules are too weak and brittle to serve as a tool for chromosome segregation, microtubules are organized in a higher order structures, microtubule bundles. Here I focus only on the antiparallel bundle formation. Microtubules are present in high abundance in all parts of the spindle, especially around the spindle poles. Cells expressing labeled tubulin or staining of tubulin with tubulin-binding dyes show high signal around the spindle pole, obstructing the view on microtubule bundles in the middle of the spindle due to the high noise. In this work, the main goal was to discover how the antiparallel bundles form *in vivo*. Since the labeling of tubulin for those purposes does not give a clear insight in microtubule bundles as noted above, using a specific protein that labels only the bundles was necessary for their succesfull visualization. There is no such protein known for parallel bundles. PRC1 protein, on the other hand, binds specifically on the antiparallel bundles and allows their visualization (Bieling et al., 2010). This is the reason I used HeLa cell line expressing GFP labeled PRC1 protein. Knowing that parallel and

antiparallel bundles are closely linked and that number of antiparallel bundles equals the number of kinetochore pairs, and therefore equals the number of kinetochore bundles (Polak et al., 2017), visualization of only antiparallel bundles makes a good insight in the localization and arrangement of parallel bundles, too. Although studying the mitotic spindle from vertical perspective is quite demanding and time consuming due to the low percentage of cells that undergo mitosis with vertically oriented spindle, relatively short duration of the prometaphase and propensity of the spindle to rotate, it provides a unique insight into the formation of microtubule bundles.

As the nuclear envelope dissembles, it was noticed that microtubules growing from different spindle poles form a dense amorphous mesh. In HeLa PRC1-GFP cell line, this mesh looks like a mist from vertical perspective, so I have called it the mist of PRC1. PRC1 is attracted to the spindle territory, presumably by interactions with individual microtubules, forming clear outline of the spindle (Mollinari et al., 2002). Those interactions and their nature are still ambiguous. PRC1 natively binds antiparallel microtubules in a form of dimer and his affinity is regulated by phosphorylation (Bieling et al., 2010, Fu et al., 2007). PRC1 is a substrate for several cyclin-dependent kinases (CDKs) (Jiang et al., 1998). PRC1 is inactivated until anaphase onset by CDK1 mediated phosphorylation, preventing its dimerization. Just before the anaphase onset, inhibitory CDK1 phosphorylation is removed from the PRC1, and it forms homodimers. These homodimers specifically recognize antiparallel microtubule overlaps, found at the spindle midzone, and bind, allowing microtubule sliding and tethering of other proteins (Bechstedt et al., 2013). While most of the PRC1 protein is localized on the spindle in anaphase, recent evidence suggests that overlapping antiparallel bundles connected by PRC1 have an important function in metaphase (Jagrić et al., 2019). In metaphase, PRC1 localizes to the bridging fibers which are mixed polarity microtubule bundles connecting opposing sister kinetochore fibers. As the spindle reorganizes in anaphase as a consequence of the decreasing activity of Cdk1/cyclin B kinase, PRC1 is dephosphorylated and concentrates at the forming spindle midzone. Also, recent work shows that PRC1 is present on the spindle already in the early prometaphase (Zhu et al., 2005). Presumably, PRC1 can bind weakly on the lateral surface of microtubules before the formation of antiparallel bundles, but those interactions are probably much weaker. As soon as the nuclear envelope breakdown appears, PRC1 localizes to the spindle (Asthana et al., 2020). During metaphase when chromosomes were aligned in the spindle center, PRC1 localized evenly to the microtubule bundles throughout the entire spindle, as noted previously by immunostaining PRC1 in fixed cells (Neef et al., 2007). Also, in HeLa cells over-expressing GFP-tagged PRC1 in bridging fibers of metaphase spindles in live cells was also seen (Kajtez et al., 2016, Polak et al., 2017). This

would suggest that the mesh of microtubules serves as a microtubule scaffold between two poles, functioning as a docking place for PRC1. The fact that PRC1 interacts with microtubules suggests that the chemical balance of PRC1 binding is shifted towards the spindle, resulting with the unequal distribution of PRC1 in the cell (**Figure 59**). Therefore, the concentration of PRC1 is higher in the spindle territory and lower in the cytoplasm.
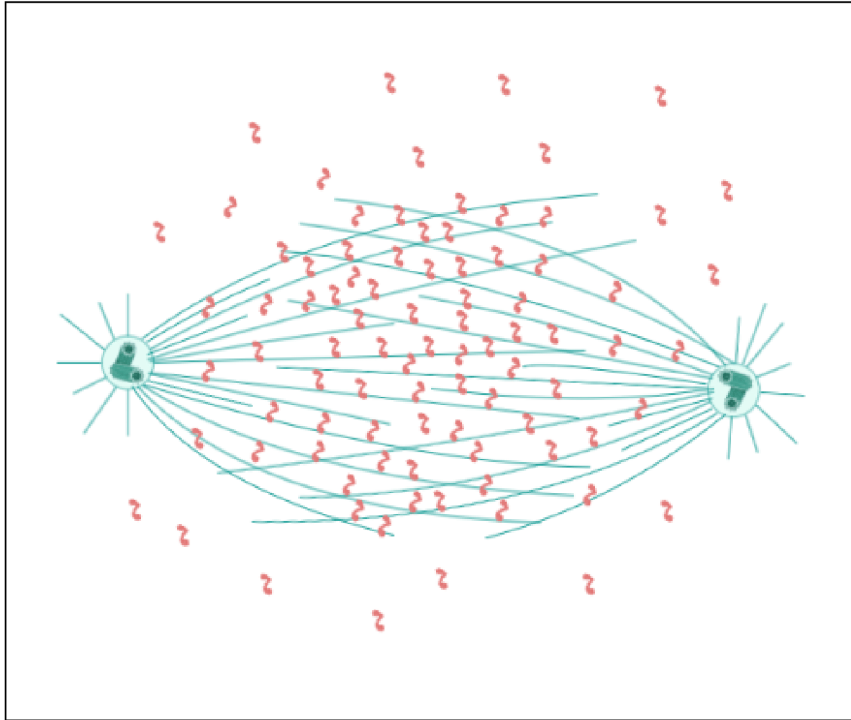
Figure 59. Schematic view of PRC1 localization on the spindle territory in the early prometaphase. This model shows higher concentration of PRC1 on the spindle in regard to the cytoplasm, due to the weak interactions of PRC1 with microtubules. Microtubules are colored green. PRC1 is colored orange.

However, it seems that PRC1 does not localize to the regions of the spindle with highest density of microtubules. Just the opposite, it seems that the highest density of microtubules is present around the spindle poles in the prometaphase, while PRC1 intensity seems highest in the middle of the spindle between two spindle poles where the density of microtubules is lower. Presumably, the proportion of antiparallel overlaps is the highest in the middle of the spindle where the probability of finding two microtubules emerging from opposite pole is the highest. If PRC1 is deposited predominantly on the microtubules forming antiparallel overlaps, is it possible that center of the spindle forms small overlapping bundles, unnoticeable under the microscope, that serve as a platform for PRC1 binding (**Figure 60**). It is highly unlikely that these small overlaps are stable in the early prometaphase due to the

highly dynamic nature of PRC1 (Asthana et al., 2020, Manenica, 2020). If those overlaps even exist, it is likely that they are in constant dynamic balance, forming and reforming in time as the PRC1 protein binds and dissociates from microtubules. On time lapse images of early vertical prometaphase in HeLa PRC1-GFP cell line, transient formation of small patches of higher intensity are shown in time interval before the formation of bundles. These patches of higher intensity seemed to be highly unstable, forming in one frame in one location and reforming later in other locations. They could represent small overlaps that assemble and disassemble in time.

Moreover, direct interaction of PRC1 with microtubules is not necessarily only mode of PRC1 localization to the spindle in the early prometaphase. PRC1 protein has intrinsically unconstructed parts of the structure (Subramanian et al., 2010). Intrinsically unconstructed regions do not have defined 3D structure, allowing the protein to perform a wide range of protein-protein interactions, expanding the pool of binding partners (Uversky et al., 2013). It is possible that localization of PRC1 to the spindle is accomplished by binding indirectly with some other proteins localized to the spindle. All these questions remain unanswered, but for sure, high concentration of PRC1 in the early prometaphase spindle is important for bundle assembly, as proven in my experiments.

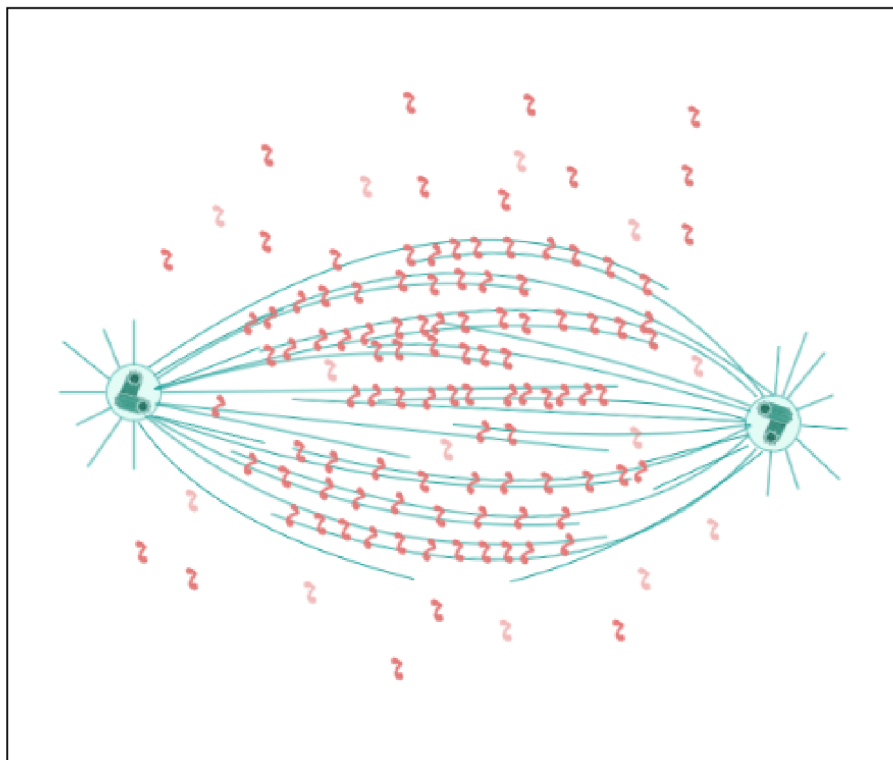**Figure 60.** Upgraded schematic view of the early prometaphase spindle. PRC1 localizes mainly in the middle of the spindle where interaction of microtubules emanating from the

opposite poles is most likely. Model presumes that prometaphase mist seen in HeLa PRC1-GFP cell line is composed of small antiparallel overlaps that bind PRC1 protein.

5.2 Antiparallel bundle focusing

As we already said, PRC1 protein localizes on the spindle in the early prometaphase forming a characteristic structure that looks like a mist under the microscope in a vertically oriented prometaphase HeLa-PRC1 cells. After the mist is formed, in one instant, signal of PRC1 started to concentrate in discreet spots of higher intensity. Occurrence of those spots represented the formation of antiparallel bundles. Intensity analysis showed that in one plane mean intensity of the spindle cross section slightly increases in time, but mean intensity of the whole spindle doesn't change indicating that only the relocalization of PRC1 inside the spindle area appears. There is no significant withdrawal of the soluble PRC1 from the cytoplasm, at least on the large scale. On the other side, maximum intensity of the middle cross section and the whole spindle increases, indicating that the amount of PRC1 bound to the spindle is not changing. Furthermore, squash analysis confirms the same. Analysis of the vertical prometaphase spindles shows that the low intensity mist of PRC1 is fragmented into smaller segments of higher intensity. As larger segments of lower intensity fragment, number of smaller segments with higher intensity increases. Furthermore, it is shown that large segments drop in size abruptly. Intensity analysis and squash segmentation indicate that there is some kind of grouping of microtubules bearing PRC1 protein in time. That brings us to the model of antiparallel bundle formation; mesh of microtubules between two spindle poles, or small previously formed antiparallel overlaps gradually group to form large stabile antiparallel bundles. I called this process antiparallel bundle focusing. Analysis of one bundle intensity also supports this thesis. Intensity analysis of individual bundle formation shows that most bundles form from the mist of PRC1 protein, and that the mean intensity of the bundle increases at the expense of intensity drop in immediate vicinity of the bundle (**Figure 61**). As it is indicated from the line plot, there is a very steep growth of intensity. Precise measurements should be made to show an exponential growth of intensity. After some time it seems that the size of the cross section of the bundle does not increase, while intensity continues to increase in time. Possibly, after most microtubules have been used in the formation of bundles, a part of soluble PRC1 protein loads on. But in the early prometaphase no withdrawal of the soluble PRC1 from the cytoplasm is shown. Presumably, the rest of PRC1 is loaded further in anaphase, on formed overlaps as the phosphorylation state of PRC1 decreases, resulting in an increase of its affinity. In the prometaphase, the bundle intensity grows, presumably until all the PRC1 is used from the mist and concentrated in the newly

formed bundle without a shift in chemical balance in cytoplasm. That means that all PRC1 used in bundle formation in the early prometaphase is already bound to the microtubules. But a slight growth of cross section middle plain mean intensity proves that, even the most of PRC1 protein is probably already bound to the microtubules during the bundle focusing, certain amount of soluble PRC1 fraction is deposited in the bundles during their formation. That would suggest that some fraction of soluble PRC1 is used already in the prometaphase and that the concentration of PRC1 drops in the cytoplasm. Those changes are probably small, and precise measurements and methods are necessary to prove that.
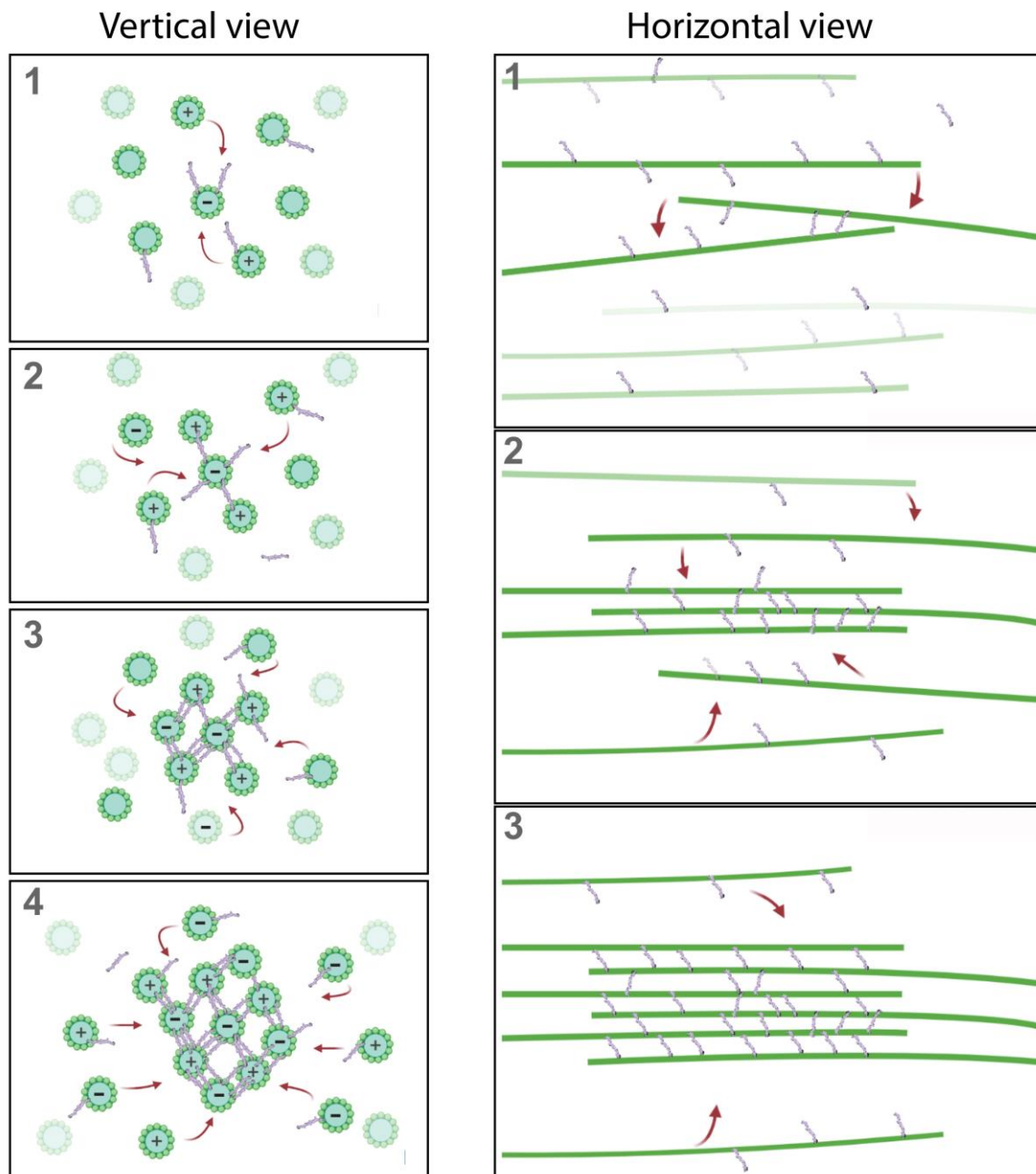

Figure 61. Model for antiparallel bundle focusing. First row (1-4) represents vertical view of antiparallel bundle formation. Microtubules emanating from the opposite spindle poles bear

laterally attached PRC1 protein. Two microtubules of opposite polarity are connected by PRC1 protein forming a core of antiparallel bundle. As the focusing advances, intensity of the cross section increases and bundle forms. Second row shows the same process, but in the horizontal orientation. Microtubules are colored green and PRC1 protein pink. Arrows represent direction of microtubule movement.

In cross section of the prometaphase spindle, spindle has semicircular shape. As already addressed, cross section of prometaphase spindle in HeLa PRC1-GFP cell line showed that the mist of PRC1 is surrounded with chromosomes except in the one region, forming chromosome gap. If cross sections of all imaged prometaphase cells are aligned in a way that the gap is facing upwards, then all spindles had the same morphology. Bottom part of the cross section is encircled with chromosomes and in the early prometaphase forms the characteristic mist of PRC1. That configuration corresponds to the cross section of the prometaphase rosette, structure that forms only in the prometaphase pathway of the mitosis (Itoh et al., 2018). Almost all early vertical prometaphase cells that have been found have this configuration. So, my work is mostly dealt with the prometaphase pathway of the spindle assembly. The question was, why the vertical prometaphase spindle formed in the prophase pathway of mitosis wasn't found under the microscope. Possibly, searching for vertical prometaphase cells selected only cells with prometaphase pathway because of technical limitations of the microscope. In the prometaphase pathway, smaller distance between centrosomes in time of NEBD resulted in higher density of microtubules and GFP labeled PRC1 that forms characteristic mist between them. Higher in density, prometaphase pathway spindle mist makes it visible under the microscope. On the other hand, prophase pathway spindles probably had smaller concentration of PRC1 between poles because of the longer distance between them and the smaller density of overlaps, so they passed unnoticed under the microscope. Also, with the fact that prometaphase pathway lasts much longer than the prophase (Kaseda et al., 2012), the probability of finding one in progress is higher.

My results suggest that all the bundles in the spindle show abrupt increase in the intensity at the same time. It seems that there is some external factor that simulates antiparallel bundle formation. It is possible that small transiently formed antiparallel bundles, seen in the time interval before focusing started, are temporary and spatially stabilized by some kind of a trigger in the cell. Those small overlaps could possibly be assembling and disassembling in time until one moment when small transient overlap becomes stabilized and forms a core of the antiparallel bundle. Then focusing of the bundle proceeds until the fully functional bundle is formed. The question is why that small unstable overlaps even form in the beginning? And

why there is an abrupt stabilization of certain overlaps later, forming antiparallel bundles. Those small overlaps could form passively in the early prometaphase because of the high density of microtubules that grow from the opposite poles, so PRC1 spontaneously crosslinks them. Also, it has been noticed that even larger bundles can fuse in the early prometaphase. That goes in support to the theory of fusion. Fusion of small overlaps could explain formation of larger bundles from smaller overlaps that then become visible under the microscope. Those data refute the theory of bundle splitting. It seems that microtubule bundles have a high propensity for fusion. Splitting of already formed bundles would require investment of energy to disturb the interactions between the bundles generated by PRC1 protein and possible some other motor proteins. While formation of transient unstable overlaps in the early prometaphase could be a result of passive crosslinking by PRC1 protein due to high density, localized focusing and formation of antiparallel bundles is highly unlikely passive process. Focusing is localized in space and synchronous in time, suggesting that activation of this event is necessary. Participation of some motor protein/proteins is possible. In vitro experiments show that some overlap formation is dependent of Kif4 proteins (Birling et al., 2010). Kif4A is essential for central spindle midzone formation and it is localized to the spindle only in anaphase A (Kurasawa et al., 2004). It is possible that some other motor proteins localize on the overlapping microtubules in the prometaphase and bundles them. The question is which one.

5.3 Lateral attachments of kinetochores to the microtubules could be a trigger for bundle formation

Since most of the bundles start to focus at the same time on the side of the spindle encircled with chromosomes the question arises whether kinetochores or some proteins of kinetochore are responsible for antiparallel bundle focusing? Since kinetochores are places of microtubule nucleation in some models of the spindle assembly (Sikirzhytski et al., 2018), it is a logical assumption that the kinetochore proteins could trigger antiparallel bundle formation. It is known that the dominant binding mechanism of chromosomes to the prometaphase spindle is through the lateral attachment of kinetochores to the microtubules (Itoh et al., 2017). Furthermore, adaptive changes in the kinetochore architecture are observed in different modes of microtubule binding (Magidson et al., 2015). To determine whether lateral attachment of kinetochores is important for antiparallel bundle formation, I inhibited specifically aurora B kinase. Aurora B is the main kinase responsible for phosphorylation and activation of proteins that are localized in the kinetochores during lateral attachment (Shrestha et al., 2017, Itoh et

al., 2017). It is known that inhibition of aurora B causes unsuccessful attachment of kinetochores to the spindle and failure in chromosome congression, but its impact on the microtubule bundle formation was never reported. Strikingly, the inhibition of aurora B caused failure in chromosome attachment, but also disturbed the formation of antiparallel bundles, as I expected. As reported in results section, inhibition of aurora B acutely and chronically resulted in different phenotypes. In both treatments, the formation of antiparallel bundles was reduced, but in the cells in which inhibitor of aurora B was added after the prometaphase mist was already formed, certain degree of focusing appeared. In acutely inhibited aurora B cells, number of bundles increases in time, although in smaller extend in regard to the wild type, suggesting that aurora B phosphorylates and presumably activates some protein/proteins responsible for focusing of antiparallel bundles. In acute inhibition of aurora B, this protein is already phosphorylated to some degree. On the other hand, if aurora B kinase is inhibited before NEBD, then there is no activation of target protein/proteins and there is no bundle focusing (**Figure 62**). Without focusing there is no growth of maximum intensity in the spindle as the data suggested.
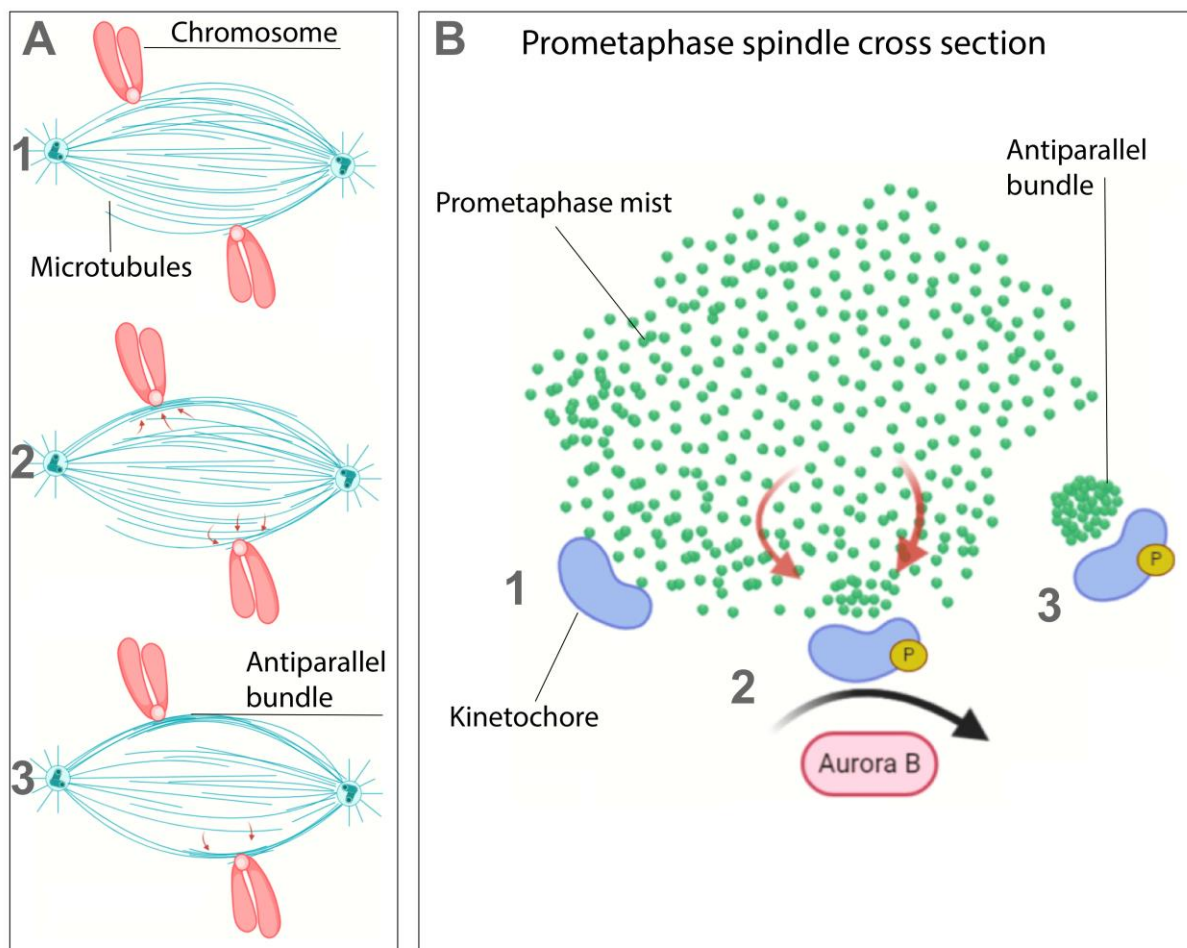
Figure 62. Model of antiparallel bundle focusing depends on aurora B kinase activity. **A.** Schematic view of the antiparallel bundle focusing (1-3) in the vicinity of laterally attached kinetochore to the spindle (horizontal view). **B.** Vertical view of antiparallel bundle focusing. After the lateral attachment of kinetochores to the microtubules, phosphorylation of specific proteins by aurora B kinase triggers bundle focusing (2). **C.** Antiparallel bundle forms (3) with kinetochore attached to it.

To exclude end-on attachment as potential trigger of antiparallel bundle formation, Ndc80 complex was silenced in the HeLa PRC1 – GFP cell line. As expected, overlaps formed normally (Cifferi et al., 2007). Their number was smaller than in the wild type, but they were of high intensity and fully formed. That excludes the end-on attachment as an important factor for focusing of bundles and leaves lateral attachment as an only cause of bundle focusing.

Next step was the depletion of a specific kinetochore protein that could be possible effector of aurora B pathway. One candidate that seemed like a possible target was spindly protein. It is known that spindly protein is a part of the protein complex in lateral attachment of kinetochores on the microtubules (Itoh et al., 2017). However, the depletion of spindly by siRNA method didn't affect the assembly of the spindle in HeLa cells. Just the opposite, depletion of spindly resulted in an increased number of antiparallel bundles in the metaphase of HeLa cells. This result raises further questions. Obviously, spindly affects the number of PRC1 labeled bundles. There are few possible explanations for that. Spindly could be a negative regulator of the number of antiparallel bundles in HeLa cells. The mechanism how it performs that function remains a question. Maybe there is a mechanism for "counting" the number of bundles that have to be formed in the cell. This could imply that cells can regulate number of bundles in some way and that spindly is involved in that function. Metaphase spindles in spindly siRNA targeting cells were of normal morphology and metaphase cells were no different than in the wild type except of higher number of bundles. Another explanation for an increased number of bundles in metaphase is that the loss of spindly causes ectopic focusing of bundles. Presumably, based on my model, antiparallel overlaps should focus only in the region where kinetochore is laterally attached to the microtubules and spindly could be responsible for that localization of focusing. When spindly is silenced, some overlaps may form in the other locations along chromosomes. Therefore, the number of bundles would increase until all microtubules and PRC1 protein are depleted from the mist and incorporated into the overlapping bundles. That would indicate its function as a scaffold for localization of some still unknown kinetochore proteins that could directly be involved in focusing of antiparallel bundles. To confirm this hypothesis, visualization of kinetochores in

HeLa PRC1-GFP protein is necessary. Another explanation is that cells with depleted spindly are aneuploid or polyploid. This would mean that in the previous mitosis complement of chromosomes or some chromosomes are retained in one dividing cell, while the other daughter cell dyes. Even if we couldn't visualize kinetochores, this scenario is highly unlikely because in the dish there were no dead cells. Interestingly, in the most cells with depleted spindly or Ndc80, bundles seem to form in a different location of the spindle cross section. In Ndc80 siRNA targeting, the largest overlaps are in the middle of the cross section, while in the spindly depleted cells, bundles with the largest intensity were formed on the periphery. Also, it seems that PRC1 intensity in bundles of Ndc80 siRNA targeting is higher than in the spindly siRNA treated cells. Because of the variable expression of PRC1 and variable number of chromosomes in HeLa PRC1-GFP cells, intensity measurements should be performed in non-tumor cell lines with stabile expression of PRC1 for precise quantification and comparison.

One possible problem is that aurora B has multiple protein targets. Not only that the pursuit for candidate protein could be hard-labor, cross talk between aurora B and some other kinases (aurora A, Polo-like kinases) makes the situation much more complicated, expanding the number of target proteins and their interactions (Kettenbach et al., 2011). Furthermore, this network of phosphorylation could directly or indirectly have impact on PRC1 protein activity. Since we focused on the cells expressing PRC1 protein, direct visualization of tubulin was not performed in HeLa cells. It is possible that inhibition of aurora B inhibits PRC1 binding on the microtubules, seemingly resulting in the absence of focusing. In order to discard that possibility, inhibition of aurora B should be performed in cells with direct visualization of tubulin using tubulin-dyes or cell line expressing labeled tubulin. Our data and image sequences of aurora B inhibited HeLa-PRC1 cells acquired from NEBD suggest that that is not the case. Most of the spindles didn't show any dynamics and growth in time, suggesting that bundles of microtubules were not formed.

During inspection of the cross section of the prometaphase spindle, one observation drew attention. On the top of the cross section of aligned prometaphase spindles, two or more bundles, called central bundles, were fully formed from the first frames of the time sequence. Those bundles were positioned just between the chromosome gap. The question arises how these bundles focus if they were not in contact with the kinetochores. It is known that first overlaps that form between the centrosomes enable spindle pole separation before NEBD (Kaseda et al., 2012). Main protein that performs sliding of the centrosomes and separates spindle poles is kinesin 5. The fact that kinesin 5 loads on the antiparallel bundles before

NEBD raises a question, whether Eg5 focuses those bundles, and possibly the newly formed bundles later in the prometaphase? Addition of STLC, specific inhibitor of Eg5 seems to inhibit the pole separation and elongation of the prometaphase spindle, but my data shows that antiparallel bundles still focus. As there is no elongation of the spindle, bundles that form are deflected from the spindle axis. Under the microscope these spindles look like asters in the cross section. That suggests that Eg5 does not focus microtubules later in the prometaphase. There must be some other protein or proteins that carry out this role.

Lots of work is ahead to determine the mechanism of antiparallel bundle formation. To determine which proteins of aurora B kinase pathway are essential, detailed depletion analysis with proper visualization should be performed. As most of aurora B targets are localized on the kinetochores, they should be tested first. Labeling of different proteins using genetic engineering approach should provide an insight in temporal and spatial localization of targeted proteins. Most likely candidates are proteins that transiently form complexes on the kinetochores during lateral attachment (Itoh et al., 2018). Temporal and spatial colocalization of candidate proteins with the start of antiparallel bundle formation should reveal the main players in this process. One important notion is that probably, main protein that starts the cross linking is motor protein, presumably from kinesin family. Furthermore, my data suggests that lateral attachment is not only important for proper positioning of chromosomes to the spindle and their congression, but it rather may also have an essential role in formation of antiparallel overlaps. Antiparallel overlaps are integral parts of the spindle apparatus, balancing forces exerted on kinetochores and performing segregation of chromosomes in anaphase as shown in previous studies (Vukušić et al., 2017). Cells in which aurora B is inhibited are arrested in mitosis and do not progress through the anaphase. Their overlaps are not fully formed, and their number is much lower in comparison to the wild type.

5.4 Microtubule branching by augmin complex is responsible for the prometaphase mist formation

Inhibition of aurora B arrests prometaphase cells in a state prior to the antiparallel bundle formation, but it seems that it does not influence the formation of the prometaphase mist. The question is then how the mist of PRC1 forms in HeLa PRC1-GFP cell line? As the formation of antiparallel overlaps was studied in cells expressing PRC1 protein, localization of PRC1 in the territory of prometaphase spindle was an indication that PRC1 binds on the microtubules by some specific interactions. So, the assumption was that the mesh of microtubules between

two poles serves as a scaffold for PRC1 protein binding in the prometaphase spindle even before overlaps form. The next question was, how this mesh of microtubules is formed and why all the cells that were found having it, were using a prometaphase pathway of mitosis? In order to answer the first question, haus6 protein of augmin complex was silenced. Augmin complex nucleates new microtubules on the lateral sides of existing ones and forms a branch (Uehara et al., 2009). Strikingly, silencing of Haus6 protein, resulted in no mist formation. Prometaphase vertical spindles containing the mist of PRC1 were never found in a dish containing cells treated with haus6 siRNA. The cells with chromosome configuration of prometaphase rosette were found. Chromosomes were forming a circle around the spindle territory with open gap on top of the cross section. However, instead of PRC1 mist, fully formed bundles were found encircled with chromosomes in the cross section. Furthermore, some bundles were present not only inside the circle of chromosomes, but between the chromosomes surrounding the cross section as well. When imaged in time, those bundles did show a slight decrease in intensity. There was also a slight increase in their number, leaving most of the bundles present in the first frames. However, squash analysis showed an interesting phenomenon. Two subpopulations of segments differing by their intensity arise in time. Moreover, maximum intensity of the spindle cross section grows, indicating that focusing exists, but as the number of bundles increases only slightly in time, there is predominant focusing on preexisting bundles. On the other hand, maximum intensity of the whole spindle didn't change significantly showing lower degree of focusing in regard to the wild type. The explanation for absence of PRC1 mist in the prometaphase spindle suggests that augmin complex is essential for its formation. That suggests that branching of microtubules between two spindle poles enables formation of dense microtubule mesh. This mesh of microtubules, together with bound PRC1, serves as a pool of building blocks for antiparallel bundle focusing in aurora B dependent manner. But the question is how then haus6 depleted cells form any spindle at all? Imaging of the spindle formation in HeLa PRC1-GFP cell line from NEBD answers that question. In the interphase, microtubules also form bundles. These interphase bundles form a network in the cytoplasm that expands from the centriole localized near the nucleus (Lodish et al., 2008). This network of cytoplasmatic microtubules is known as cytoskeleton. As the nuclear envelope breaks, depolymerization of the cytoplasmatic microtubules appears and the soluble tubulin dimer serves as the building blocks for spindle assembly (Lodish et al., 2008). However, it is noticed that the largest and most stable interphase bundles do not depolymerize. They are retrieved and incorporated in the spindle driven by cytoplasmatic dynein protein (Vaisberg et al., 1993). Large quantity of the bundles is encircling the nucleus already in the interphase. In the prophase pathway of

mitosis, where centrosomes are positioned on the opposite poles of the nucleus, it is practical for the cell to just incorporate those bundles in the spindle without dissolution and rebuilding of new microtubules and bundles. But in the prometaphase pathway, long thick interphase bundle incorporation could be a problem because of the small length of the spindle. So it seems that in the prometaphase pathway, augmin complex nucleates microtubules extensively, forming a dense microtubule mesh. This mesh is formed by polymerization of newly nucleated microtubules using soluble tubulin dimers from cytoplasm (**Figure 63**). As the mesh is formed, the cytoplasmatic tubulin is withdrawn from the cytoplasm and incorporated in the spindle by polymerization of microtubules, shifting the chemical balance to a new formation of microtubules, resulting in depolymerization of microtubules from the interphase bundles. This is also probably enhanced by accumulation of nucleation factors dependent of Ran-GDP gradient in the vicinity of chromosomes (Carazo-Salas, 1999). Probably the same process drives the spindle formation in the prophase pathway, but because of the larger distance between poles, this mesh is not so dense and is unnoticed under the microscope. That would explain also why only prometaphase pathway spindles in vertical orientation were found under the microscope. Moreover, that explains the specific phenotype of metaphase cells treated with haus6 siRNA. In the metaphase, haus6 targeting cells, most of the bundles in the spindle had large overlaps. The number of bundles is significantly lower than in the wild type cells. That is because of the different origin of bundles in Haus6 targeting cells. Live cell time lapse imaging revealed extensive interphase bundle retrieval during spindle formation presumably forming large overlaps in the metaphase. Since the augmin complex is silenced, cell cannot produce new bundles by focusing because there is no microtubule mesh formation at all. Driven by the dynein, those stable bundles are then incorporated into the spindle, resulting in the specific morphology of haus6 targeting metaphase cells. As expected, this process is much more evident in the cells with prometaphase pathway of mitosis where the mist formation and focusing is a dominant way of bundle formation. However, detailed inspection of 3D structure of metaphase spindle in haus6 targeting showed the inner small bundles that are barely visible. It seems that those small bundles of lower intensity form by focusing due to small residual presence of functional augmin complex in haus6 siRNA treated cells or small density of microtubules nucleated at the spindle poles. That means that the small amount of the mist still formed and resulted in the low intensity bundle formation in inner part of the spindle, while external bundles with large overlaps are of interphase origin. These two types of bundles of different origin can be seen in the squash analysis as two populations of segment differing in intensity. Segments of higher

intensity match large interphase bundles retrieved to the spindle from the cytoplasm, while low intensity segments match to population of small, newly focused bundles.

Even greater effect that confirms the same thesis is seen in non-tumor immortalized RPE1 cells. During spindle formation, there was an extensive retrieval of microtubule bundles from the cytoplasm even in wild type cells. But regarding the haus6 targeting, in the wild type there were lagging fragments of microtubule bundles that accumulated on the cell membrane. In haus6 targeting those fragments have not been seen, indicating that all bundle fragments are retrieved to the spindle by dynein. Presumably interphase bundles in wild type cells showed higher disintegration due to spindle microtubule polymerization and interphase bundle fragmentation. In haus6 depleted cells, on the other hand, even the most distant interphase bundles were retrieved to the spindle suggesting that there is no fragmentation of the interphase bundles due to decreased polymerization in the spindle territory as a consequence of microtubule branching failure.

Moreover, inspection of the phenotype of metaphase cells showed that in haus6 depleted cells, spindle was bound to the bottom membrane of the cell. Since the RPE1 cells are adhesive epithelial cells, they show a rich network of cortical microtubule bundles (Youn et al., 2006). Those cortical bundles participate in the cell to cell and cell to plate adhesion. Data indicate that in RPE1 cell line, as in HeLa cell line, there is impaired branching of the microtubules and usage of soluble cytoplasmatic tubulin during spindle formation. Cortical interphase bundles can't depolymerize because the chemical balance is not shifted towards the spindle microtubule polymerization. Small amount of microtubule plus ends in the spindle has no capacity to consume high amount soluble tubulin in cytoplasm and shifts the balance toward interphase bundle disintegration due to absence of branching. Thus, the interphase bundles remain mostly intact. Highest concentration of interphase bundles is on the bottom membrane of the cell due to extensive cell adhesion to the dish plate. When spindle forms, those bundles remain intact and they are only dragged to the bottom of the spindle. Therefore, the spindle remains attached to the bottom membrane of the cell, mediated by those cortical bundles. In the wild type, metaphase spindle is compact and detached from the membrane and floats in the cytoplasm because the cortical bundles are depolymerized, while tubulin is used for the formation of new microtubules and bundles.
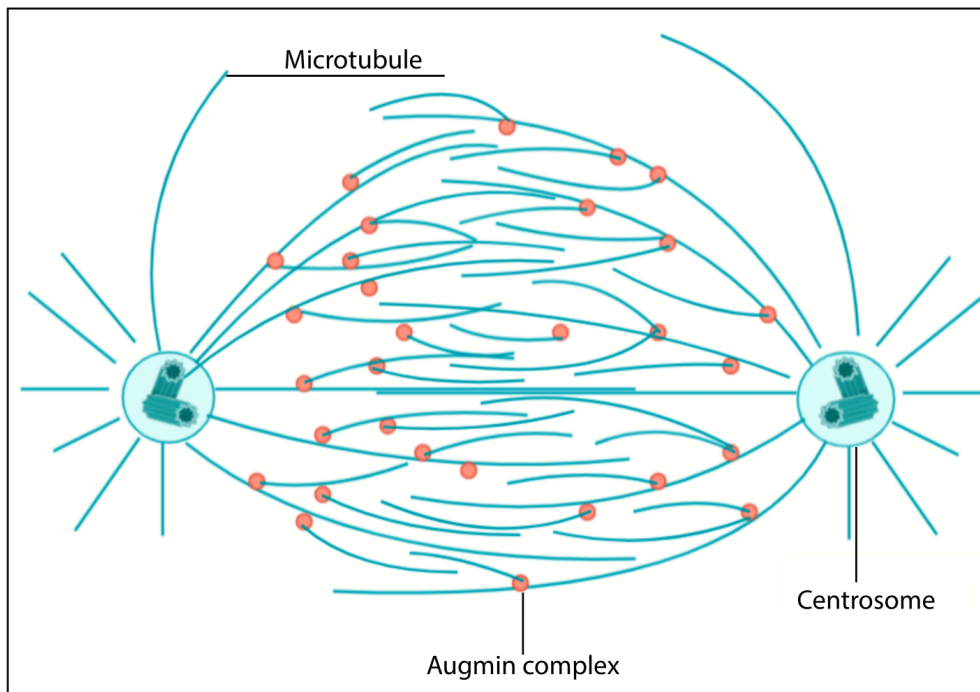
Figure 63. Schematic view of the mist formation by branching of microtubules by augmin complex. Augmin complex enables nucleation of new microtubules on the lateral surface of existing microtubules emanating from the opposite spindle poles, forming a mesh of microtubules. That mesh then serves as a platform for PRC1 binding and mist formation in the prometaphase.

The significance of those results could have great impact on our understanding of the spindle assembly. The data suggests that two important factors are prerequisite for a proper antiparallel bundle assembly in cells. First is the formation of PRC1 mist, formed by binding of PRC1 to the mesh of microtubules formed by augmin complex. Then overlaps form in aurora B dependent way, presumably by lateral attachment of kinetochores to the microtubules. Since the exact proteins and mechanisms responsible for the latter process are still unknown, their discovery would greatly clarify the process of the spindle assembly. Also, the contribution of those mechanisms on the spindle assembly in normal and cancer cells could have significance in biology of cancer. Since cancer cells show a high degree of aneuploidy and heavy chromosome instability, they often carry a larger number of chromosomes. For their segregation, larger spindle with a larger number of overlapping bundles is required. Therefore, cancer cells with higher number of chromosomes have a higher demand for antiparallel overlaps. It is possible that some specific protein responsible for focusing of those overlaps might be overexpressed in cancer cells. These cells would then be more sensitive to specific inhibition of that protein. Also, mutation of some proteins, like spindly, could provide a selective benefit to those cells by increasing the number of

antiparallel bundles. Further research and understanding of these complex processes could provide potential targets in the cancer treatment. Moreover, since the prometaphase pathway of the spindle assembly is dominant in some documented tumors, cells that enter mitosis through that pathway could be more depended on bundle focusing and mist formation by augmin complex than others (Kaseda et al., 2012). Different mechanism of the spindle assembly could provide the selective difference between them.

5.5 Spindle morphology in the prometaphase pathway reveals complementarity of different mechanism of antiparallel bundle formation

Recognition of vertical prometaphase spindle was mainly based on the prometaphase mist in PRC1 and semicircular collar of chromosomes around the cross section of the spindle. It is noticed that some prometaphase spindles had different morphology than the others. Some spindles were much more "tufted" in the cross section, with some bundles emanating from the spindle territory. So spindles were categorized in 3 groups based on their "roughness". Those groups showed different length and different "coverage" with chromosomes. These categories represent prometaphase spindle formation in different stages of centrosome separation. As it is already said, centrosome separation is uncoupled with nuclear envelope breakdown. If NEBD happens when centrosomes are very close to each other, then they will be positioned laterally regarding the nucleus. Because of Ran gradient, microtubules emanating from the spindle pole will grow towards the chromosomes at a greater deflection from the spindle pole axis. Since the mesh of microtubules will form preferentially between two spindle poles by augmin, deflected microtubules grow outside the spindle territory (mist). As they meet kinetochores on the other side of the nucleus, they form the antiparallel overlap outside the spindle territory in aurora dependent pathway, while most of the kinetochores close to the centrosomes form overlaps in spindle territory. As the spindle elongates, those distant overlaps are retrieved to the spindle territory dragging the attached kinetochore along. If the distance between centrosomes is higher in the time of NEBD, then the microtubules grow with smaller deflection towards the chromosomes because the nucleus is partially surrounded by centrosomes. That way, most of the kinetochores are already close to the prometaphase mist, and a smaller amount of bundle focusing outside the spindle territory and retrieval is present. There is a continuum of centrosome distance in cells with prometaphase pathway of mitosis, probably resulting in different frequencies of antiparallel bundle formation. As centrosomes become more separated, lower frequency of retrieval should be seen. However, it seems that in the prophase pathway, higher amount of retrieval is present. Those retrieval events probably have an origin of interphase bundle. This data suggests that spindle assembly

is not a uniform process, at least from the biophysical point of view. A lot of different mechanisms are involved, depending on the centrosome topology, time of NEBD and presence of different proteins.

5.6 Antiparallel bundle dynamics in the prometaphase

When imaging the prometaphase cells in time, it was almost impossible not to notice another strange phenomenon. In all vertical cross sections, bundles were not static in time of focusing and after their formation. In all cells, bundles showed a characteristic pattern of movement. Results showed that, all newly formed bundles, focused in the region encircled by chromosomes, moved in the same direction, towards the two central bundles present from the beginning of the imaging. Those central bundles are formed first, before NEBD, and they separate two spindle poles by sliding driven by kinesin-5 (Eg5). Along with the movement of bundles, the spindle expands. Even more interesting was that in parallel to the movement of newly formed bundles, movement of chromosomes was reported. Chromosome followed the upward movement of newly formed bundles and closed the circle around the spindle cross section. These observations lead to a hypothesis that movement of bundles is influenced by movement of chromosomes or vice versa. Since the movement of chromosomes to the metaphase plate, known as chromosome congression was known long since, inhibition of Cenp-E is performed. Cenp-E is a motor protein that drives the congression of chromosomes by walking toward the plus end of microtubules (Yu et al., 2019). After inhibition of Cenp-E, part of chromosomes does not reach the metaphase plate in vertically oriented spindles as previously reported (Yu et al., 2019). Strikingly, acute inhibition of Cenp-E showed different pattern of bundle movement in most cells. In some cells, newly formed bundles traveled in the opposite direction of the central bundles. The fact that in the prometaphase pathway of mitosis all chromosomes are initially located on the side of the prometaphase spindle facing the nucleus, their simultaneous congression could explain bundle dynamics. That suggests that as the antiparallel bundle focus, they serve as the tracks for Cenp-E driven chromosome tethering to the metaphase plate. As they are all congressing to the same plate from the whole spindle surface, crowding of chromosome arms leads to steric hindrance in the center of the spindle. The steric forces of chromosomes arms then push the chromosomes one from another to make place in the tone plane (**Figure 64**). Since all the bundles are beneath the central bundles together with chromosome attached to them, only place they can go is on the other side of the central bundles. Since the chromosomes are attached to the antiparallel bundles,

repulsion of chromosome arms drives the bundles along. Moreover, the cross section of the spindle expands. This expansion is probably also a consequence of chromosomes pushing due to Cenp-E mediated movement towards the metaphase plate. After the period of expansion, area of spindle does not change, possibly due to the arrival of chromosomes into metaphase plate. This data suggest that expansion of the spindle is a consequence of steric repulsion of chromosome arms, as a consequence of chromosome congression.
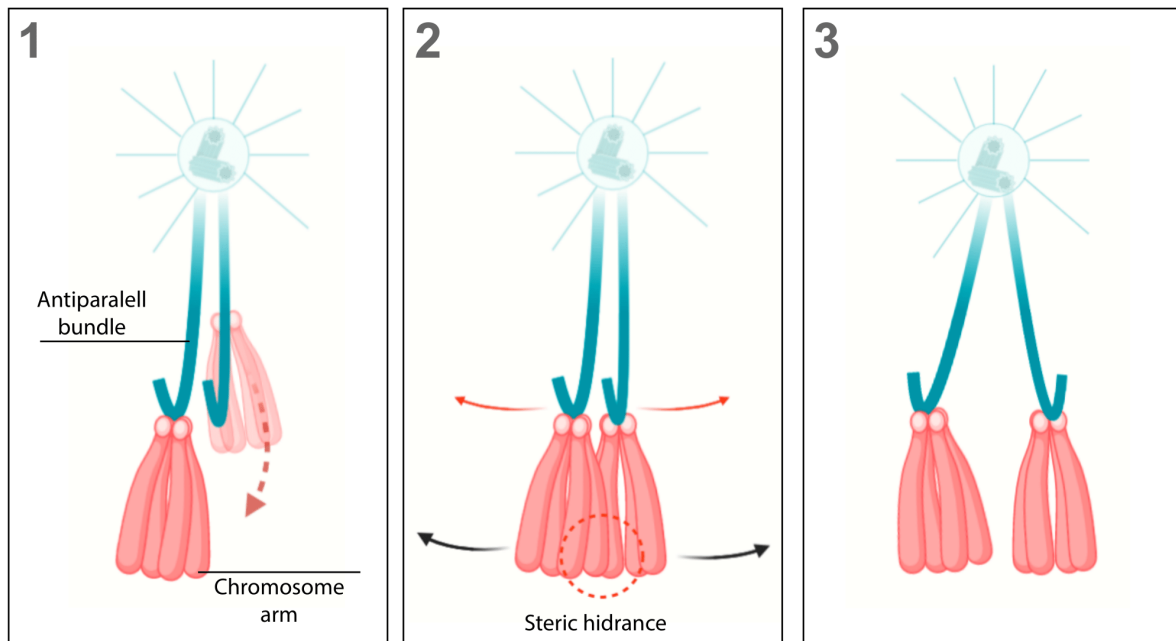

Figure 64. Model for antiparallel bundle dynamics. Schematic view shows two congressing chromosomes on two bundles positioned next to each other (1). As the chromosomes arrive in the same plane, their arms clash (2) and they repel each other moving the bundles along (3). Arrows represent the direction of movement.

Since the live cell imaging of the vertical prometaphase spindle in time is not the simplest way to further investigate that indication, spindle in metaphase cells treated with Cenp-E inhibitor was inspected. Metaphase cells in both HeLa and RPE1 cell line treated with GSK showed smaller width of the spindle, as expected. To exclude possibility that the smaller width and abnormal bundle dynamics is a consequence of a specific effect of Cenp-E inhibition, mitosis with un-replicated genome was induced. In cells with induced MUG only DNA was removed from the spindle, while the position of kinetochores was not disrupted (Wise and Brinkley, 1997). All three cell lines showed decreased width in the metaphase due to DNA removal proving that steric hindrance between chromosome arms is responsible for spindle expansion and observed bundle dynamics.

6. CONCLUSION

There are two pathways of mitosis differing by the position of centrosomes regarding to the cell nucleus. In the prophase pathway centrosomes are on the opposite sides of the spindle before nuclear envelope breakdown, while in the prometaphase pathway nuclear envelope breaks before centrosomes are fully separated. Here, the antiparallel bundle formation in the prometaphase pathway was investigated using vertical spindles as an experimental system. My data shows that in the prometaphase pathway of mitosis, after nuclear envelope breakdown, structure I called prometaphase mist is formed. This prometaphase mist shows very dynamic behavior. Then in one instant, focusing of antiparallel bundles begins. My data shows that during the bundle formation, only redistribution of PRC1 occurs in the spindle. Inhibition of aurora B kinase, main kinase responsible for lateral attachment of kinetochores to the spindle, inhibits formation of antiparallel bundles. On the other hand, inhibition of Ndc80 complex, responsible for end-on attachment does not affect the antiparallel bundle formation. Inhibition of spindly resulted in an increased number of bundles. Also, inhibition of Haus6 protein, one of the components in the augmin complex, inhibited the formation of prometaphase mist indicating an important role of microtubule branching in formation of the prometaphase mist. After the bundles formed, they showed a consensus pattern of movement. All the newly formed bundles were moving in the direction of the two central bundles that focused before the nuclear envelope breakdown and that drive the spindle pole separation driven by Eg5. Irregular movement of bundles in cells with inhibition of Cenp-E protein suggest that specific movement of bundles was a consequence of chromosome congression and steric repulsion forces exerted by the chromosome arms during the concentration of chromosomes in the metaphase plate. Displacement of DNA from the spindle resulted in extreme decrease of metaphase spindle width confirming the fact that steric repulsions of chromosomes are indeed responsible for expansion of the spindle and bundle dynamics. To conclude, antiparallel microtubule bundles form from the mist of microtubules and spindle proteins including PRC1, which is formed by branching of microtubules by augmin complex. Focusing was induced by aurora B dependent lateral attachment of kinetochores to the spindle. After the bundles form, they move driven by the steric repulsion forces of chromosome arms that are a consequence of Cenp-E depended chromosome congression.

7. LITERATURE:

Alberts B., Johnson A., Lewis J., Raff M., Roberts K., Walter P. (2002): Molecular Biology of The Cell, Fourth Edition, Garland Science.

Asthana J., Cade N. I., Lim W. M., Surrey T. (2020): PRC1 and EB1 Binding Dynamics Reveal a Solidifying Central Spindle during Anaphase Compaction in Human Cells. BioRxiv.

Bancaud A., Huet S., Rabut G., Ellenberg J. (2010): Fluorescence Perturbation Techniques to Study Mobility and Molecular Dynamics of Proteins in Live Cells: FRAP, Photoactivation, Photoconversion, and FLIP. Cold Spring Harb Protoc. Chapter 5.

Bechstedt S. and Brouhard G. J. (2013): Motors and MAPs Collaborate to Size Up Microtubules. Developmental Cell. **26:** 118-120.

Bennett A., Bechi B., Tighe A., Thompson S., Procter D. J., Taylor S. S. (2015): Cenp-E inhibitor GSK923295: Novel synthetic route and use as a tool to generate aneuploidy. Oncotarget. **6:** 20921-20932.

Bieling P., Telley I. A., Surrey T. (2010): A minimal midzone protein module controls formation and length of antiparallel microtubule overlaps. Cell. **142**: 420-432.

Bratman S.V., Chang F. (2008): Mechanisms for maintaining microtubule bundles. Trends in Cell Biology. **18**: 580-586.

Brinkley B. R., Zinkowski R. P., Mollon W. L., Davis F. M., Pisegna M. A., Pershouse M., Rao P. N. (1988): Movement and segregation of kinetochores experimentally detached from mammalian chromosomes. Nature. **336:** 251-254.

Carazo-Salas R. E., Gruss O. J., Mattaj I. W., Karsenti E. (2001): Ran-GTP coordinates regulation of microtubule nucleation and dynamics during mitotic-spindle assembly. Nat Cell Biol. **3:** 228-234.

Cifferi C., Musacchio A., Petrovic A. (2007): The Ndc80 complex: Hub of kinetochore activity. FEBS Letters. **15:** 2862-2869.

Fu J., Bian M., Jiang Q., Zhang C. (2007): Roles of Aurora Kinases in Mitosis and Tumorigenesis. Mol Cancer Res. **5:** 1-10.

Gaska I., Armstrong M., Alfieri A., Forth S. (2019): The mitotic crosslinking protein PRC1 acts as a mechanical dashpot to resist microtubule sliding. BioRxiv.

Haren L., Gnadt N., Wright M., Merdes A. (2009): NuMA is required for proper spindle assembly and chromosome alignment in promethaphase. BMC Reaserch Notes. **2:** 64.

Helfrich B. A., Kim J., Gao D., Chan D. C., Zhang Z., Tan A., Bunn P. A. (2016): Barasertib (AZD1152), a Small Molecule Aurora B Inhibitor, Inhibits the Growth of SCLC Cell Lines *In Vitro* and *In Vivo*. Molecular cancer therapeutics. **15**: 2314-2322.

Heald R., Khodjakov A. (2015): Thirty years of search and capture: The complex simplicity of mitotic spindle assembly. J. Cell Biol. **211**: 1103-1111.

Helfrich B. A., Kim J., Gao D., Chan D. C., Zhang Z., Tan A. C., Bunn Jr P. A. (2016): Barasertib (AZD1152), a Small Molecule Aurora B Inhibitor, Inhibits the Growth of SCLC Cell Lines In Vitro and In Vivo. Mol. Cancer Ther. **15**: 2314-2322.

Iemura K., Tanaka K. (2015): Chromokinesin Kid and kinetochore kinesin CENP-E differentially support chromosome congression without end-on attachment to microtubules. Nat. commun. **6**: 6447.

Itoh G., Ikeda M., Iemura K., Amin M. A., Kuriyama S., Tanaka M., Mizuno N., Osakada H., Haraguchi T., Tanaka K. (2018): Lateral attachment of kinetochores to microtubules is enriched in prometaphase rosette and facilitates chromosome alignment and bi-orientation establishment. Sci. Rep. **8**: 3888.

Jagrić M., Risteski P., Martinčić J., Milas A., Tolić I. M. (2019): Optogenetic control of PRC1 reveals its role in kinetochore alignment at the methaphase plate. BioRxiv.

Jiang W., Jimenez G., Wells N. J., Hope T. J., Wahl G. M., Hunter T., Fukunaga R. (1998): PRC1: A Human Mitotic Spindle-Associated CDK Substrate Protein Required for Cytoinesis. Molecular Cell. **6:** 877-855.

Kajtez J., Solomatina A., Novak M., Polak B., Vukušić K., Rudiger J., Cojoc G., Milas A., Sumanovac Sestak I., Risteski P., Tavano F., Klemm A. H., Roscioli E., Welburn J., Cimini D., Gluncic M., Pavin N., Tolic I. M. (2016): Overlap microtubules link sister k-fibers and balance the forces on bi-oriented kinetochores. Nat Commun. **7:** 10290.

Kalinina I., Nandi A., Delivani P., Chacon M. R., Klemm A. H., Ramunno-Johnson D., Krull A., Lindner B., Pavin N., Tolić-Nørrelykke I. M. (2013): Pivoting of microtubules around the spindle pole accelerates kinetochore capture. Nat. Cell Biol. **15**: 82–87.

Kaseda K., McAinsh A. D., Cross R. A. (2012): Dual pathway spindle assembly increases both the speed and the fidelity of mitosis. Biol. Open. **1**: 12-18.

Kettenbach A. N., Schweppe D. K., Faherty B. K., Pechenick D., Pletnev A. A., Gerber S. A. (2011): Quantitative phosphoproteomics identifies substrates and functional modules of Aurora and Polo-like kinase activities in mitotic cells. Sci. Signal. **4:** rs5.

Krull A., Steinborn A., Ananthanarayanan V., Ramunno-Johnson D. Petersohn U., Tolić I. M. (2014): A divide and conquer strategy for the maximum likelihood localization of low intensity objects. Optics Express. **22:** 210-228.

Kurasawa Y., Earnshaw W.C., Mochizuki Y., Dohmae N., Todokoro K. (2004): Essential roles of KIF4 and its binding partner PRC1 in organized central spindle midzone formation. EMBO J. **23**:3237–3248.

Lancaster O. M., Berre M. L., Dimitracopoulus A., Bonazzi D., Zlotek-Zlotkiewicz E., Picone R., Duke T., Piel M., Baum B. (2013): Mitotic rounding alters cell geometry to ensure efficient bipolar spindle formation. Dev. Cell. **25:** 270-283.

Leary A., Nazarova E., Sim S., Shulist K., Francois P., Vogel J. (2018): Kinesin-5 froms a stable bipolar spindle in a fast, irreversible snap. BioRxiv.

Lodish H., Berk A., Kaiser C.A., Krieger M., Scott M.P., Bretscher A., Ploegh H. (2008): Molecular cell biology, Sixth Edition, New York, W.H. Freeman and company.

Magdison V., O'Connel C. B., Lončarek J., Paul R., Mogilner A., Khodjakov A. (2011): The Spatial Arrangement of Chromosomes during Prometaphase Facilitates Spindle Assembly. Cell. **146**: 555-567.

Magidson V., Paul R., Yang N., Ault J. G., O'Connell C. B., Tikhonenko I., McEwen B.F., Mogilner A., Khodjakov A. (2015): Adaptive changes in the kinetochore architecture facilitate proper spindle assembly. Nat. Cell Biol. **17**: 1134-1144.

Mahoney N. M., Goshima G., Douglass A. D., Vale R. D. (2006): Making Microtubules and Mitotic Spindles in Cells without Functional Centrosomes. Curr. Biol. **16:** 564-569.

Maiato H., Rieder C. L., Khodjakov A. (2004): Kinetochore-driven formation of kinetochore fibers contributes to spindle assembly during animal mitosis. J Cell Biol. **167:** 831-840.

Manenica M. (2020): Biophysical properties of the protein regulator of cytokinesis 1, PRC1, in the phases of the human cell mitosis. Dabar.

McCleland M. L., Gardner R. D., Kallio M. J., Daum J. R., Gorbsky G. J., Burke D. J., Stukenberg P. T. (2003): The highly conserved Ndc80 complex is required for kinetochore assembly, chromosome congression, and spindle checkpoint activity. Genes Dev. **17:** 101-114.

McEwen B. F., Heagle A. B., Cassels G.O., Buttle K. F., Rieder C. L. (1997): Kinetochore fiber maturation in PtK1 cells and its implications for the mechanisms of chromosome congression and anaphase onset. J Cell Biol. **137:** 1567-1580.

McEwen B. F., Chan G. K., Zubrowski B., Savoian M. S., Sauer M. T., Yen T. J. (2001): CENP-E is essential for reliable bioriented spindle attachment, but chromosome alignment can be achieved via redundant mechanisms in mammalian cells. Mol Biol Cell. **12:** 2776-2789.

Mitchison T. J., Kirschner M. (1984): Dynamic instability of microtubule growth. Nature. **312**: 232-237.

Molodtsov M. I., Mieck C., Dobbelaere J., Dammermann A., Westermann S., Vaziri A. (2016): A force-induced directional switch of a molecular motor enables parallel microtubule bundle formation. Cell. **167:** 539-552.

Mollinari C., Kleman J-P., Jiang W., Schoehn G., Hunter T., Margolis R. L. (2002): PRC1 is a microtubule binding and bundling protein essential to maintain the mitotic spindle midzone. J Cell Biol. **157:** 1175-1186.

Murata-Hori M., Wang Y. (2002): The Kinase Activity of Aurora B Is Required for Kinetochore-Microtubule Interactions during Mitosis. Science Direct. **12:** 894-899.

Nakayama Y., Matsui Y., Takeda Y., Okamoto M., Abe K., Fukumoto Y., Yamaguchi N. (2012): c-Src but Not Fyn Promotes Proper Spindle Orientation in Early Prometaphase. JBC. **287:** 24905-24915.

Neef R., Gruneberg U., Kopajtich R., Li X., Nigg E.A., Sillje H., Barr F.A. (2007): Choice of Plk1 docking partners during mitosis and cytokinesis is controlled by the activation state of Cdk1. Nat. Cell Biol. **9**:436–444.

O'Connell B. C., Khodjakov A. L. (2007): Cooperative mechanisms of mitotic spindle formation. J. Cell. Sci. **120**: 1717-1722.

Pavin N., Tolić-Norrelykke I. M. (2014): Swinging a sword: how microtubules search for their targets. Syst. Synth. Biol. **8**: 179-186.

Polak B., Risteski P., Lesjak S., Tolić I. M. (2017): PRC1-labeled microtubule bundles and kinetochore pairs show one-to-one association in metaphase. EMBO Rep. **18**: 217-230.

Prelogovic M., Winters L., Milas A., Tolić I. M., Pavin N. (2019): Pivot-and-bond model explains microtubule bundle formation. Phys. Rev. E. **100**: 012403.

Putkey F. R., Cramer T., Morphew M. K., Silk A. D., Johnson R. S., McIntosh J. R., Cleveland D. W. (2002): Unstable Kinetochore-Microtubule Capture and Chromosomal Instability Following Deletion of CENP-E. Dev. Cell. **3:** 351-365.

R Core Team. (2016): R: A Language and Environment for Statistical Computing. R Foundation for Statistical Computing, Vienna, Austria.

Rieder S. L., Salmon E. D. (1994): Motile kinetochores and polar ejection forces dictate chromosome position on the vertebrate mitotic spindle. J. Cell Biol. **124**: 223-233.

Rizk A., Paul G., Incardona P., Bugarski M., Mansouri M., Niemann A., Ziegler U., Berger P., Sbalzarini I. F. (2014): Segmentation and quantification of subcellular structures in fluorescence microscopy images using Squash. Nature protocols. **9:** 586-596.

Royle S. J., Bright N. A., Lagnado L. (2005): Clathrin is required for the function of mitotic spindle. Nature. **434:** 1152-1157.

Saeidi H., Lohrasebi A., Mahnam K. (2014): External electric field effects on the mechanical properties of the αβ-tubulin dimer of microtubules: a molecular dynamics study. J. Mol. Model. **20:** 2395.

Sikirzhytski V., Magidson V., Steinman J. B., He J., Le Berre M., Tikhonenko I., Ault J. G., McEwen B. F., Chen J. K., Sui H., Piel M., Kapoor T., Khodjakov A. (2014): Direct kinetochore-spindle pole connections are not required for chromosome segregation. J. Cell Biol. **206**: 231–243.

Silkworth W. T., Nardi I. K., Paul R., Mogilner A., Cimini D. (2012): Timing of centrosome separation is important for accurate chromosome segregation. Mol Biol Cell. **23:** 401-411.

Simunic J., Tolić I. M. (2016): Mitotic spindle assembly: building the bridge between sister K-fibers. Trends Biochem Sci. **41**: 824-833.

Subramanian R., Wilson-Kubalek E. M., Arthur C. P., Bick M. J., Campbell E. A., Darst S. A., Milligan R. A., Kapoor T. M. (2010): Insights into antiparallel microtubule crosslinking by PRC1, a conserved Nonmotor microtubule binding protein. Cell. **142**: 433-443.

Tolić I. M. (2017): Mitotic spindle: kinetochore fibers hold on tight to interpolar bundles. Eur. Biophys. J. **47**: 191-203.

Toso A., Winter J. R., Garrod A. J., Amaro A. C., Meraldi P., McAinsh A. D. (2009): Kinetochore-generated pushing forces separate centrosomes during bipolar spindle assembly. J. Cell Biol. **184**: 365-372.

Uehara R., Nozawa R., Tomioka A., Petry S., Vale R. D., Obuse C., Goshima G. (2009): The augmin complex plays a critical role in spindle microtubule generation for mitotic progression and cytokinesis in human cells. **106: 6998-7003.**

Uverski V. N. (2013): A decade and a half of protein intrinsic disorder: Biology still waits for physics. Protein Science. **6: 693-724.**

Shrestha R., Conti D., Tamura N., Braun D., Ramalingam R. A., Cieslinski K., Ries J., Draviam V. M. (2017): Aurora-B kinase pathway controls the lateral to end-on conversion of kinetochore-microtubule attachments in human cells. Nature communications. **8: 150.**

Vaisberg E. A., Koonce M. P., McIntosh J. R. (1993): Cytoplasmatic dynein plays a role in mammalian mitotic spindle formation. JCB. **123: 849-858.**

Vukušić K., Buđa R., Bosilj A., Milas A., Pavin N., Tolić I. M. (2017): Microtubule sliding within the bridging fiber pushes kinetochore fibers apart to segregate chromosomes. Dev Cell. **43**: 11-23.

Walczak C. E., Shaw S. L. (2010): A MAP for Bundling Microtubules. Cell. **142: 364-367.**

Wise D. A., Brinkley B. R. (1997): Mitosis in cells with unreplicated genomes (MUGs): spindle assembly and behavior of centromere fragments. Cell Motil Cytoskeleton. **36**: 291-302.

Wollman R., Cytrynbaum E.N., Jones J.T., Meyer T., Scholey I.M., Mogilner A. (2005): Efficient chromosomes capture requires a bias in the 'search-and-capture' process during mitotic-spindle assembly. Curr Biol. **15**: 828-832.

Wu W., Jingbo S., Xu W., Liu Y., Huang Y., Sheng Q., Lv Z. (2018): S-trityl-L-cysteine, a novel Eg5 inhibitor, is a potent chemotherapeutic strategy in neuroblastoma. Oncol. Lett. **16: 1023-1030.**

Youn Y., Hong J., Burke J.M. (2006): Cell Phenotype in Normal Epithelial Cell Lines with High Endogenous N-Cadherin: Comparison of RPE to an MDCK Subclone. Invest. Ophthalmol. Vis. Sci. **47: 2675-2685.**

Yu K., Zhong N., Xiao Y., She Z. (2019): Mechanisms of kinesin-7 CENP-E in kinetochore-microtubule capture and chromosome alignment during cell division. Biol. Cell. **111: 143-160.**

Zhu C., Jiang W. (2005): Cell cycle-dependent translocation of PRC1 on the spindle by Kif4 is essential for midzone formation and cytokinesis. PNAS. **102:** 343-348.

8. CURRICULUM VITAE

Personal information:

Jurica Matković

08. January 1997

Zagreb, Croatia

Education:

Graduate program in Molecular biology, Department of Biology, Faculty of Science, University of Zagreb, Zagreb (Croatia

Undergraduate program in Biology, Department of Biology, Faculty of Science, University of Zagreb, Zagreb (Croatia)

Gymnasium Vladimir Prelog, Natural Science High School Vladimir Prelog, Zagreb (Croatia)

Conferences:

Simunić J., Manenica M., Matković J., Tolić I. M.

Mitotic spindle: From living and synthetic systems to theory 2019,

Split (Croatia), poster presentation.

Science popularization:

Night of Biology 2018, Faculty of Science, University of Zagreb, Zagreb (Croatia).